공학박사 학위논문

Integration of Stem Cells and Graphene for Myocardial Infarction Treatment

줄기세포와 그래핀의 융합을 통한 심근경색의 치료

2015 년 8 월

서울대학교 대학원

화학생물공학부

박 주 연

Integration of Stem Cells and Graphene for Myocardial Infarction Treatment

줄기세포와 그래핀의 융합을 통한 심근경색의 치료

지도교수 김 병 수
이 논문을 공학박사 학위논문으로 제출함

2015 년 8 월

서울대학교 대학원
화학생물공학부
박 주 연

박주연의 박사학위논문을 인준함
2015 년 8 월

위 원 장	황석연	(인)
부 위 원 장	김병수	(인)
위 원	한지숙	(인)
위 원	오유경	(인)
위 원	박한수	(인)

Abstract

Integration of Stem Cells and Graphene for Myocardial Infarction Treatment

Jooyeon Park

School of Chemical and Biological Engineering

The Graduate School

Seoul National University

Myocardial infarction (MI) is one of the major causes of death worldwide. However, the clinical therapies to treat MI is very limited, and the number of patients increases every year. Therefore, there is an urgent need to develop alternative therapeutic methods for cardiac repair after MI. Recently, stem cell and tissue engineering emerged as a potential strategy for MI treatment. In addition, graphene has also drawn much attention for their application in the field of biomedical engineering due to its unique electrical, chemical, optical, and physical properties.

Therefore, in this dissertation presents the integration of stem cells and graphene for the treatment of MI. The major goals of this study is summarized as follows. 1) Development of a graphene platform to promote stem cell differentiation towards cardiac lineage, and the investigation of its mechanisms. 2) Improvement of

stem cell therapy efficacy for MI treatment by utilizing reduced graphene oxide (RGO) to promote paracrine factor secretion and gap junction protein expression by stem cells. 3) Utilizing graphene oxide (GO) flakes to prevent stem cell anoikis when implanted to ischemia and reperfusion injury after MI.

First, we showed that graphene can promote cardiomyogenic differentiation process of mesenchymal stem cells (MSCs). MSCs have drawn much attention as a source of MI therapy because MSCs are easy to isolate and expand, and are capable of differentiating into various cell types. However, the conventional methods to differentiate stem cells to cardiomyocytes require expensive growth factors or toxic chemical inducers. In this study, we demonstrated that the cardiomyogenic differentiation process of MSCs could be promoted simply by culturing MSCs on graphene without using additional inducers for the differentiation. This may be attributed to the enhanced expression of extracellular matrix (ECM) proteins related to cardiomyogenic differentiation. In addition, the signaling molecules required for cardiomyogenic differentiation are upregulated in MSCs cultured on graphene. Collectively, graphene was able to promote cardiomyogenic gene expressions in MSCs.

Second, we showed that the incorporation of RGO flakes into MSC spheroids enhanced the expression of angiogenic growth factors and gap junction proteins in MSCs, and resulted in the attenuation of cardiac remodeling after MI. The secretion of paracrine factors and the formation of gap junctions by the implanted cells promote cardiac repair. The formation of spheroids by MSC clustering is known to promote growth factor secretion by promoting cell-cell interactions. However, cell-ECM interactions, which can further promote growth factor secretion, is very limited in MSC spheroids. Therefore, in this study, we

incorporated RGO, which can adsorb ECM proteins, in MSC spheroids to promote cell-ECM interactions. As a result, the secretion of paracrine factors was further enhanced in MSC-RGO hybrid spheroids. The enhanced secretion of paracrine factors by the incorporation of RGO upregulated the gap junction protein expression in MSCs. The implantation of MSC-RGO spheroids promoted cardiac repair compared to the implantation of MSC spheroids.

Finally, the adhesion of GO flakes to MSCs prior to implantation enhanced the therapeutic efficacy of MSCs in MI. The restoration of blood flow after MI results in a burst of reactive oxygen species (ROS). ROS hinders the adhesion of the implanted MSCs to the injured myocardium, resulting in cell anoikis (i.e. cell death due to the loss of adhesion). Therefore, we have protected MSCs from undergoing anoikis by adhering GO flakes to MSCs prior to their implantation to the injured myocardium. GO is capable of effectively adsorbing ECM proteins. ECM protein-adsorbed GO flakes protected MSCs from undergoing anoikis when MSCs-GO were exposed to ROS condition *in vitro*. *In vivo*, MSCs-GO showed enhanced engraftment in the reperfused myocardium after MI compared to MSCs alone. The enhanced engraftment of MSCs-GO resulted in enhanced paracrine factor secretion. Therefore, the adhesion of GO flakes to MSCs promoted cardiac tissue repair and cardiac function restoration.

Keywords: mesenchymal stem cells, graphene, myocardial infarction, cell function, cell implantation

Student number: **2010-23330**

Table of contents

List of figures

List of tables

Abbreviations

Ad_{hVEGF}	VEGF-encoded adenoviral vectors
AFM	Atomic force microscopy
CCK-8	Cell Counting Kit-8
Col I	Type I collagen
Col III	Type III collagen
Col IV	Type IV collagen
CSCs	Cardiac stem cells
cTnT	Cardiac troponin T
CVD	Chemical vapor deposition
Cx43	Connexin 43
DAPI	4,6-diamidino-2-phenylindole
DCFDA	2′-7′-dichlorofluorescin diacetate
DMEM	Dulbecco's modified Eagle's medium
EB	Ethidium bromide
ECM	Extracellular matrix
EF	Ejection fraction
ELISA	Enzyme-linked immunosorbent assay
ERK	Extracellular signal-regulated kinases
ESCs	Embryonic stem cells
FAK	Focal adhesion kinase
FBS	Fetal bovine serum
FDA	Fluorescein diacetate
FGF-2	Fibroblast growth factor-2

FN	Fibronectin
FS	Fractional shortening
FT-IR	Fourier transform infrared spectroscopy
GO	Graphene oxide
H&E	Hematoxylin and eosin
HGF	Hepatocyte growth factor
ICP-MS	Inductively coupled plasma-mass spectrometry
IGF-1	Insulin growth factor-1
iPSCs	Induced pluripotent stem cells
JNK	C-Jun N-terminal kinases
LVIDd	Left ventricular internal diameter at end diastole
LVIDs	Left ventricular internal diameter at end systole
MI	Myocardial infarction
MLC2a	Atrial myosin light chain 2
MLC2v	Ventricular myosin light chain-2
MNBs	Magnetic nanobeads
MSCs	Mesenchymal stem cells
NT	No treatment
PBS	Phosphate buffered saline
PCNA	Proliferating cell nuclear antigen
PDGF-BB	Platelet-derived growth factor-BB
PEI	Polyethylenimine
pERK	Phosphorylated ERK
pFAK	Phosphorylation of FAK
PI3K	Phosphatidylinositol 3-kinase

PlGF	Placental growth factor
PMMA	Poly (methyl methacrylate)
PS	Penicillin–streptomycin
PVA	Polyvinyl alcohol
qRT-PCR	Quantitative reverse transcriptase polymerase chain reaction
RGO	Reduced graphene oxide
ROS	Reactive oxygen species
SAED	Selected area electron diffraction
SDF-1	Stromal cell-derived factor-1
SMA-α	Smooth muscle actin alpha
TEM	Transmission electron microscopy
TTC	Triphenyl tetrazolium chloride
TUNEL	Terminal deoxyribonucleotidyl transferase-mediated biotin-16-dUTP nick-end labelling
VEGF	Vascular endothelial growth factor
VN	Vitronectin
vWF	Von Willebrand Factor
β-MHC	Beta-type myosin heavy chain

Chapter 1.

Research backgrounds and objectives

1.1. Myocardial infarction (MI)

Cardiovascular diseases remain one of the leading causes of death worldwide[1,2]. Over 80 million individuals have one or more cardiovascular diseases in the United States.[2] Myocardial infarction (MI) serves as the major contributor to cardiac-associated disorders.[1,3,4] Various therapeutic approaches, including thrombolytic treatments and surgical coronary artery bypass, have been introduced to treat MI. However, these therapies merely promote cardiac tissue regeneration.[5-7] MI is a kind of ischemic heart disease characterized by reduced blood supply to the heart, which results in cardiac tissue damage, ventricular malfunction, and heart failure.[4] Because MI originates from low blood supply and cardiac cell death, successful treatments for MI depend on recovering blood vessels and regenerating cardiac tissues.[4,7] In other words, tissue regenerative approaches are required for effective MI treatment.

Recently, significant advances have been made in the fields of stem cells for MI treatment.[8-10] A number of clinical trials with stem cells have shown encouraging results.[11-14] Stem cells have regenerative potentials to replace the dead cardiomyocytes, salvage dying cells, and induce angiogenesis at the infarcted region.[7] A number of different cell types, including mesenchymal stem cells (MSCs),[11-14] embryonic stem cells (ESCs),[15-17] induced pluripotent stem cells (iPSCs),[18-20] and cardiac stem cells (CSCs)[21] have all shown salutary effects in MI treatment. Among the various cell types, MSCs are a reliable source for cell therapy as MSCs have shown safe and promising results in long-term clinical trials.[12,14,22] Upon implantation into the infarcted heart, a fraction of MSCs can differentiate into functional cardiomyocytes and replace the damaged cardiac tissues for heart function improvement.[23-25] Additionally, MSCs are known to secrete various therapeutic

paracrine molecules for cardiac cell protection, angiogenesis, and immune modulation for cardiac repair.[1,26-28]

In addition to the stem cell therapy, biomaterial-based MI treatments have drawn significant attention as new therapeutic approaches for cardiac repair.[29,30] Treatment options that utilize nanobiomaterials, including nanoparticles, nanofibrous scaffolds, self-assembling peptides, and many others, have addressed significant improvements in myocardial repair.[29] Nanobiomaterials have been used to deliver therapeutic molecules, including proteins, drugs, and genes.[31-35] Additionally, biomaterials utilized as cell carriers have improved the therapeutic efficacy of the cells.[36,37] Previous studies showed that the cells implanted into infarcted myocardium with functional biomaterials exhibited improved cell survival and engraftment, resulting in enhanced cardiac repair.[36,37] More recently, nanobiomaterials that can modulate cell functions have provided a new approach of biomaterial-incorporated cell therapy for MI. Nanomaterials with unique topographical, electrical, or chemical characteristics have been extensively studied to create synergistic effects with cell therapy. Indeed, a combination of cells and biomaterials proposed promising therapeutic options for MI.[38-51]

1.2. MSCs for MI treatment

A number of preclinical and clinical studies have been performed using stem cells to repair the damaged heart.[8,15-20,52,53] Most of these cells, including MSCs, ESCs, iPSCs, and CSCs, improved cardiac function and suggested promising therapeutic approaches for MI. ESCs and iPSCs represent ideal cell sources for MI repair due to their pluripotency. ESCs can differentiate into functional cardiomyocytes when implanted into the injured myocardium.[16,17] Differentiation of ESCs at the lesion site further restores contractile function of the heart and attenuates cardiac remodeling.[15] Similarly, the implantation of iPSCs into the injured myocardium resulted in cell engraftment and differentiation into cardiomyocytes, which led to enhanced cardiac function.[18-20] Despite their therapeutic potentials, however, ESCs pose potential risks of teratogenicity and ethical concerns, while the generation efficiency of iPSCs is still very low.[54,55] As an alternative, CSCs have drawn attention as a cell source to repair the damaged heart. CSCs are c-kit-positive heart-resident stem cells can differentiate into cardiomyocytes.[55] However, the extremely small portion of CSCs in hearts and the difficulties in obtaining these cells limits the clinical applications of CSCs even with their high therapeutic efficacy.[55] Meanwhile, MSCs have been extensively investigated as the optimal cell source for MI. Although the cardiac differentiation potential of MSCs is comparatively limited than ESCs, iPSCs, and CSCs, MSCs can easily be isolated from the patients, expanded *ex vivo*, and utilized in an autologous manner.[7] Additionally, the secretion of therapeutic paracrine molecules from MSCs, including various types of growth factors and cytokines, is known to repair the injured myocardium.[1,56-60] The therapeutic efficacy of MSCs has been exhibited in a number of clinical studies. The POSEIDON trial have demonstrated that the implantation of autologous or allogenic human MSCs

improved cardiac function after MI.[52] Also, the APOLLO trial showed enhancements in cardiac function, perfusion, and neovasculogenesis after the transplantation of adipose-derived stem cells.[53] Various other trials, including the ANGEL, ATHENA, and MyStromal Cell, are currently undergoing clinical phase trials for chronic myocardial ischemia.[8] In the following sections, the two major therapeutic mechanisms of MSC therapy for MI, namely 1) the differentiation of MSCs into cardiac lineage and 2) the paracrine actions of MSCs, are reviewed (Figure 1.1).

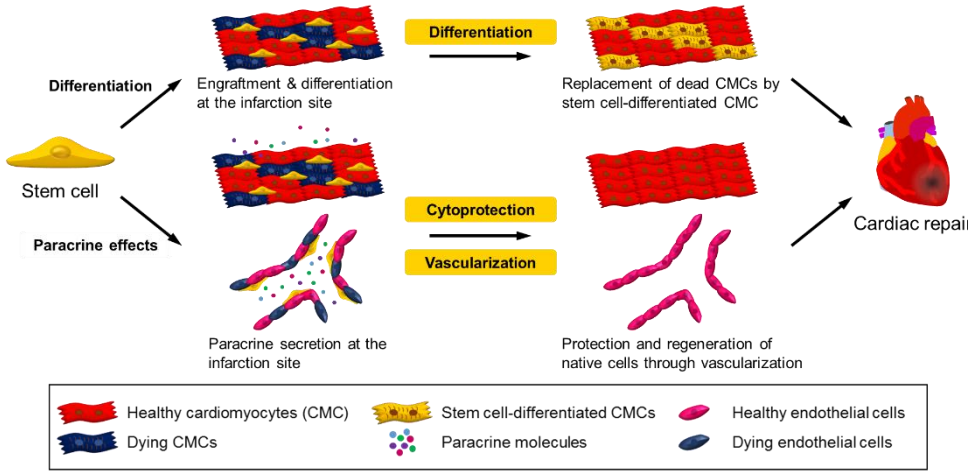

Figure 1.1. Therapeutic mechanisms involved in stem cell therapy for MI treatment. Stem cells can either differentiate into cardiomyocytes or secrete therapeutic paracrine molecules to salvage and regenerate heart tissue.

1.2.1. Differentiation of MSCs into cardiac lineage

Direct differentiation of the implanted MSCs into cardiac lineage cells has originally been proposed as the principal mechanism of stem cell therapy for MI.[7] Hence, cardiac differentiation of MSCs *in vitro*, which can be achieved by chemicals, small molecules, growth factors, and co-culture with cardiac cells, has been extensively investigated to improve the therapeutic efficacy of MSCs. MSCs are capable of differentiating into cardiomyocytes *in vitro*.[61] To differentiate MSCs into cardiomyocytes using chemicals, 5-azacytidine has been widely utilized as the key chemical facilitator.[62,63] It has also been reported the fluid shear stress in combination with 5-azacytidine treatment further enhances cardiomyogenic differentiation of MSCs.[64] Besides 5-azacytidine, small molecules such as phorbol myristate acetate can also promote cardiomyogenic differentiation of MSCs, and stimulate electromechanical integration of MSCs with resident cardiomyocytes.[65] Bartunek *et al*. further showed that pretreatment of MSCs with cardiomyogenic growth factors prior to implantation can induce cardiac lineage differentiation of MSCs and enhance the therapeutic efficacy of the MSCs.[66] The co-culture of MSCs with cardiac cells can also promote cardiomyogenesis of MSCs, which can further be promoted through pretreatment of nanobiomaterials[51] or alignment of the cells[67]. Upon implantation into the damaged heart, MSC-differentiated cardiomyocytes can reduce fibrosis, improve angiogenesis, preserve gap junctions, and enhance cardiac functions compared to the implantation of undifferentiated MSCs.[51,65,66]

MSCs have also been demonstrated to differentiate into cardiac cells *in vivo* following implantation. Yoon *et al*. have shown that MSCs implanted to the infarcted myocardium differentiated into cardiomyocytes, endothelial cells, and smooth muscle cells, which led to cardiac function improvement.[68] Differentiation of

adipose-derived and cortical bone-derived stem cells into cardiomyocytes and vascular cells has also been observed after *in vivo* implantation.[69,70]

1.2.2. Paracrine factor secretion of MSCs for cardiac repair

Even though the cardiac function improvements after MSC implantation were accompanied with the differentiation of the MSCs, other studies have addressed that the number of newly differentiated or generated cardiomyocytes was too small to explain the benefits of the MSC therapy.[71] After MI, more than a billion of cardiomyocytes undergo apoptosis and necrosis, hence, the small fraction of MSCs-differentiated cardiomyocytes cannot elicit meaningful benefits for MI therapy. Growing evidences now suggest that growth factors and cytokines secreted from the implanted MSCs play a critical role in promoting cardiac repair.[56,60] MSCs are known to secrete a variety of growth factors and cytokines that can exert protective effects on damaged tissues and organs.[57-59] These paracrine molecules are involved in cardiac tissue regeneration, neovascularization, contractility, cardiac metabolism, myocardial protection and even immune responses for cardiac repair.[72]

The therapeutic effects of paracrine molecules for cardiac repair were demonstrated in the studies where the administration of conditioned medium of stem cell cultures recapitulated the benefits of stem cell implantation.[27,71] Gnecchi *et al.* demonstrated that the conditioned medium from MSC cultures showed cytoprotective effects on rat cardiomyocytes *in vitro* and significantly reduced cardiac fibrosis *in vivo*.[27] Paracrine factors secreted by the implanted MSCs have shown to protect adjacent cardiomyocytes from undergoing cell death, attenuate left ventricular remodeling in ischemic heart, and induce angiogenesis and vasculogenesis.[28] To enhance the paracrine secretion of MSCs and elicit better tissue regeneration, previous studies have introduced hypoxic culture conditions or MSC spheroids generating mild hypoxia on MSCs.[51,73-76] It has also been demonstrated that hypoxia preconditioning of MSCs not only stimulates the growth factor

secretion of MSCs but also results in enhanced survival of the implanted MSCs in the infarcted myocardium.[26]

These observations regarding the differentiation capability and paracrine action of MSCs have prompted studies with the development of new therapeutic strategies that can exert synergistic effects with MSCs. Recently, nanobiomaterials that can improve the cardiac differentiation and harness the paracrine action of MSCs have gained much attention.

1.3. Nanobiomaterial-incorporated stem cell therapy for cardiac repair

Mounting evidences for stem cell-derived paracrine action along with their cardiac lineage differentiation for cardiac repair suggested a crucial step forward for stem cell therapy. Recently, studies that have utilized nanobiomaterials to potentiate the therapeutic efficacy of stem cells have made great advances. Biocompatible nanomaterials have been used to deliver therapeutic molecules for angiogenesis and stem cell recruitment to promote cardiac repair. Also, co-implantation of functionally designed nanomaterials with stem cells exploited synergistic effects for cardiac repair. Nanomaterials can not only enhance the engraftment of the implanted stem cells *in vivo*, but also regulate stem cell function in a more cardiac repair-favorable manner. In the following sections, we provide an overview of integration of nanobiomaterials with stem cells for enhanced cardiac repair after MI (Figure 1.2).

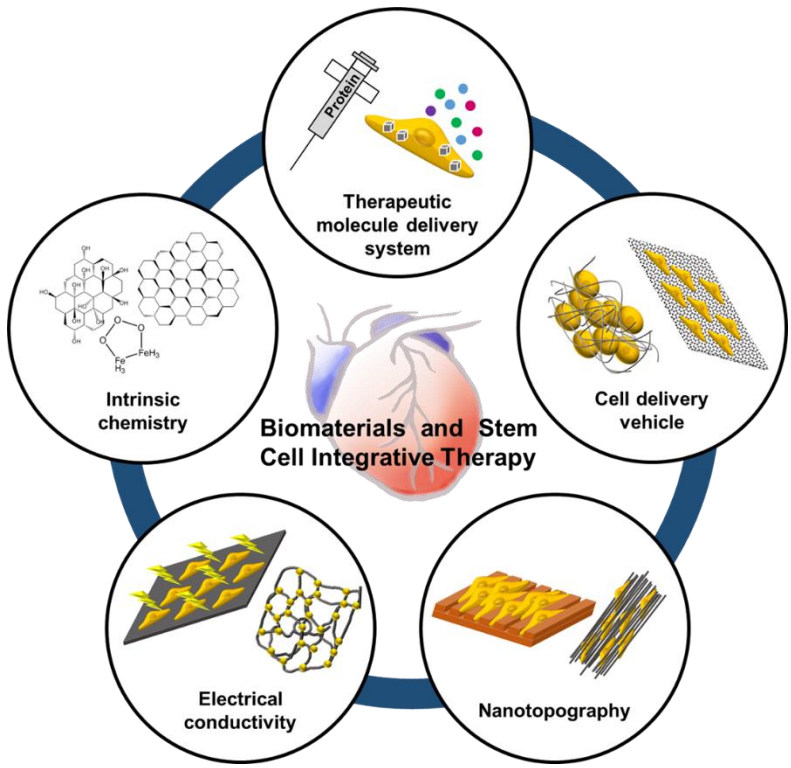

Figure 1.2. Integration of nanobiomaterials with stem cells for MI treatment. Nanobiomaterials can enhance the delivery efficacy of therapeutic molecules and cells for cardiac repair. In addition, nanotopographical, electrical, and chemical cues of nanobiomaterials can regulate stem cell functions for enhanced therapeutic efficacy for MI treatment.

1.3.1. Therapeutic molecule delivery system

The delivery of therapeutic molecules, including genes and proteins, has improved cardiac repair after MI by promoting angiogenesis[34,77] or recruiting stem cells[78]. The delivery of angiogenic proteins, such as platelet-derived growth factor-BB (PDGF-BB)[35] and placental growth factor (PlGF)[31], using nanobiomaterials have significantly attenuated cardiac remodeling and improved cardiac function after MI. Angiogenic proteins were delivered in a sustained and controlled manner using nanobiomaterials to prolong the expression of these proteins.[31,32,35,79] PDGF-BB has previously been delivered to infarcted myocardium using injectable self-assembling peptide nanofibers, which enabled effective delivery of the growth factor.[35] PDGF-BB delivered without self-assembling peptides rapidly disappeared from the injected site after 24 hours, and a negligible amount of PDGF-BB was detected after 3 days. On the other hand, self-assembling peptide nanofibers loaded with PDGF-BB achieved sustained release of PDGF-BB at the injection sites for 14 days. PDGF-BB released from self-assembling peptide showed protection of cardiac cells *in vivo* and enhanced cardiac function after MI, while the delivery of PDGF-BB alone demonstrated insignificant improvements in cardiac function. Similarly, chitosan-alginate nanoparticles delivered PlGF in a sustainable manner.[31] Chitosan-alginate nanoparticles showed over a 120-hour period sustained release of PlGF *in vitro*, and the implantation of PlGF-bound nanoparticles significantly restored cardiac function and promoted vessel regeneration.

In addition to the direct delivery of therapeutic proteins to the MI region, nanobiomaterials have also been engaged with gene delivery. Zhang et al. have utilized magnetic nanobeads for enhanced gene delivery efficacy of vascular endothelial growth factor (VEGF)-encoded adenoviral vectors (Ad_{hVEGF}).[79] The

conjugation of magnetic nanobeads (MNBs) with adenoviral vectors (MNBs/Ad) enabled higher gene transduction efficacy in cultured cells under magnetic field stimulation compared to Ad alone *in vitro*. When MNBs/Ad_{hVEGF} complexes were intravenously injected *in vivo*, epicardial placement of magnet effectively attracted the complexes to the injured myocardium. Gene delivery approach using MNBs significantly reduced cardiac remodeling and improved left ventricular function by enhancing the gene delivery efficacy.[79]

Cells are often transfected with genes using nanocarriers *in vitro* prior to being implanted to the lesion site. For example, PEI nanoparticles were able to effectively transfect VEGF genes into skeletal myoblasts.[80] Implantation of VEGF-transfected skeletal myoblasts into the infarcted myocardium showed significantly improved cardiac repair compared to skeletal myoblasts without transfection. Transfection of insulin growth factor-1 (IGF-1) into cardiomyocytes[33] and cardiac progenitor cells[81] enhanced the survival of the implanted cells in the infarcted heart and promoted heart repair. In addition, the transfection of angiopoietin-1 gene to adipose-derived stem cells prior to implantation promoted angiogenesis in the infarcted heart with enhanced secretion of angiopoietin-1.[82] Collectively, cell-based gene delivery to the infarcted myocardium proposes a novel approach for cardiac repair, and nanobiomaterials play a crucial role in efficient gene transfection of the cells.

For stem cell homing and tissue repair, the delivery of stromal cell-derived factor 1 (SDF-1) has shown much potential.[83,84] SDF-1 is a chemokine involved in stem cell homing.[85] The expression of SDF-1 is stimulated by the induction of MI, which in turn, recruits stem cells to the injured myocardium.[84] The migration of stem cells to the infarcted myocardium was further enhanced with SDF-1 over-expression though SDF-1 gene delivery to left ventricular wall after MI induction using

adenovirus vector.[84] It has been reported, however, that locally delivered SDF-1 protein is vulnerable to rapid diffusion and cleavage. Therefore, to overcome these barriers, Segers et al. designed SDF-1 that is resistant to cleavage, and tethered this chemokine to self-assembling peptides. SDF-1-bound self-assembling peptides retained chemotactic activity and allowed local delivery of SDF-1 at the infarcted region. Subsequently, nanobiomaterial-integrated SDF-1 delivery significantly enhanced the stem cell homing, increased capillary density, and improved cardiac function.[86]

1.3.2 Cell delivery vehicle

Although stem cell therapy has emerged as a promising treatment option for MI, its therapeutic benefit still remains limited due to poor engraftment and survival of the implanted cells.[87] Efficient delivery and prolonged survival of the stem cells have been one of the major challenges in the stem cell therapy and its translational application for MI.[8] Therefore, the development of new therapeutic strategies that can enhance the survival and extend the reparative action of the implanted cells is suggested as the critical factor that determines the beneficiary outcomes of the stem cell therapy.[88] A number of nanobiomaterial-based approaches have been utilized as efficient cell delivery systems, including cardiac patches and injectable nanomaterials, and their therapeutic efficacy for cardiac repair has previously been investigated.

To improve stem cell retention after implantation *in vivo*, nanostructured cardiac patches and injectable peptides have been studied.[29,89-91] Cardiac patches are placed on the epicardial surface of the infarcted heart. Thus, the patches require proper structural and chemical properties that are compatible with the native cardiac tissue. For this reason, fabrication of cardiac patches with collagen, the predominant extracellular matrix protein in the heart tissue, has drawn much attention with its environmental compatibility.[29] Simpson *et al.* have previously demonstrated that collagen patches seeded with MSCs improved MSC survival *in vitro* and restored cardiac function after implantation.[92] Compared to previous studies that showed less than 11% of cell engraftment after implantation, MSCs delivered with collagen patches achieved a cell engraftment of 23%, resulting in better cardiac function improvement. Cardiac patches without MSCs showed no improvements in cardiac function, suggesting that the major therapeutic efficacy was attributable to the

implanted stem cells. Along with the natural materials such as collagen, synthetic materials have also been investigated.[29] Among various types of synthetic polymers, poly(lactide-co-ε-caprolactone) has been suggested as a suitable candidate for cardiac patch due to its elasticity and biodegradability.[93] When MSCs were seeded onto poly(lactide-co-ε-caprolactone)-based cardiac patch and implanted onto the infarcted heart, MSC survival and cardiac function were both greatly improved.[93] Injection of MSCs alone also showed partial improvement in cardiac function. However, the patch provided a fertile environment that increased MSC viability and cardiac repair efficacy. Cardiac function restoration was not observed with poly(lactide-co-ε-caprolactone) cardiac patch alone. Even though aforementioned studies showed that cardiac patch alone did not improve cardiac function,[92,93] contradictory results have been obtained in other cardiac patch studies.[94,95] Therefore, further studies are required to fully investigate the efficacy of acellular patches and their effects on stem cell therapy for cardiac repair.

Bio-inspired self-assembling peptide nanofibers can be utilized as a cell-delivery vehicle for MI treatment.[96-98] Attributable to the biocompatibility and biodegradability, self-assembling peptides have been utilized not only in drug delivery but also in cell delivery for cardiac repair. Previous studies showed that self-assembling peptides as a cell-delivery vehicle greatly improved the survival of the implanted cells and significantly facilitated myocardial regeneration after MI when implanted with either MSCs, skeletal myoblasts, or bone marrow mononuclear cells.[96-98] This is majorly because self-assembling peptides formed nanofibrous structure and provided cell-friendly environment for the implanted cells. Furthermore, Guo *et al.* have integrated self-assembling peptides with cardiac stem cells and demonstrated their therapeutic applications in rat MI model.[99] Self-

assembling peptides modified with cell adhesion motifs, RGDSP, facilitated cardiac stem cell adhesion and survival *in vivo*. Upon implantation, CSC-seeded self-assembling peptides readily bundled into nanofiber scaffolds, provided suitable microenvironment for CSC survival, and protected CSCs from apoptosis and necrosis caused by anoxia. Subsequently, increased survival of CSCs implanted with self-assembling peptides resulted in enhanced cardiac differentiation of CSCs, resulting in better cardiac repair. Compared to the groups treated with CSCs or self-assembling peptides alone, the combination of CSCs with the peptides significantly improved cardiac function and reduced collagen deposition. Collectively, these studies suggest that self-assembling peptides can serve as an efficient cell delivery vehicle providing cell-friendly microenvironments, which can promote the therapeutic efficacy of stem cells in MI repair.

1.3.3. Nanotopographical cues of nanobiomaterials

Nanobiomaterials with nanotopographical cues have been applied to modulate cell behaviors, such as cell differentiation, function, and gap junction expression, for cardiac tissue repair. For the development of therapeutic nanobiomaterials for MI, researchers have mainly focused on the innate properties of the heart, because cardiac-mimetic characteristics may pose significant effects on the cells.[9,10,29] Heart is a constantly working, dynamic organ with complexity. For functional activity of the heart, cardiac cells comprising heart muscles require a quick and efficient signal transfer. For cell signal transduction and synchronous contraction of the heart, cardiac cells alignment and proper gap junction protein distribution are required.[100] To mimic the anisotropic property of the heart, various nanotopography-associated approaches have been introduced to modulate cell behaviors and integrated with stem cells for cardiac repair.

A previous study has demonstrated that contact guidance of the cells by aligned topography or electrical field stimulation is crucial in the orientation and elongation of cardiomyocytes.[38] Interestingly, this study showed that while the combination of nanotopography and electrical stimulation can promote the contractile property of cardiomyocytes, the topographical cue is a stronger determinant of cardiomyocyte alignment than electrical field stimulation. Several studies demonstrated that aligned nanofibers, which mimic the nanostructures of natural extracellular matrix (ECM) of the heart tissue,[39] can improve the alignment[40] and beating of the cardiomyocytes[42]. Cardiomyocytes cultured on aligned nanofibrous electrospun patches showed higher beating frequency and amplitude compared to those cultured on randomly-oriented cardiac patches. Upon implantation *in vivo*, cardiomyocyte-seeded aligned cardiac patch improved the therapeutic outcomes of the cell therapy, while randomly-

oriented patch induced serious cardiac deterioration and worsened cardiac function.[42] This study indicates that the function of cardiomyocytes can be modulated using anisotropic characteristics of the nanobiomaterials.

Anisotropic property of the nanobiomaterials was further shown to affect stem cell behaviors for higher therapeutic efficacy. Kim *et al.* have previously shown that cardiac niche-mimicking aligned nanotopography could enhance the adhesion, proliferation, and cardiomyogenic differentiation of CSCs.[41] Implantation of stem cell-seeded anisotropic polymer scaffolds showed better integration with the host tissue due to the cardiac ECM-mimicking nanostructures. Subsequently, CSC-seeded aligned cardiac patch reduced cardiac fibrosis and improved cardiac function.[41] Anisotropic property of nanobiomaterials has also shown to improve paracrine action of stem cells as well. Kang *et al.* recently demonstrated that MSCs cultured on aligned fibronectin-immobilized polycaprolactone nanofibers exhibited enhanced expression of angiogenic and cardio-protective genes.[101] This study showed that MSCs cultured on anisotropic polycaprolactone nanofibers exhibited aligned cellular phenotypes found in native cardiac tissue. The implantation of MSC-seeded anisotropic scaffolds significantly improved cardiac function in rat MI model.[101] The mechanisms of fibronectin-immobilized polycaprolactone nanofibers-mediated cellular signaling and paracrine molecule expression were not clarified in this study. However, the interactions between stem cells and nanotopographical cues of nanobiomaterials led to enhanced paracrine effects of stem cells for cardiac repair. Collectively, the topographical cues can not only enhance the cardiac differentiation of stem cells, but also improve paracrine factor secretion from stem cells for cardiac repair.

Topographical alignment has shown synergistic effects with conventional cardiac differentiation methods. Pijnappels *et al.* showed that forced alignment of MSCs in the patterned substrate can significantly improve cardiac differentiation of MSCs and their functional integration with cardiomyocytes in MSC-cardiomyocyte co-culture.[67] The functional integration between MSCs and cardiomyocytes enhanced the MSCs' conduction velocity and gap junction protein, connexin 43 (Cx43), expression. In addition, buckled structure on patterned nanofibrous scaffold has exhibited a synergistic effect with 5-azacytidine treatment to improve cardiomyogenic differentiation and Cx43 expression of MSCs.[102] These studies show the anisotropic property of biomaterials can not only independently enhance the reparative action of MSCs, but also exert synergistic effects with other therapeutic approaches for MI treatment.

1.3.4. Electrically conductive nanobiomaterials

Along with the topographical characteristic, electrical conductivity is another unique property of the heart that is critical in developing therapeutic biomaterials for cardiac repair. Unlike cells in other organs, cardiac cells need gap junction-based intercellular coupling and electrical conduction for natural heart function. Thus, therapies that are electrochemically unsuitable may pose electrophysiological inharmony with native cardiac tissues and cause arrhythmic risks upon application.[100] To mimic and preserve the electrically conductive characteristics of the heart, previous studies have focused on developing conductive nanobiomaterial-integrated therapeutics that are electrically compatible with native cardiac tissues. Various nanobiomaterials, including carbon- and gold-based nanomaterials, have shown electrical conductivity,[103-105] and researchers have integrated these nanomaterials with stem cell therapy for MI treatment.

A number of previous studies showed that the integration of carbon nanofibers or carbon nanotubes with polymer scaffolds can promote the adhesion and proliferation of cardiomyocytes[43] and cardiac progenitor cells.[44] In addition, these conductive nanomaterials significantly promoted the expression of Cx43 in cardiac cells and stimulated electrical coupling between cells. Expression of Cx43 is particularly important for MI repair because it is essential for intercellular coupling, arrhythmic risk reduction, and functional cardiomyogenic differentiation of MSCs for cardiac repair.[65,74,100,106] Even though the mechanisms for Cx43 upregulation on conductive materials have not been clearly elucidated, overexpression of Cx43 certainly suggests the potential of conductive nanobiomaterials for cardiac repair. To better elicit the therapeutic potentials of conductive materials, Martines *et al.* and Kharaziha *et al.* have demonstrated the improvements in the electrophysiological

functions of cardiomyocytes seeded onto the chitosan matrix incorporated with carbon nanofibers[48] and poly(glycerol sebacate):gelatin scaffolds embedded with carbon nanotubes[50], respectively. Cardiac cells seeded onto the conductive nanobiomaterial-integrated scaffolds exhibited synchronous beating behavior and showed increased expression of cardiac-specific genes involved in cardiac muscle contraction and electrical coupling.

Gold nanomaterials have also been utilized to improve Cx43 expression and therapeutic efficacy of the cell therapy. Cardiomyocytes cultured in hydrogel scaffolds integrated with gold nanoparticles[45] or gold nanowires[46] showed increased Cx43 expression compared to cardiomyocytes cultured in hydrogels without gold nanomaterial integration. Dvir *et al.* incorporated gold nanowires to porous alginate scaffolds to develop three-dimensional conductive nanocomposites.[46] Non-conducting alginate pore walls were bridged with conductive gold nanowires and demonstrated enhanced electrical signal propagation, enabling the electrical communication between the cardiomyocytes seeded on the scaffolds. Therefore, cardiomyocytes grown on conductive hydrogel scaffolds showed synchronous contraction upon electrical stimulation.[46] Collectively, these studies suggest the integration of electrically conductive nanomaterials with polymeric scaffolds may improve the therapeutic efficacy of the current treatment options.

To examine whether conductive materials can provide cardiomimetic cues to MSCs for cardiac differentiation, a number of studies have investigated MSCs' phenotype changes upon the treatment of conductive materials. Mooney *et al.* have demonstrated that electrical stimulation of carbon nanotube-embedded scaffolds significantly enhanced cardiomyogenic differentiation of MSCs seeded on the scaffolds.[47] Electrical stimulation reoriented the cells perpendicular to the direction

of the current and significantly augmented the expression of cardiac-specific biomarkers including Cx43. To differentiate the effect of electrical stimulation from the conductive properties of the materials, Crowder *et al.* further investigated carbon nanotube-containing synthetic polymer scaffolds without electrical stimulation on cardiac differentiation of MSCs.[49] This study observed that electrically conductive nanobiomaterials alone without electrical stimulation can also promote stem cells' cardiac differentiation. Aforementioned studies, however, did not clarify the mechanisms involved in cardiac differentiation and Cx43 enhancement of MSCs cultured on conductive materials. Further studies elucidating the effects of conductive materials on cell function modulation and differentiation are required for therapeutic application of conductive materials for MI.

Conductive nanobiomaterials have actively participated in intercellular coupling and cardiac differentiation, showing a great potential in therapeutic applications for MI treatment. However, the mechanisms behind their effects on stem cells' behavior still remain elusive. Furthermore, conductive nanobiomaterials need to properly mimic the electrical conductivity of the native heart to reduce the arrhythmic risks upon *in vivo* application.[100] Future studies elucidating the mechanisms involved in MSCs behavior modulation by conductive nanomaterials and the development of *in vivo* mimetic conductive materials would provide a better therapeutic window for the application of conductive nanobiomaterials for MI.

1.3.5. Intrinsic chemistry of nanobiomaterials

Along with topographical and electrical properties of the biomaterials, the intrinsic chemical properties can also be applied for stem cell therapy for MI. For example self-assembling peptide nanofibers that can capture paracrine molecules have been utilized to promote cardiac repair.[107] Self-assembling peptides comprised of short peptide sequences linked to a fatty acid tail can spontaneously assemble into nanofibers under various physiological conditions. These peptides are biodegradable and apt to functional modifications, making a better candidate for MI treatment. Webber *et al.* have demonstrated that heparin-presenting self-assembling peptides can bundle into a matrix consisting of fibrillar nanostructures similar to natural cardiac ECM.[107] The presentation of heparin further enabled the binding of growth factors secreted from the stem cells *via* heparin-binding domains.[107] Using recombinant proteins of VEGF and fibroblast growth factor-2 (FGF-2) loaded in nanofibers, the effects of nanofiber-captured growth factors from the stem cell-conditioned medium were recapitulated. When implanted into the damaged heart, the growth factor-bound nanofibers successfully restored the hemodynamic function of the heart by modulating cardiac metabolism.[107] This study showed the therapeutic potentials of synthetic materials with stem cells' paracrine factors as an acellular therapy for MI.

Owing to their innate chemical characteristics, nanoparticles have also been utilized for cell function modulation and cardiac repair. Iron oxide nanoparticles, which have been widely used for *in vivo* imaging, have recently been applied to modify the cell functions of H9C2 cells, a cardiomyoblast cell line, in MSC-H9C2 co-culture.[51] The co-culture of MSCs with cardiac cells has previously been demonstrated to prime MSCs toward cardiac lineage, and the implantation of cardiac

primed-MSCs into the infarcted heart was shown to improve cardiac function.[65] For co-culture, the rat cardiomyoblast cell line H9C2 has drawn much attention due to the ease of accessibility compared to primary cardiomyocytes. However, the low level of Cx43 expression in H9C2 cells[108] limits the efficacy of MSC cardiac priming by MSC-H9C2 co-culture.[51] Han *et al.* have recently showed that the internalization of iron oxide nanoparticles can augment the Cx43 expression in H9C2 cells without exhibiting cytotoxicity by modulating intracellular c-Jun N-terminal kinase (JNK) signaling.[51] The enhanced Cx43 expression stimulated the intercellular crosstalk between H9C2 cells and MSCs. MSCs co-cultured with iron oxide nanoparticle-internalized H9C2 cells showed improved cardiac differentiation and paracrine molecule secretion. Subsequently, the implantation of the co-cultured MSCs reduced fibrosis, enhanced angiogenesis, and improved cardiac function.[51] Collectively, defining the intrinsic chemical properties of the nanomaterials that can influence the stem cell function would provide a basis for the development of better therapeutic options for the future MI therapy.

1.4. Limitations of previous stem cell therapies for MI treatment

Although significant advances have been made in the development of stem cell therapies for MI treatment by integrating nanobiomaterials, there are still some limitations that need to be overcome to achieve even better therapeutic efficacy. Here, some limitations regarding stem cell differentiation toward cardiomyogenic lineage, stem cell spheroids, and cell delivery vehicles are discussed.

First, 5-azacytidine is one of the widely used inducers to promote cardiomyogenic differentiation of stem cells toward cardiomyogenic lineage.[62,63] However, 5-azacytidine has potential to interfere with deoxyribonucleic acid methylation.[109] Therefore, non-cytotoxic methods should be developed to induce cardiomyogenesis of stem cells for clinical applications.

Second, stem cell spheroids have drawn much attention because they can generate mild hypoxia and enhance the paracrine factor secretion on stem cells.[75] However, stem cell spheroids show very limited cell-ECM interactions.[110] The provision of cell-ECM interactions to stem cells in spheroids would further improve the therapeutic efficacy of stem cells as cell-ECM interactions can promote paracrine factor secretion and enhance Cx43 expression.[111,112] In addition, it has been demonstrated that electrically conductive materials can stimulate the expression of Cx43.[113] Therefore, the incorporation of electrically conductive materials that can provide cell-ECM interactions into stem cell spheroids would facilitate better therapeutic outcome after stem cell spheroid implantation into the MI-treated heart.

Finally, many methods have been developed to deliver cells into the infarcted myocardium to improve cell engraftment and survival. Polymer scaffolds

and hydrogels have been widely studied to promote stem cell survival after implantation. However, polymer scaffolds and hydrogels have certain disadvantages. Generally, the delivery of stem cells using polymer scaffolds require invasive surgical procedures and would only be delivered to the epicardial surface.[114] In addition, stem cell delivery using hydrogels often require accurate control of time as rapid gelation is required for the improvement in cell retention whereas sufficient gelation time is required for injection.[115] Therefore, a facile method to deliver cells by injection with no need for the control of gelation time would provide a better option for cell delivery to improve cell engraftment after implantation into the infarcted myocardium.

1.5. Graphene for tissue engineering applications

Graphene is a single-atom-thick material composed of sp^2-bonded carbon atoms in hexagonal lattice structure, showing extraordinary chemical, electrical, thermal, and mechanical properties.[116] Graphene has attracted great interests from many fields of research, including chemistry, electrical engineering, physics, material science, and bioengineering, due to its uniqe intrinsic characteristics.[117-120] Recently, many researchers started to focus on the application on graphene and its derivatives for biomedical applications, including stem cell regulation, therapeutic molecule delivery, cancer therapy, and bioimaging. Especially for tissue engineering applications, graphene and its derivatives have emerged as a candidate with great potential.

Previous studies reported that graphene can promote cell adhesion. MSCs culture on graphene show a spindle-like morpholgy while MSCs culture on SiO_2 subsrates show a polygonal shape.[121] In addition, osteoblasts grew confluently in a monolayer on graphene while islands of round-shaped cells were observed on SiO_2 substrates due to insufficient cell adhesion.[121] Similarly, fibroblasts cultured on reduced graphene oxide (RGO) and graphene oxide (GO) showed enhanced number of focal adhesions and smaller focal adhesion area compared to the fibroblasts cultured on coverslips, showing a stronger attachment of cells on RGO and GO substrates comapared to the coverslips.[122]

Stem cells cultured on graphene showed significantly enhanced differentiation potential toward osteogenic lineage.[123] The extent of osteogenesis of MSCs promoted by graphene is comparable to that by the growth factors.[123] Lee et al. have demonstrated that graphene can preconcentrate and enhance the local concentration of osteogenic inducers in cell culure media, and thereby promote

osteogenic differentiation of MSCs.[124] The degree of RGO functionalization was able to regulate the extent of osteogenic differentiation of MSCs by altering the amount of protein adsorption on the substrate through controlling the non-colvalent interactions (electrostatic forces, hydrogen bonding, hydrophobic interactions, and π-π interactions) between functionalized RGO and proteins.[125] In addition to protein and osteogenic inducer adsorption, the roughness of the surface created by GO coating also influnced the extent of bone mineralization of MSCs.[126]

Graphene has also been demonstrated to influence the behavior of neural cells. Graphene was not only biocompatible to neural cells such as hippocampal cells, but also was able to increase the number and average neurite length compared to tissu culture polystryrene substrates.[127] In addition, the differentiation of neural stem cells into neurons was enhanced on graphene, which may have been attributed to the upregulation of laminin-related receptors on cells cultured on graphene.[128] Furthermore, the fluorination and patterning of graphene significantly enhanced the degree of neurogenic differentiation of MSCs by facilitating cell alignment and elongation.[129]

Moreover, recent studies have demonstrated the commitment of stem cells toward various other lineages could be enhanced by graphene derivatives. GO was shown to enhance the adipogenic differentiation of MSCs by preconcentrating insulin and promoting fatty acid synthesis.[124] In addition, the myogenic differentiation of myoblasts was enhanced on RGO and GO substrates, with higher enhancement on GO substrates, compared to glass substrates.[130] This study attributed the promotion of myogenic differentiation to the adsorption of serum protein and nanotopography by RGO and GO substrates.[130] Graphene and GO also regulated the

behaviors of iPSCs.[131] The endodermal differentiation of iPSCs was augmented on GO, whereas graphene suppressed the differentation.[131]

The integration of graphene and graphene derivatives with polymers and hydrogels have been investigated to utilize graphene and graphene derivatives for three-dimensional (3D) scaffolds. GO has been incorporated into polyvinyl alcohol (PVA) hydrogels to form GO/PVA composite hydrogels.[132] The incorporation of GO siginificantly enhanced the mechanical property of the hydrogels, and GO/PVA composite hydrogels did not show significant toxicity on fibroblasts when examined by the cell morphology and number.[132] Furthermore, graphene-doped chitosan-PVA nanofibers promoted wound healing compared to chitosan-PVA nanofibers in a mouse model.[133] The promotion of wound healing may have been attributed to the antibacterial effects by electrons that escaped from graphene.[133]

Graphene derivatives have also been investigated as a therapeutic molecule delivery system to control cell function for enhnaced tissue regeneration efficacy. For example, GO was used to deliver transforming growth factor-β3 and bone morphogenetic protein-2 in a sustainable manner, resulting in in enhanced chondrogenic differentiation[110] and bone regeneration[134], respectively. The loading of therapeutic proteins on GO is relatively easy as GO can readily adsorb proteins through hydrophobic interactions, electrostatic forces, and hydrogen bonding.[125]

1.6. Research objectives of this dissertation

Stem cell therapy has become one of the most encouraging treatment options for MI. Simple delivery of stem cells has been applied in a number of pre-clinical and clinical studies. However, the therapeutic efficacy of stem cells needs improvements, and stem cell therapy's efficient clinical translation remain elusive. To potentiate the therapeutic efficacy of stem cells, nanobiomaterials have been utilized in a number of different forms. Nanobiomaterial-integrated strategies include efficient delivery of therapeutic molecules or cells, development of cardiac niche-mimicking biomaterials with electrical conductivity or anisotropic nanotopography, and utilization of chemical properties of the nanomaterials. However, there are still some limitations in these stem cell therapies.

Therefore, in this dissertation, we proposed various methods to utilize the unique properties of graphene and its derivatives to overcome the limitations of previous stem cell therapies to improve the therapeutic efficacy for MI treatment. We investigated the effects of intrinsic chemistry of graphene, GO, and RGO on MSC differentiation, growth factor secretion, gap junction expression, and survival. Moreover, the effects of electrical conductivity of RGO on gap junction expression was also examined. The therapeutic efficacy of GO- and RGO-integrated MSC implantation was evaluated using mouse and rat MI models.

Chapter 2.

Experimental procedures

2.1. Preparation of graphene and graphene derivatives

2.1.1. Graphene preparation

First, high-quality, large-scale monolayer graphene was synthesized on a copper foil by chemical vapor deposition (CVD) process. Second, 300 nm thin poly(methyl methacrylate) (PMMA), called the 'supporting layer', was coated on graphene films, and annealed at 140 ºC for 1 min to cure it. Then, the graphene on the other side of the copper foil was removed by reactive ion etching process with a power of 100 W and O_2 etching gas of 20 sccm. Next, PMMA/graphene on copper foil was floated on the surface of an aqueous solution of 0.1 M ammonium persulphate [$(NH_2)_4S_2O_8$] to etch away copper foil. After all of the copper layers were etched away, the floating PMMA/graphene film was collected using a clean PET film and transferred to deionized water, and washed five times with deionized water. After that, PMMA/graphene was transferred to the coverslips. The samples were dried with nitrogen gas immediately after the transfer and baked for 8 h on a hot plate at 60 ºC. The samples were cleaned using acetone at room temperature for 30 min to remove the PMMA support layer. The samples were then dried and baked for 8 h on a hot plate at 60 ºC. Finally, the graphene on coverslip was obtained.

2.1.2. GO and RGO preparation

Graphite powder (< 20 μm) was purchased from Sigma-Aldrich and used as received. GO was synthesized using a modified Hummers method.[135] The synthesized GO was suspended in water (0.05 wt.%) to give a brown dispersion. The exfoliation of GO was achieved by ultrasonication for 3 h, and the mixture was subsequently dialyzed (12–14 kDa cut-off) for 6 h to remove any residual salts and acids. The obtained solution was then subjected to centrifugation at 3000 rpm for 20 min to remove the unexfoliated GO. The resulting homogeneous dispersion (100 mL) was mixed with 1 mL of hydrazine solution (35 wt.% in water) and 7 mL of ammonia solution (28 wt.% in water). RGO powder was then obtained by filtration and drying in vacuum.

2.2. Characterization of graphene and graphene derivatives

The samples were characterized by atomic force microscopy (AFM), Raman spectroscopy, ultraviolet–visible spectrometer, transmission electron microscopy (TEM), selected area electron diffraction (SAED), fourier transform infrared spectroscopy (FT-IR), and inductively coupled plasma-mass spectrometry (ICP-MS). The surface morphology examination ofthe samples was conducted through non-contact mode AFM (XE-100 system, Park Systems, Korea). The structural properties of the graphene on the coverslip were further investigated through Raman spectroscopy (RM 1000-Invia, Renishaw, UK). The Raman spectra were recorded by using an argon ion laser (514 nm) as the excitation source with a notch filter of 50 cm^{-1}. The typical scan range was from 1000 to 3000 cm^{-1} and the instrumental resolution was 10 cm^{-1}. The optical transmittance of the graphene on the coverslip was measured using an ultraviolet–visible spectrometer (UV-3600, Shimadzu, Japan). The TEM and SAED analyses were conducted on a TEM (JEOL 2100, JEOL, Japan) operated at 200 kV. The rotation between the TEM images and the corresponding SAED patterns was calibrated using molybdenum trioxide crystals. The sheet resistances of the graphene on the coverslip were measured through the van der Pauw four-probe method using a Hall measurement system. The FT-IR spectra were obtained on a Fourier Transform Infrared spectrometer (Thermo Scientific Nicolet 6700 spectrometer). The samples for FT-IR measurement were prepared by grinding the dried GO powder. The heavy metal content in GO was measured using ICP-MS (820-MS, Varian, Mulgrave, Australia).

2.3. Cell preparation

2.3.1. MSC culture on graphene-coated coverslips

Human bone marrow-derived MSCs were purchased from a commercial source (Lonza, USA) and cultured in Dulbecco's modified Eagle's medium (DMEM, Gibco BRL, USA) containing 10% (v/v) fetal bovine serum (FBS; Gibco-BRL) and 1% (v/v) penicillin–streptomycin (PS; Gibco-BRL). MSCs at passage 4 were plated at 1 × 10^3 cells/cm^2 for the experiments. The medium was changed every 2 days.

2.3.2. MSC-RGO spheroid formation

MSC or MSC-RGO spheroids were fabricated through the hanging-drop method with slight modifications.[136] Three thousand MSCs (passage 5) in 30 μl of DMEM containing 20% (v/v) FBS, 1% (v/v) PS, and RGO (0, 2.5, 5, or 10 μg/ml) were incubated hanging on the lid of a Petri dish for two days to form a spheroid. To evaluate the morphology of the spheroids and the presence of RGO in the spheroids, the spheroids were fixed in 4% (v/v) paraformaldehyde for 30 min and embedded in OCT compound. The spheroids were cut into 10-μm sections and stained with H&E. Cell apoptosis was evaluated using a terminal deoxyribonucleotidyl transferase-mediated biotin-16-dUTP nick-end labelling (TUNEL) assay kit (Millipore Corp., Billerica, MA, USA) according to the manufacturer's instructions. For comparison, MSCs were cultured on a cell culture plate in a monolayer, and incubated with RGO flakes (0, 2.5, 5, or 10 μg/ml) for two days (Mono-0, Mono-2.5, Mono-5, and Mono-10, respectively).

2.3.3. GO adhesion to MSCs

Human bone marrow MSCs were purchased from Lonza (Walkersville, MD, USA). The MSCs were cultured DMEM (Gibco, NY, USA) growth medium supplemented with 10% (v/v) FBS, 100 units/ml penicillin, and 100 μg/ml streptomycin. MSCs at passage 6 were used for this study. To prepare the MSCs-GO, GO flakes were added to the culture medium and allowed to adhere to MSCs for 24 h. The cytotoxicity of GO was measured using Cell Counting Kit-8 (CCK-8, Dojindo Laboratories, Kumamoto, Japan). Three samples were analyzed per group.

2.4. *In vitro* assays

2.4.1. TEM analyses

The spheroids were fixed with Karnovsky's solution (EMS Hatfield, PA, USA) for 24 h at 4°C and washed three times with a 0.05 M sodium cacodylate buffer. The specimens were then fixed with 2% osmium tetroxide (Sigma) for 2 h at 4°C, washed three times with cold distilled water, dehydrated through a series of graded ethanol (50, 60, 70, 80, 90, 95, 98, and 100%) and propylene oxide rinses, and finally embedded in Spurr's resin (Agar Scientific, Essex, UK). The samples were then polymerized at 60°C for 24 h and cut into thin slices using an ultramicrotome (MTX, RMC, Arizona, USA). The thin sections were observed with a Libra 120 microscope (Carl Zeiss, Oberkochen, Germany).

2.4.2. Quantitative reverse transcriptase polymerase chain reaction (qRT-PCR)

The total RNA was extracted using 1 ml of TRIzol reagent (Invitrogen) and 200 μl of chloroform. The samples were centrifuged at 12,000 rpm at 4°C for 10 min. The RNA pellets were washed with 75% (v/v) ethanol and dried. After the drying procedure, the samples were dissolved in RNase-free water. The RNA (500 ng) from each sample was reverse-transcribed to obtain cDNA using GoScript Reverse Transcriptase (Promega, USA). SYBR green-based qRT-PCR was performed using a StepOnePlus Real-Time PCR System (Applied Biosystems, USA) instrument with the TOPreal qPCR Premix (Enzynomics, Korea). Forty amplification cycles were performed, and each cycle consisted of three steps: 30 s at 94 °C, 45 s at 55 °C, and 45 s at 72 °C. The primer sequences for the qRT-PCR analyses are listed in Table 2.1. All of the data were analyzed using the $2^{-\Delta\Delta Ct}$ method. Three samples were analyzed per group.

Table 2.1. Primer sequences for qRT-PCR

GAPDH	5’-CCA CTC CTC CAC CTT TGA C-3’	5’ACC CTG TTG CTG TAG CCA-3’
Bcl-2	5’-TTG GCC CCC GT GCT T-3’	5’-CGG TTA TCG TAC CCC GTT CTC-3’
Caspase-3	5’-CTG GTT TTC GGT GGG TGT-3’	5’CAG TGT TCT CCA TGG ATA CCT-3’
Col I	5’-CAG CCG CTT CAC CTA CAG C-3’	5’-TTT TGT ATT CAA TCA CTG TCT T-3’
Col III	5’-GGG AAT GGA GCA AAA CAG TCT T-3’	5’-CCA ACG TCC ACA CCA AAT TCT-3’
Col IV	5’-TGT CCA ATA TGA AAA CCG TAA AGT G-3’	5’-CAC TAT TGA AAG CTT ATC GCT GTC TT-3’
Fibronectin	5’-TCC ACG GGA GCC TCG AA-3’	5’-ACA ACC GGG CTT GCT TTG-3’
Laminin	5’CAC AAC AAC ATT GAC ACG ACA GA-3’	5’-GCT GGA GGG CAT CAC CAT AGT-3’
Cardiac actin	5’-GCA AGG ACC TGT ATG CCA ACA ATG-3’	5’-GCC TCA TCG TAC TCT TGC TTG CTA-3’
GATA4	5’-TTT TTA AGC GAG TTG GTT TTT TCC-3’	5’-CGA CGG CAA CAA CGA TAA TAT G-3’
β-MHC	5’-CCA CCC AAG TTC GAC AAA ATC-3’	5’-CGT AGC GAT CCT TGA GGT TGT A-3’
cTnT	5’-CAG GAT CAA CGA TAA CCA GAA AGT C-3’	5’-GTG AAG GAG GCC AGG CTC TA-3’
MLC2a	5’-CCC CAG CGG CAA AGG-3’	5’-CCA CCT CAG CTG GAG AGA ACT T-3’
MLC2v	5’-ACC GCC TCT GTC CCT ACC TT-3’	5’-GCC ACC CAG GCT GCA A-3’
VEGF	5’-GAG GGC AGA ATC ATC ACG-3’	5’-CAC CAG GGT CTC GAT TGG AT-3’
FGF-2	5’-GAC GGC CGA GTT GAC GG-3’	5’-CTC TCT CTT CTG CTT GAA GTT-3’
HGF	5’-GAT GGC CAG CCG AGG C-3’	5’-TCA GCG CAT GTT TTA ATT GCA-3’
Cx43	5’-TCT GAG TGC CTG AAC TTG C-3’	5’-ACT GAC AGC CAC ACC TTC C-3’

2.4.3. Analyses of cell viability

Fluorescein diacetate (FDA) and ethidium bromide (EB) solution was prepared by mixing 10 μl FDA solution (Sigma, 5 mg/ml in acetone) and 10 ml EB solution (Sigma, 10 μg/ml in PBS). Spheroids were incubated in FDA and EB solution for 3–5 min at 37 ^{o}C. After staining, the samples were examined using a fluorescence microscope (IX71 inverted microscope, Olympus, Tokyo, Japan). Live and dead cells were assessed by calcein-AM and ethidium homodimer, relatively, using two-color fluorescence live/dead assay kit (Molecular Probes, USA). The cell viability was quantitatively measured using CCK-8 (Sigma).

2.4.4. Enzyme-linked immunosorbent assay (ELISA)

The spheroids were incubated in DMEM without FBS for 24 h. The amount of growth factors in the supernatant was then determined quantitatively using an ELISA assay kit (n = 3 per group, R&D Systems, USA).

2.4.5. Western Blot

The analysis was performed through 10% (w/v) SDS-polyacrylamide gel electrophoresis (n = 3 per group). The proteins were first transferred to an Immobilon-P membrane (Millipore Corp., USA) and then probed with antibodies (all purchased at Abcam, UK). The proteins were then incubated with a horseradish peroxidase-conjugated secondary antibody (Santa Cruz Biotechnology, USA) for 1 h at room temperature. The blots were developed using an enhanced chemiluminescence detection system (Amersham Bioscience, USA).

2.4.6. Immunocytochemistry

For MSCs cultured on graphene, proliferating cells were analyzed by immunofluorescence staining using antibodies against proliferating cell nuclear antigen (PCNA, Abcam). Samples were mounted in 4,6-diamidino-2-phenylindole (DAPI, Vector Laboratories, USA) for nuclear staining.

The MSC-RGO sections were immunocytochemically stained with antibodies against Cx43 (Abcam). The immunostaining signal was visualized with rhodamine isothiocyanate-conjugated secondary antibodies (Jackson ImmunoResearch Laboratories, USA). The slides were counterstained with DAPI (Vector Laboratories, USA) to stain the nuclei of the cells.

2.4.7. Dye transfer

MSCs were stained with either 10 μM DiI or 10 μM Calcein AM. After washing, the DiI-labeled MSCs and Calcein AM-labeled MSCs with or without RGO (5 μg/ml) were mixed in equal proportions to form spheroids. The spheroids were imaged using a Leica TCS SP8 X Confocal Microscope (Leica Microsystems, Mannheim, Germany).

2.4.8. Analyses of GO adhesion on MSCs

GO flakes were labelled with DiI (1 μg/ml, Sigma) for 12 h at 37°C. After labeling, the MSCs were labeled with DAPI and PKH67 (Sigma) according to the manufacturer's instructions. The GO flakes and MSCs were washed 3 times with phosphate buffered saline (PBS). GO flakes (10 μg/ml) were added to the MSC culture, and the GO flakes were allowed to adhere to MSCs for 24 h. The cells were collected by trypsinization and analyzed with fluorescent microscopy (Model IX71, Olympus, Tokyo, Japan). After trypsinization, the cells were examined under a fluorescent microscope to ensure that none of the GO flakes had detached. The adhesion of GO to the MSCs was analyzed using TEM. First, the MSCs-GO were fixed with Karnovsky's solution (EMS Hatfield, PA, USA) for 24 hours at 4°C and washed 3 times with a 0.05 M sodium cacodylate buffer. The specimens were then fixed with 2% osmium tetroxide (sigma) for 2 hours at 4°C, washed three times with cold distilled water, dehydrated using a series of graded ethanol and propylene oxide rinses, and finally embedded in Spurr's resin. The samples were then polymerized at 60°C for 24 hours and sectioned using an ultramicrotome (MTX, RMC, Arizona, USA). The thin sections were observed with a Libra 120 microscope (Carl Zeiss, Oberkochen, Germany).

2.4.9. Assays for cell adhesion and viability with or without GO under reactive oxygen species (ROS) condition

The MSCs and MSCs-GO were seeded on cell culture plates in the presence of 0 or 200 μM H_2O_2, an exogenous ROS source. The number of live cells was determined by CCK-8 after 90 min and 24 h according to the manufacturer's protocol (n = 3 per group). The adhesion of the cells was visualized with rhodamine-conjugated phalloidin (Millipore).

To determine the effect of GO flakes on the prevention of cell anoikis, MSCs and MSCs-GO were plated on agar-coated plates, which prevents cell adhesion to the plate. The number of live cells was determined by CCK-8 after 24 h (n = 3 per group).

2.4.10. Detection of ROS

The amount of ROS is detected using hydrogen peroxide assay kit (Biovision, CA, USA) according to the manufacturer's instructions (n = 4). The intracellular ROS was detected by staining cells with 2′-7′-dichlorofluorescin diacetate (DCFDA, 10 μM, Sigma) for 30 min.

2.4.11. Adhesion of fibronectin (FN)- or vitronectin (VN)-adsorbed GO flakes to MSCs

To adsorb FN or VN on GO, GO flakes (10 μg/ml) were incubated with FN (50 μg/ml) or VN (50 μg/ml) in PBS for 3 h.[125] Unbound FN and VN were removed by washing with PBS for three times. FN- or VN-adsorbed GO flakes (10 μg/ml) were added to the MSC culture, and allowed to adhere to MSCs for 24 h.

2.4.12. Competition between free ECM proteins and ECM proteins adsorbed on GO for their interactions with MSCs

MSCs were incubated with ECM protein-adsorbed and DiI-labeled GO flakes in serum-free medium or serum-containing medium for 24 h. The serum-containing medium contains free ECM proteins. Unbound GO flakes were removed by washing several times with PBS. ECM protein-adsorbed GO flakes were also incubated in serum-free medium and serum-containing medium without MSCs for 24 h in order to confirm GO attachment to MSCs, rather than the dish. The adhesion of GO flakes to MSCs was analyzed with fluorescent microscopy.

2.5. Experimental procedures *in vivo*

2.5.1. MI induction and MSC-RGO spheroid implantation

The animal experimental protocol was approved by the Chonnam National University Animal Care and Use Committee (CNU IACUC-H-2014-22). MI was induced in 8-week-old male athymic BALB/c nude (nu/nu) mice (n = 8 per group, Central Lab Animal Inc., Seoul, Korea) by occlusion of the coronary artery. Briefly, the mice were anesthetized with an intramuscular injection of ketamine (50 mg/kg) and xylazine (10 mg/kg), and the left coronary artery was occluded within the myocardium between the left atrial appendage and the right ventricular outflow tract using a curved needle and a 5-0 silk suture. One week after MI, PBS, RGO flakes, Sph-0 (3×10^5 cells), or Sph-5 (3×10^5 cells) in a volume of 50 μL were injected into the border zone. Age-matched mice that were subjected to a sham operation were used as the non-MI group. The mice were sacrificed two days after MSC implantation.

2.5.2. Induction of MI and MSC-GO implantation

Myocardial infarction was induced in 8-week-old Sprague-Dawley rats (n = 16 per group, 240 ± 10 g, Samtako Bio, Osan, Korea) as previously described.[137] Briefly, the rats were placed under general anesthesia and the heart was exposed at the left costal rib using an incision. The left anterior descending artery was ligated with a 6-0 silk suture (Ethicon, Cincinnati, OH, USA) for 1 hour and then reperfused. The infarction was macroscopically visualized as blanching in the left ventricle. No ligation was performed for the normal group. The animals were sacrificed 14 days after the implantation unless stated otherwise. The animals were used in accordance with the International Guide for the Care and Use of Laboratory Animals. The experimental protocol was approved by the Animal Research Committee of Yonsei University College of Medicine (IACUC No. 2012-0202-2).

To track MSCs *in vivo*, the MSCs were labeled with DAPI by adding DAPI solution to the culture medium according to the manufacturer's instruction. One million MSCs were suspended in 60 μl PBS, and injected using a 30-guage needle after reperfusion at the anterior and lateral aspects of the infarction border zone. For the PBS injection, 60 μl of PBS was injected at the same sites. The site of injection was examined to analyze surviving cells, and the infarction site was examined to assess cardiac regeneration.

2.5.3. Analyses of surviving MSCs

The animals were sacrificed 3 or 14 days after cell implantation. The heart tissues were fixed with 10% (v/v) formaldehyde, embedded in paraffin, and sliced into 5 μm sections. The sections were deparaffinized and rehydrated. A TUNEL assay was performed to detect the apoptotic activity in the implanted MSCs using an ApopTag Red in Situ Apoptosis Detection Kit (Millipore) according to the manufacturer's instruction. Four separate slides were photographed using a fluorescent microscope and DAPI-labeled cells and TUNEL-positive cells were counted (n = 3 hearts per group).

The amount of human VEGF secreted by implanted human MSCs was determined by staining tissue sections with anti-VEGF antibody (ab52917, Abcam) that reacts specifically with human VEGF. VEGF fluorescently stained using a fluorescein isothiocyanate (FITC) secondary antibody (Jackson ImmunoResearch Laboratories, n = 3 hearts per group).

2.5.4. Histochemical and immunohistochemical staining

Two weeks after cell injection, the hearts were excised and transversely sectioned into two blocks across the infarct zone. The tissue blocks were frozen in liquid nitrogen with the Tissue-Tek OCT compound, and sectioned to 4-μm-thick sections.

For immunohistochemical analysis, the slides were treated with 3% hydrogen peroxide in PBS for 10 min at room temperature to block endogenous peroxidase activity. After nonspecific binding was blocked with 5% normal goat serum (Sigma), the slides were incubated with primary antibodies against Cx43 (Abcam, Cambridge, MA, USA) or von Willebrand Factor (vWF, Abcam) for 18 h at 4°C. The sections were washed three times with PBS, and then incubated for 1 h with Alexa-Fluor 488- or 594-conjugated-secondary antibodies. After washing, the slides were mounted with a mounting medium (VectaMount mounting medium, Vector Labs Inc., Burlingame, CA, USA). Images were obtained and digitized on a computer using an Olympus CX31 microscope (Olympus) equipped with an Infinity 1 camera (Lumenera Scientific, Ottawa, Canada). Five mice were analyzed for quantification.

Cardiac fibrosis was evaluated by Masson's Trichrome staining. The fibrotic areas were determined by visualizing the blue-stained fibrotic deposits using the NIS-Elements Advanced Research program (Nikon, Japan). The percentage of ventricular fibrosis was calculated as the blue-stained area divided by the total ventricular area. Three samples were analyzed per group. Hematoxylin and eosin staining was performed to evaluate inflammatory cell infiltration at the site of MSC and MSC-GO implantation.

. To measure the infarct size of the myocardium, the rat hearts were transaxially sectioned and incubated in triphenyl tetrazolium chloride (TTC, Sigma)

for 20 min at 37°C, followed by 10% (v/v) formalin fixation at 2-8°C overnight. The infarcted region appeared yellow-white, and the viable myocardium appeared red. The heart sections were photographed with a digital camera, and the area was measured using planimetry and the ImageJ software (National Institutes of Health, Bethesda, MD, USA). The area of the infarct is expressed as the percentage of yellow-white infarct tissue to the total left ventricle. Three heart samples per group were used for the analyses. A TUNEL assay was performed to detect the apoptotic activity in the implanted MSCs using an ApopTag Peroxidase *In Situ* Apoptosis Detection Kit (Millipore) according to the manufacturer's instructions.

2.5.5. Evaluation of cardiac function

Left ventricular function was assessed by transthoracic echocardiography (n = 5 per group). Two weeks after spheroid injection, the animals were anesthetized, and intubated. Echocardiography was performed to evaluate the left ventricular function. The echocardiography was performed with a 15-MHz linear array transducer system (MSC-RGO spheroid implantation study, iE33 system, Philips Medical Systems) and 10.0 MHz transducer (MSC-GO implantation study, GE Medical System, Fairfield, CT) by an expert who was not aware of the experimental conditions to exclude bias.

2.6. Statistical analysis

The quantitative data are expressed as the means ± standard deviations. The statistical analyses were performed through one-way analysis of variance (ANOVA) with Tukey's significant difference post hoc test using the SPSS software (SPSS Inc., USA). A value of $p<0.05$ was considered to denote statistical significance.

Chapter 3.

Graphene-regulated cardiomyogenic differentiation process of mesenchymal stem cells by enhancing the expression of extracellular matrix proteins and cell signialing molecules

3.1. Introduction

Stem cell-based regenerative medicine provides a promising strategy for the treatment of heart failure, which is one of the common causes of mortality in the world.[25] Specifically, MSCs have been shown to have great potential to repair heart diseases. However, the therapeutic efficacy of the treatment is quite limited as MSCs hardly differentiate into cardiomyocytes *in vivo*.[138] For example, it has been known that the transplantation of cardiomyogenically differentiated MSCs greatly improved myocardial contractility.[65] Therefore, many researchers have attempted to develop methods for the promotion of *in vitro* cardiomyogenic differentiation of MSCs. Specifically, 5-azacytidine has been utilized to commit MSCs toward the cardiomyogenic lineage.[62] However, 5-azacytidine-treated MSCs are not clinically suitable because it has been anticipated to interfere with normal cell activity by inhibiting deoxyribonucleic acid methylation,[109] suggesting that other methods for MSC commitment toward the cardiomyogenic lineage without using exogenous chemical inducers that may interfere with normal cell activity should be developed for clinical stem cell therapies for myocardial infarction.

It is reported that MSC differentiation could be modulated through cellular interactions with culture substrates *in vitro*.[139] However, only a few studies have studied the effect of cell culture substrates on cardiomyogenic differentiation of MSCs. Recently, graphene has drawn attention as a platform for cell culture due to its unique physical, chemical, and mechanical properties and its effects on stem cell lineage specifications.[140,141] Guided by these considerations, here we propose for the first time that graphene can promote the expression of cardiomyogenic genes of MSCs. We also investigated a potential mechanism of the effects of graphene on the enhanced cardiomyogenic differentiation process through analyzing the expressions

of ECM proteins and cell signaling molecules that are known to promote the cardiomyogenic differentiation of stem cells.

3.2. Results and discussion

3.2.1. Fabrication of graphene

Figure 3.1 shows the fabrication method for the preparation of the high-quality and large-scale graphene on coverslips. The graphene used in this study was synthesized through the CVD method on copper foils.[18] After synthesis, the copper foil was etched and the same batch of graphene was transferred to coverslips.

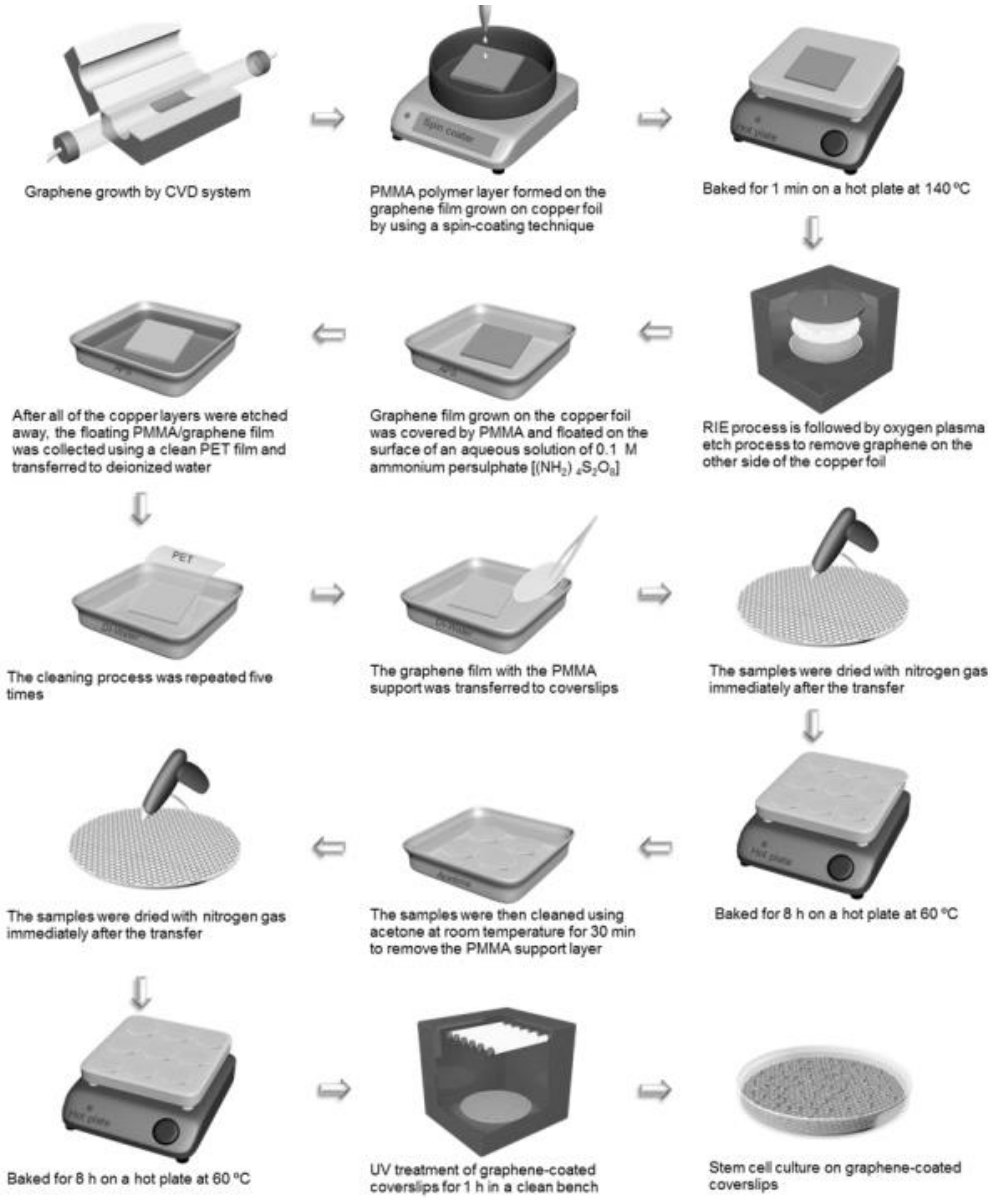

Figure 3.1. Fabrication method of graphene on coverslip

3.2.2 Characterization of graphene

AFM images of the coverslips and graphene-coated coverslips showed that the surface roughness (root-mean-square deviation, Rq) were 4.87 nm and 4.93 nm, respectively, indicating that the monolayer graphene film did not change the surface roughness of the substrate (Figure 3.2a). Optical images of the coverslip and the graphene-coated coverslip showed that both are transparent (Figure 3.2b). The contact angle measurements showed that the graphene-coated coverslip was slightly hydrophobic (73.9 ± 1.2°), whereas the contact angle of the coverslip was 64.7 ± 2.8° due to the hydrophobic property of graphene, a finding that is consistent with recent report (Figure 3.2c).[124] To confirm the presence of monolayer graphene, the transferred graphene film was characterized through Raman spectroscopy (Figure 3.2d). The Raman spectrum of graphene is characterized by three main characteristic peaks.[19] The peak located at ~2700 cm^{-1} (G′ band) exhibits a full width at half-maximum of 26~33 cm^{-1}. The I_{2D}/I_G ratio is more than three-fold as intense as the peak located at ~1600 cm^{-1} (the G band) and there is no measurable peak observed at ~1350 cm^{-1} (the D band), which indicates the synthesis of high-quality monolayer graphene. In addition, the graphene-coated coverslip exhibited high transparency with a transmittance that exceeded 97.4% at a wavelength of 550 nm (Figure 3.2e), which confirms the presence of uniform and monolayer graphene. Figure 3.2f shows a representative low-magnification TEM image of graphene sheet on a TEM grid. Figure 3.2g shows a TEM image of the circled region in Figure 3.2f. We have included a SAED pattern image (Figure 3.2h) to confirm the high crystallinity of the graphene used in our experiments. Six-fold symmetry, which is a typical SAED pattern for well-synthesized graphene, was observed for the graphene used in this study. The intensity profile of the equivalent Bragg reflections measured along the

line denoted showed that the intensities of the $\bar{1}0\bar{1}0$ (inner hexagon) and $\bar{1}\bar{1}20$ (outer hexagon) spots were equivalent, which indicates that the set of diffraction spots originated from a single-layer graphene sheet (Figure 3.2i). We continually investigated the sheet resistance of the graphene on the coverslip through a van der Pauw method with four probes method. The transferred graphene on the coverslip showed a sheet resistance of 500 ± 50 Ω/□ with a high uniformity.

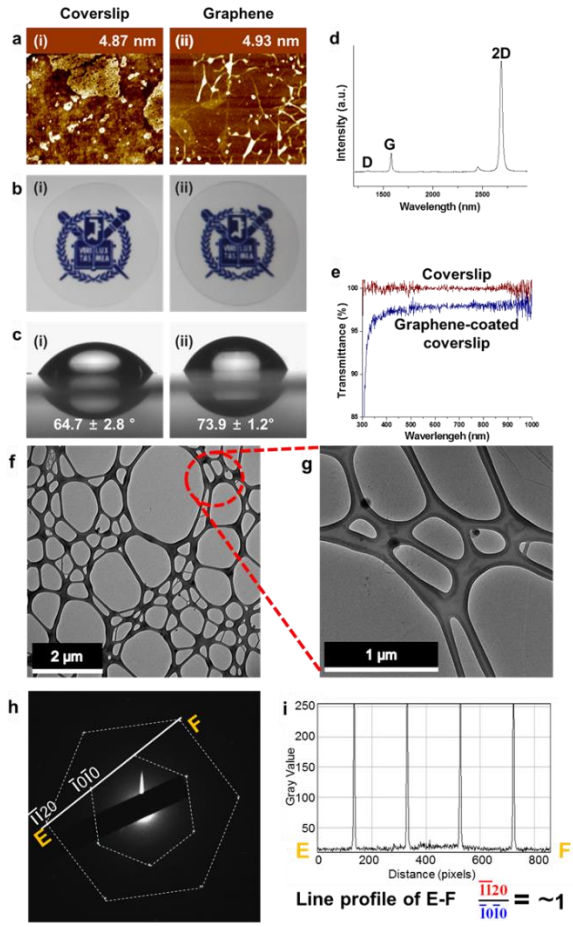

Figure 3.2. Characterization of graphene substrates. (a) AFM topography images. The values indicate the roughness of the surfaces. (b) Photographs and (c) contact angle of (i) a coverslip and (ii) graphene on a coverslip. (d) Raman spectroscopy of graphene. (e) Transparency of the graphene films transferred to a coverslip. TEM images of a graphene sheet on a TEM grid at (f) low and (g) high magnifications. (h) SAED pattern. (i) Intensity profile of the diffraction spots along a line connecting points E and F in the single-layer graphene diffraction pattern in (h). The uniform intensity profile between the inner and outer spots demonstrates that the graphene sheet consists of a single layer.

3.2.3. Biocompatibility of graphene

We first evaluated the biocompatibility of graphene by comparing the viability, apoptosis, and proliferation of MSCs cultured on graphene and coverslips. The live/dead cell staining with calcein-AM and ethidium homodimer revealed that most of the cells were alive regardless of the substrate type (Figure 3.3a). No significant difference in the relative numbers of live cells at various time points was observed in the analysis of the cells with the CCK-8 (Figure 3.3b). It was very interesting to note that Bcl-2, which is an anti-apoptotic gene, was upregulated in MSCs cultured on graphene compared to MSCs cultured on coverslips, whereas the expression of caspase-3, which is a cysteine protease that is activated during programmed cell death, was decreased on graphene compared to coverslips (Figure 3.3c). PCNA staining, which stains proliferating cells, demonstrated that the degree of cell proliferation was similar regardless of the substrate type (Figure 3.3d). Cell counting also showed that there was no significant difference in the number of cells cultured on graphene and coverslip at all time points (Figure 3.3e). Together, our results on the cell viability, apoptosis, and proliferation assay demonstrate that graphene is biocompatible and can provide a suitable environment for proliferation for MSCs *in vitro*.

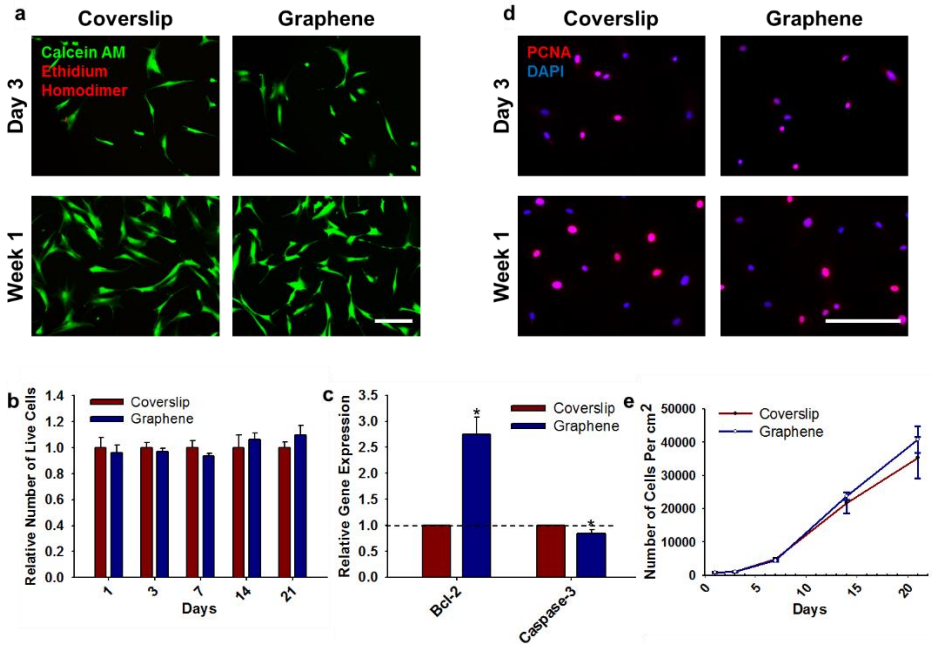

Figure 3.3. *In vitro* biocompatibility of graphene. (a) Live/dead assay of MSCs cultured on graphene and coverslips for 3 days and 1 week. The live cells were stained with calcein-AM (green), and the dead cells were stained with ethidium homodimer (red). The scale bar represents 200 μm. (b) The number of live cells is expressed relative to the number of live cells on a coverslip on day 1. The number of live cells was counted using CCK-8. (c) Upregulation of Bcl-2, an anti-apoptotic marker, and downregulation of caspase-3, a pro-apoptotic marker, in MSCs cultured on graphene for 3 weeks relative to MSCs cultured on coverslips, as evaluated by qRT-PCR. *$p < 0.05$ compared to MSCs cultured on coverslips. (d) Proliferation of MSCs cultured on coverslips and graphene. The proliferation was evaluated by PCNA staining. The proliferating cells were stained with PCNA (red), and the nuclei were stained with DAPI (blue). The scale bar represents 200 μm. (e) Growth of MSCs cultured on graphene and coverslips. The growth was evaluated by counting the number of cells at various time points using hemocytometer.

3.2.4 Cardiomyogenic lineage commitment of MSCs cultured on graphene

In a second set of cell culture experiments, we examined various cardiomyogenic markers at the transcript level to determine the cardiomyogenic commitment of MSCs cultured on graphene in a medium that does not contain any inducers for cardiomyogenic differentiation 2 and 3 weeks after cell seeding. Strikingly, the expression of many cardiomyogenesis-related markers was enhanced in MSCs cultured on graphene compared to MSCs cultured on coverslips even in the absence of cardiomyogenic inducers in the medium (Figure 3.4). The expression of an early cardiomyogenic transcriptional factor (GATA4) was upregulated in MSCs cultured on graphene compared with MSCs cultured on coverslips. The enhancement in the early marker (GATA4) expression decreased with the culture time (i.e., 3.3-fold increase at week 2 and 2.7-fold increase at week 3). Two weeks after cell seeding, the gene expression of all of the cardiomyogenic contractile proteins, including cardiac actin, beta-type myosin heavy chain (β-MHC), cardiac troponin T (cTnT), ventricular myosin light chain-2 (MLC2v), and atrial myosin light chain 2 (MLC2a), was enhanced on graphene compared to coverslips. Unlike the expression of an early cardiomyogenic differentiation marker (GATA4), these were further upregulated at week 3 in MSCs cultured on graphene compared to MSCs cultured on normal coverslips. The gene expression of the gap junction protein, Cx43, was also enhanced in MSCs cultured on graphene. Previous studies have reported that electrically conductive materials promoted cardiomyogenic differentiation of MSCs[142] and the expression of Cx43 in cardiomyocytes.[113] However, the electric conductivity of graphene did not contribute to the enhanced expression levels of cardiomyogenic genes in MSCs in our study, because MSC cultures on double-layer graphene (300

± 30 Ω/□) and triple-layer graphene (150 ± 30 Ω/□) did not exhibit an additional increase in the expression levels of cardiomyogenic genes (data not shown). In addition, the MSCs did not exhibit the functional and electrophysiological properties of mature cardiomyocytes regardless of the substrate type, which suggests that additional signals may be required to differentiate MSCs into mature cardiomyocytes. Therefore, further studies should be carried out to find additional signals that do not hamper normal cell activity and exhibit synergistic effect with graphene on cardiomyogenic differentiation of MSCs.

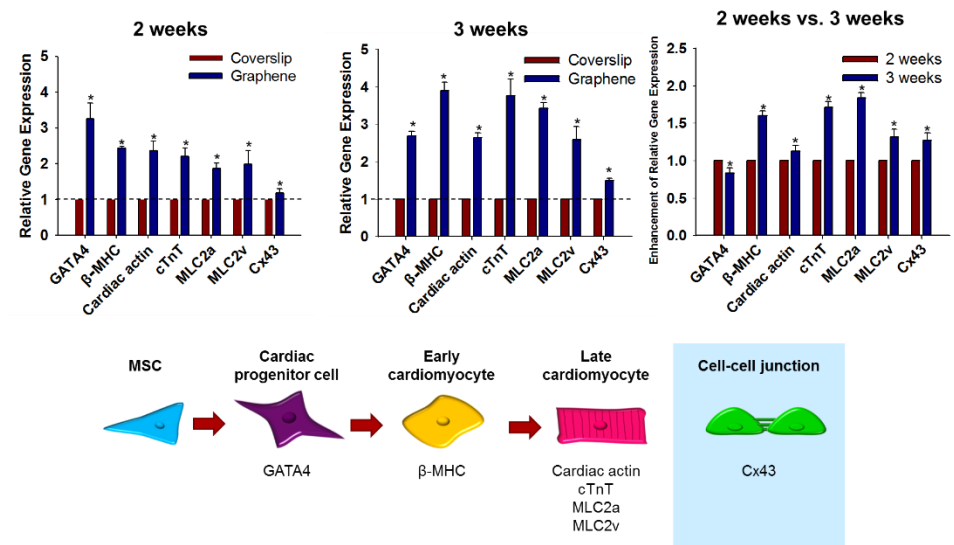

Figure 3.4. Enhanced expression of cardiomyogenic genes in MSCs cultured on graphene without using chemical inducers. Two and three weeks after cell seeding, the MSCs cultured on graphene exhibited an upregulation of the mRNA expression of an early cardiomyogenic transcriptional factor (GATA4), cardiomyogenic contractile proteins (cardiac actin, β-MHC, cTnT, MLC2a, and MLC2), and gap junction protein (Cx43) compared with MSCs cultured on coverslips. The mRNA expression levels were evaluated by qRT-PCR. *$p < 0.05$ compared to MSCs cultured on coverslips.

3.2.5. Enhanced ECM gene expression by graphene

It is widely reported that the stem cell-ECM interactions may play key roles in the cardiomyogenic differentiation of stem cells. Many studies have demonstrated that the lineage specification of stem cells could be controlled, at least in part, by the interaction of the stem cell with the ECMs.[143-145] Therefore, we investigated whether an MSC culture on graphene compared to a culture on coverslips affected the gene expression levels of cardiomyogenic differentiation-related ECM proteins in the MSCs. Among the various ECM proteins, we chose type I collagen (Col I), type III collagen (Col III), type IV collagen (Col IV), fibronectin, and laminin for analysis. It is noted that collagen, fibronectin, and laminin are known as the major components of the cardiac ECM.[146] Embryonic stem cell-derived beating cardiomyocytes are reported to be surrounded by a network of fibronectin, laminin, Col I and Col IV.[147] Col I and Col III, both of which are produced by cardiac stem cells and cardiac fibroblasts,[148] represent approximately 80% and 11% of the total collagen in the myocardium, respectively.[149] Collagen is essential for the cardiomyogenic differentiation of mouse embryonic stem cells because the use of collagen synthesis inhibitors inhibits cardiac differentiation.[150] A recent study also demonstrated that culture of embryonic stem cell-derived embryonic bodies on Col IV-coated surfaces enhanced the cardiomyogenic differentiation synergistically with hypoxia, whereas a culture on fibronectin-coated surfaces enhanced the cardiomyogenic differentiation under normoxia.[151] In addition, laminin is essential for the development of cardiomyocytes capable of propagating electrical signals between neighboring cardiomyocytes.[152] Compared with MSC culture on coverslips, the MSC culture on graphene upregulated the gene expressions of cardiomyogenic differentiation-related ECM proteins (Col I, Col III, Col IV, fibronectin, and laminin) as evaluated through

qRT-PCR (Figure 3.5). The upregulation of the ECM gene expression may, at least in part, be responsible for the enhanced cardiomyogenic differentiation of the MSCs cultured on graphene (Figure 3.4a).

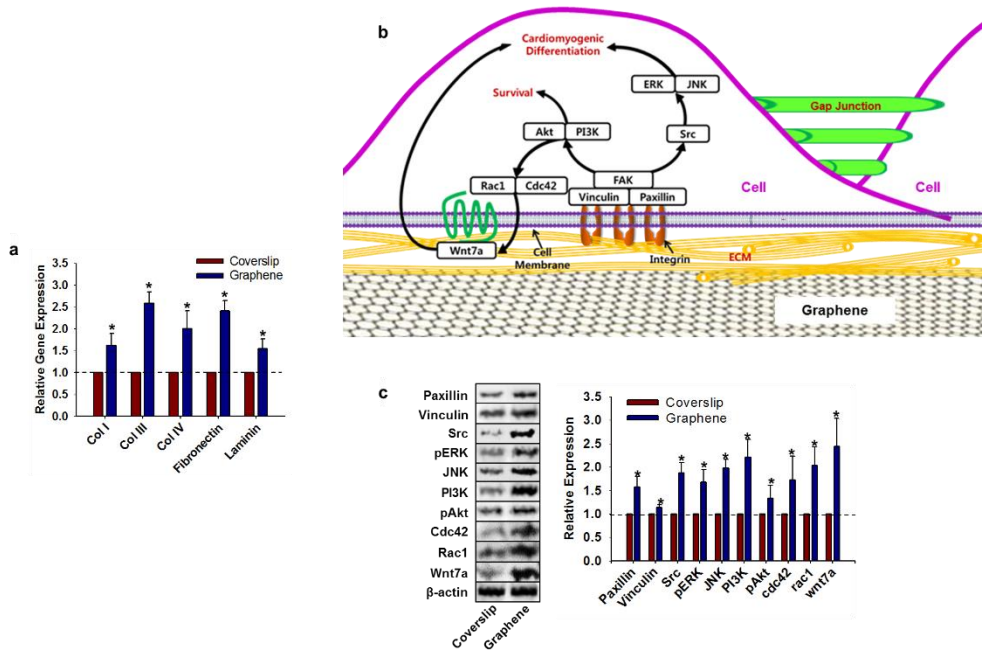

Figure 3.5. Enhanced gene expression of ECM proteins and activation of molecules involved in cardiomyogenic differentiation-related signal transduction pathways in MSCs cultured on graphene. (a) The MSCs cultured on graphene for 3 weeks exhibited an upregulation of the mRNA expression of ECM proteins known to promote the cardiomyogenic differentiation of stem cells compared with those on coverslips. *$p < 0.05$ compared to MSCs cultured on coverslips. (b) A schematic diagram of the signal transduction pathways associated with cardiomyogenic differentiation and cell survival and western blot analyses of MSCs cultured on graphene or coverslips for 3 weeks to analyze the molecules involved in the signal transduction pathways. Quantification of the relative protein expressions of the cell signaling molecules ($n = 3$). *$p < 0.05$ compared to MSCs cultured on coverslips.

3.2.6. Regulation of cell signaling pathway by graphene

The cardiomyogenic differentiation of stem cells can be regulated through the modulation of signal transduction pathways. Therefore, we investigated whether the cardiomyogenic differentiation-related signal transduction is promoted in MSCs cultured on graphene compared with MSCs cultured on coverslips (Figure 3.5b). Among various cell signaling molecules, we first examined the expression of focal adhesion components, such as vinculin and paxillin, which are recruited for the clustering of activated integrins and the remodeling of actin cytoskeletons. Graphene enhanced the expression of both paxillin and vinculin, which are focal adhesion-associated proteins. Vinculin modulates the interactions between paxillin and focal adhesion kinase (FAK), promoting FAK activation.[153] The activation of FAK mediates a variety of adhesion-dependent biological processes including cell survival, proliferation, migration, and differentiation.[154] The autophosphorylation of tyrosine 397 of FAK allows FAK to bind Src [155] and phosphatidylinositol 3-kinase (PI3K),[156] and these bindings mediate multiple signaling events that regulate stem cell survival and differentiation (Figure 3.5b).[157,158]

Extracellular signal-regulated kinases (ERK) and JNK are activated during cardiomyogenic differentiation.[159] Graphene upregulated both ERK and JNK in MSCs (Figure 3.5b). Previous studies have reported that the upregulation of PI3K/Akt enhances cardiomyogenesis,[160,161] whereas the inhibition of PI3K suppresses cardiomyogenic differentiation.[162] In the present study, both PI3K and Akt were upregulated in MSCs cultured on graphene compared to MSCs cultured on coverslips (Figure 3.5b). Moreover, the upregulation of PI3K/Akt also promotes cell survival, at least in part, through the regulation of downstream effectors, such as the members of the Bcl-2 family.[158] The enhanced Bcl-2 gene expression in MSCs

cultured on graphene (Figure 3.3c) may be, at least in part, due to the upregulation of PI3K/Akt (Figure 3.5b).

Wnt7a is known to be required for the myogenic differentiation of stem cells,[163] the development of cardiac conduction system,[164] and the modulation of the cardiomyogenic versus chondrogenic cell fate decision.[165] In our study, Wnt7a was upregulated in MSCs cultured on graphene (Figure 3.5b). Wnt 7a has been shown to be upregulated when the expression levels of Rac1 and Cdc42 are enhanced.[165] Rac1 and Cdc42 are upregulated by the activation of PI3K/Akt.[166] Our data show that both Rac1 and Cdc42 were upregulated in MSCs cultured on graphene (Figure 3.5b). Therefore, our data suggest that graphene may promote the cardiomyogenic differentiation and diverse behaviors of MSCs through specific cell-ECM interactions and regulation of cell signaling pathway even in the absence of exogenous inducers (Figure 3.5b).

Chapter 4.

Graphene potentiates the myocardial repair efficacy of mesenchymal stem cells by stimulating the expression of angiogenic growth factors and gap junction protein

4.1. Introduction

MSC implantation is a promising strategy for cardiac repair after MI.[167] Previous studies have demonstrated that MSCs implanted into the ischemic myocardium contribute to the induction of angiogenesis, attenuation of cardiac remodeling, and improvement in cardiac functions mainly through the secretion of reparative paracrine factors.[27,75,168-170] Meanwhile, MI may enhance vulnerability to arrhythmia due to gap junction remodeling as a result of cardiac fibrosis and the loss of gap junction-expressing cardiac cells.[171] The implantation of cells expressing gap junction proteins, such as Cx43, can attenuate post-infarct arrhythmia.[172] Although MSCs are capable of expressing Cx43, the amount of Cx43 expressed by naïve MSCs is minimal,[173] raising concerns regarding their proarrhythmogenic potential.[174] In addition, the upregulated expression of Cx43 in MSCs enhances their cytoprotective effect on cardiomyocytes and improves cardiac function.[175] Therefore, the upregulation of reparative paracrine factors and Cx43 expression in MSCs would enhance the therapeutic efficacy and reduce the risk of arrhythmia in MSC implantation therapy for MI.

The implantation of MSCs into the infarcted myocardium in a spheroid form may be advantageous because MSCs in spheroids show enhanced expression of angiogenic growth factors, such as VEGF and FGF-2,[176] and Cx43[177]. The enhanced cell-cell interactions in MSC spheroids promote the expression of reparative paracrine factors.[178] Additionally, this, at least in part, contributes to the upregulation of Cx43 expression.[179,180] However, cells in spheroid form show poor cell-ECM interactions,[110] which may limit further stimulation of growth factor expression and thereby Cx43 expression.[111]

In this study, we hypothesized that the incorporation of RGO flakes into MSC spheroids would improve the expression of reparative paracrine factors and Cx43 in the MSCs. RGO is a two-dimensional nanomaterial composed of carbon atoms, showing unique optical, chemical, mechanical, and electrical properties.[181,182] Cellular interactions with electrically conductive materials enhance Cx43 expression.[50] In addition, RGO is capable of adsorbing ECM proteins, such as FN, from the serum contained in the cell culture medium.[124] This feature of RGO can provide cell-ECM interactions,[124] which can enhance the expression of paracrine factors[183] and Cx43.[184] Therefore, we investigated whether the incorporation of RGO flakes into MSC spheroids can enhance the expression of reparative paracrine factors and Cx43 in the MSCs and the therapeutic efficacy of the MSCs for the treatment of MI (Figure 4.1).

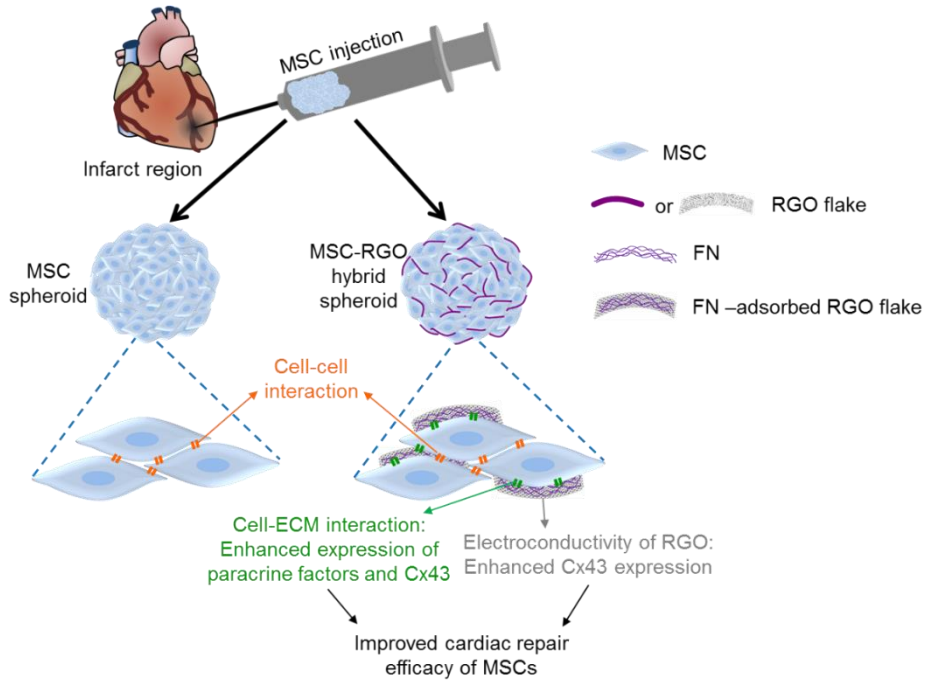

Figure 4.1. Schematic illustration of the effects of RGO flake incorporation in MSC spheroids on cardiac repair in MSC therapy for the treatment of MI.

4.2. Results and discussion

4.2.1. Characterization of RGO flakes

The Raman spectrum of RGO flakes showed two characteristic peaks of graphene at 1580 cm^{-1} and 1350 cm^{-1}, which are known as G and D band, respectively (Figure 4.2a).[185] The AFM image of RGO flakes showed that the thickness of the RGO flakes used in this study was approximately 1-2 nm (Figure 4.2b). The AFM and TEM images showed that the sizes of the RGO flakes were approximately 2-5 μm (Figure 4.2b and c). RGO flakes with such sizes were used to enhance the cell-ECM interactions and cell-cell interactions. RGO flakes larger than 2 μm were used because RGO flakes under 1 μm can be easily internalized by the cells.[186] The adhesion of RGO flakes to MSCs, rather than internalization of RGO flakes into MSCs, is needed to promote cell-ECM interactions. RGO flakes smaller than 5 μm were used to prevent RGO flakes from physically hindering cell-cell interactions between MSCs with the size ranging from 15 to 19 μm.[187] The six-fold symmetry of the SAED pattern image (inset) obtained through TEM showed the high crystallinity of the RGO used in our experiments (Figure 4.2c). The intensity profile of the diffraction peaks measured along the denoted line showed that the intensities of the $\bar{1}0\bar{1}0$ (inner hexagon) and $\bar{1}\bar{1}20$ (outer hexagon) spots were similar, which demonstrates that the RGO flakes used in this study were close to single layer (Figure 4.2c).[188]

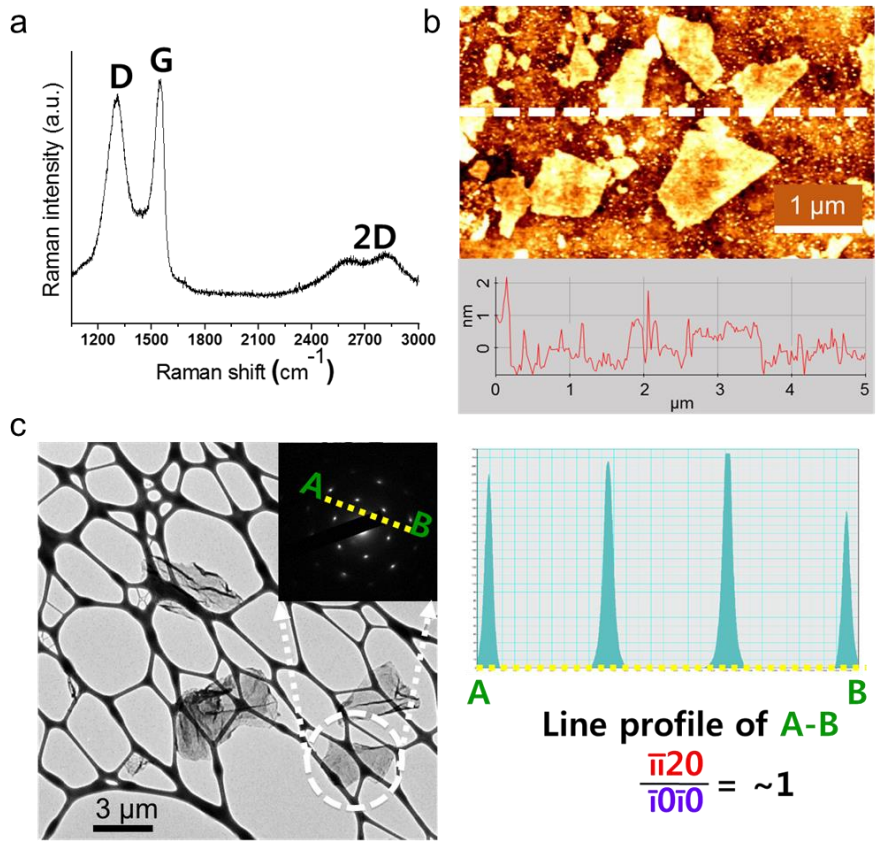

Figure 4.2. Characterization of RGO flakes. a) Raman spectroscopy, b) AFM image, and c) TEM image and corresponding SAED pattern of RGO flakes.

4.2.2. Formation of MSC-RGO hybrid spheroids

Previous studies have demonstrated that the use of various materials can influence the functions of cells in spheroids. For example, embryonic bodies cultured on hydrogel materials with controlled elasticity showed enhanced formation of cardiovascular organoids.[189] Recently, Yoon *et al.* have reported that the incorporation of transforming growth factor-β3-adsorbed graphene oxide sheets to spheroids improved the chondrogenic differentiation of the adipose-derived stem cells.[110] In this study, we utilized the potential of RGO flakes to enhance cell-ECM interactions and the electrical conductivity of RGO flakes to enhance the function of MSCs.

To determine the optimal concentration of RGO flakes for the formation of MSC-RGO hybrid spheroids, the cytotoxicity of the RGO flakes at various concentrations was examined. The TUNEL staining of apoptotic cells demonstrated that the incorporation of RGO flakes into MSC spheroids by adding RGO flakes at concentrations of 0, 2.5, 5, and 10 μg/ml to MSC suspensions in hanging drop form (Sph-0, Sph-2.5, Sph-5, and Sph-10, respectively) did not significantly alter the apoptotic activity of MSCs (Figure 4.3a). Similarly, the expression of a pro-apoptotic gene, caspase-3, was not significantly changed by differences in the RGO concentration (Figure 4.3b). However, the expression of the anti-apoptotic gene Bcl-2 was decreased significantly in MSCs incorporated with 10 μg/ml RGO flakes (Figure 4.3b). A previous study has reported that increasing RGO concentration in cell culture can exert oxidative stress on the cells, and thus induce cell apoptosis.[190] We postulated that this could be the reason for the decreased Bcl-2 expression in MSCs incorporated with 10 μg/ml RGO flakes. Therefore, RGO concentrations lower than 10 μg/ml would be preferred for the formation of MSC-RGO hybrid

spheroids. The cytotoxicity of incorporation of 5 μg/ml RGO flakes was further analyzed by staining viable and nonviable cells using FDA and EB, respectively. The FDA and EB staining demonstrated that the incorporation of 5 μg/ml RGO did not alter the viability of MSCs in spheroids (Figure 4.4a). In addition, CCK-8 analyses of Sph-0 and Sph-5 showed that there was no significant difference in the cell viability in spheroids with and without 5 μg/ml RGO incorporation (Figure 4.4b).

To examine the formation of MSC-RGO hybrid spheroids, hematoxylin and eosin (H&E) staining and TEM analysis were performed for Sph-0, Sph-2.5, Sph-5, and Sph-10. H&E staining of the spheroid sections showed that the distribution of RGO flakes within spheroids was quite homogenous (Figure 4.5a). The amount of RGO flakes incorporated in MSC spheroids increased with an increase in the RGO concentration in the MSC-RGO suspension in hanging drop form during the process of MSC-RGO hybrid spheroid formation (Figure 4.5a).

To examine the interaction of RGO flakes with MSCs in spheroids, TEM images were obtained (Figure 4.5b). In the absence of RGO flakes, the MSC spheroids (Sph-0) showed only cell-cell contacts. In contrast, cell-RGO contacts were dominant in Sph-10, and negligible cell-cell contacts were observed. In Sph-2.5 and Sph-5, cell-RGO and cell-cell contacts were observed. The comparison of these two types of hybrid spheroids revealed that Sph-5 showed a balanced combination of cell-cell and cell-RGO contacts, whereas Sph-2.5 showed mainly cell-cell contacts with very limited cell-RGO contacts. Therefore, considering the optimized combination of cell-cell and cell-RGO contacts along with the cytotoxicity data, an RGO concentration of 5 μg/ml was chosen for the formation of MSC-RGO hybrid spheroids in the following experiments.

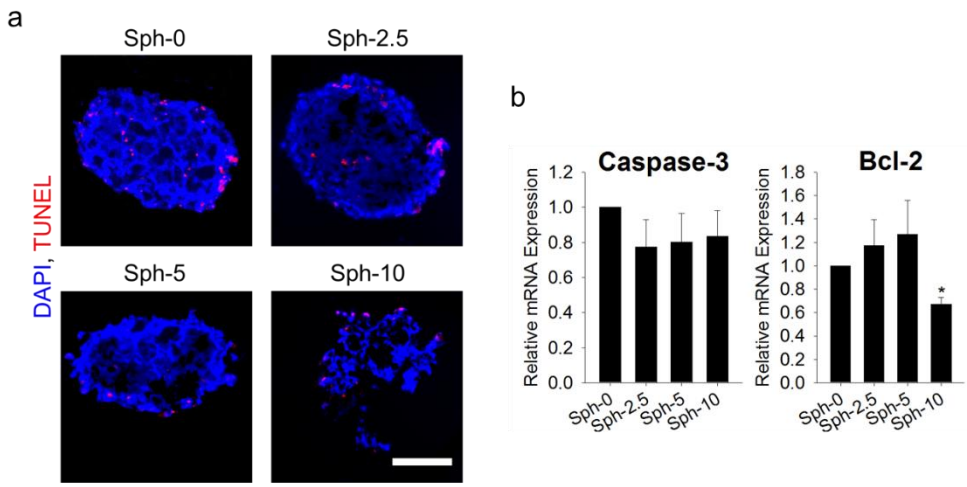

Figure 4.3. Cytotoxicity of RGO flakes. a) TUNEL staining of apoptotic cells in MSC spheroids that contain various amounts of RGO flakes. Scale bar, 100 μm. b) Relative mRNA expression of a pro-apoptotic gene, caspase-3, and an anti-apoptotic gene, Bcl-2. *$p < 0.05$ versus any other group.

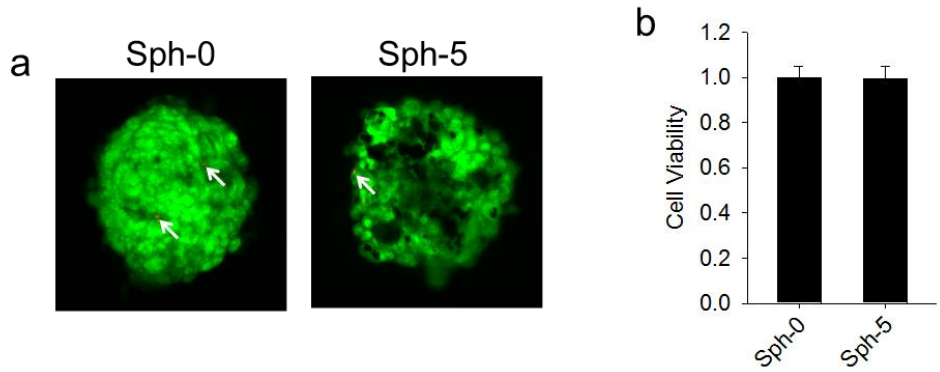

Figure 4.4. a) Fluorescence micrographic images of Sph-0 and Sph-5 stained with FDA and EB. Green and red (arrows) colors indicate viable and dead cells, respectively. b) Quantification of the cell viability in Sph-0 and Sph-5.

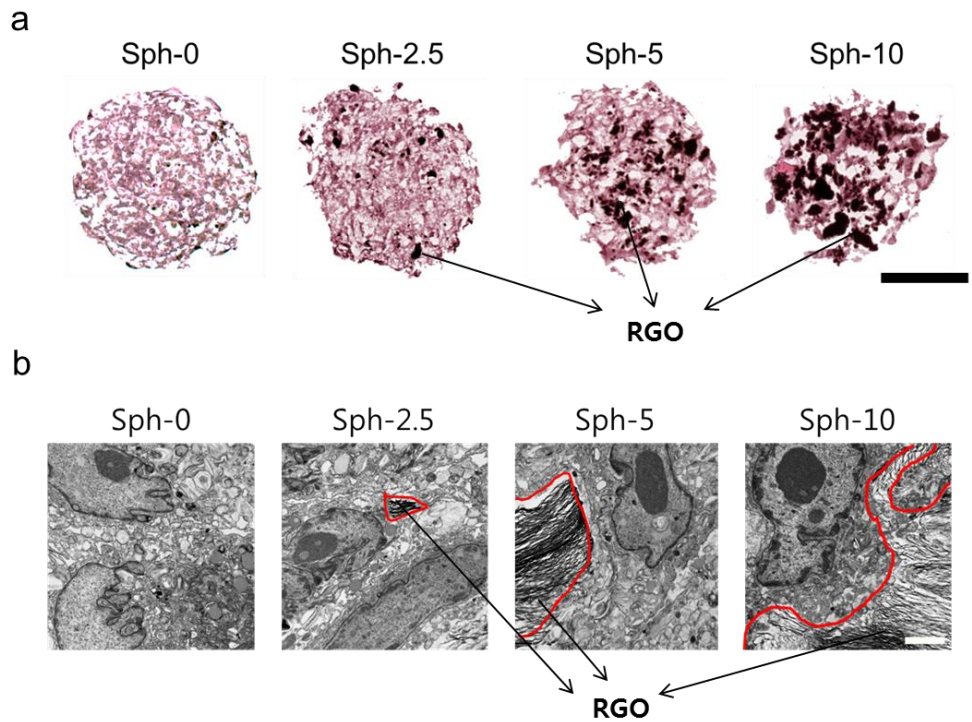

Figure 4.5. Formation of MSC-RGO hybrid spheroids that contain various amounts of RGO flakes. a) H&E staining of MSC-RGO hybrid spheroids. RGO flakes are indicated by black color. Scale bar, 100 μm. b) TEM images of MSC-RGO hybrid spheroids. Cell-RGO interactions were minimal in Sph-0 and Sph-2.5, and dominant in Sph-10. Sph-5 showed a good combination of cell-RGO and cell-cell interactions. Scale bar, 2 μm.

4.2.3. Enhanced cell-ECM interactions by RGO incorporation into MSC spheroids

A previous study has demonstrated that cell adhesion to graphene substrates is mediated by cell-ECM interactions due to the adsorption of ECM proteins, such as FN, to graphene.[125] Therefore, we evaluated the capability of RGO flakes to adsorb FN from a serum-containing culture medium. While no FN was detected in RGO flakes immersed in phosphate buffered saline (PBS), a significant amount of FN was detected in RGO flakes incubated in serum-containing culture medium (Figure 4.6a). The expression of FN was detectable only at the periphery of MSC spheroids without RGO (Figure 4.6b), which is in agreement with the results of a previous study.[191] In contrast, FN was distributed evenly throughout the MSC-RGO hybrid spheroids in Sph-5 (Figure 4.6b), because the RGO flakes in the hybrid spheroids adsorbed FN. FN in the MSC-RGO hybrid spheroids (Sph-5) can provide cell-ECM interactions via FN-integrin binding,[192,193] To confirm the enhanced cell-ECM interactions obtained through the incorporation of FN-adsorbed RGO flakes into MSC spheroids, we examined the expression of integrin β1, an integrin type that is known to bind to FN for cell-FN interactions.[194] As expected, integrin β1 was significantly enhanced in Sph-5 compared with Sph-0 (Figure 4.6c).

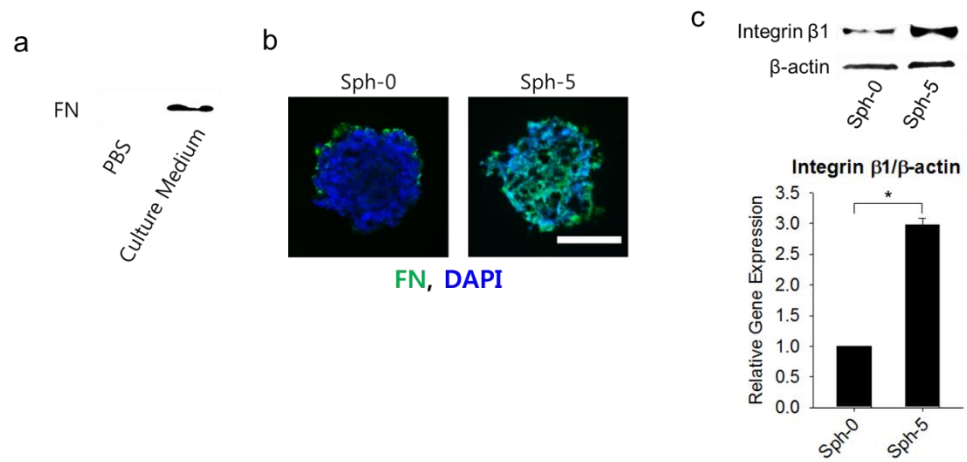

Figure 4.6. Incorporation of RGO flakes into MSC spheroids provides cell-ECM interactions. a) Incubation of RGO flakes in a serum-containing culture medium resulted in FN adsorption on the RGO flakes, whereas incubation in PBS resulted in no adsorption, as determined by western blot analysis. b) A homogenous distribution of FN was observed in the MSC-RGO hybrid spheroids, which can provide cell-ECM interactions, whereas FN was detected only at the periphery of MSC spheroids, as determined by immunohistochemistry for FN. Scale bar, 100 μm. c) Enhanced expression of integrin β1, a FN-interacting integrin, was observed in MSC-RGO hybrid spheroids, indicating enhanced cell-FN interaction, as determined by western blot analysis. *$p < 0.05$.

4.2.4. Enhanced angiogenic growth factor expression in MSC-RGO spheroids

Enhanced cell-ECM interactions trigger cell signaling cascades that upregulate the expression of growth factors.[183] Integrin-mediated cell-ECM interactions facilitate FAK activation.[195] The phosphorylation of FAK (pFAK) activates ERK thereby enhances VEGF expression.[112] In this study, the incorporation of RGO flakes into MSC spheroids enhanced the cell-ECM interaction mediated by FN-integrin binding (Figure 4.6c), which led to enhanced expressions of pFAK, phosphorylated ERK (pERK), and thus, VEGF (Figure 4.7a).

We examined the expression of angiogenic growth factors through qRT-PCR and ELISA. VEGF, FGF-2, and hepatocyte growth factor (HGF) were analyzed because these are the major growth factors that induce angiogenesis,[196] which plays a critical role in cardiac repair.[197] The expression of VEGF, FGF-2, and HGF showed similar tendencies (Figure 4.7b). The formation of spheroids enhanced the expression of proangiogenic growth factors compared with that obtained with a monolayer culture (Sph-0 versus Mono-0, Figure 4.7b), which is in accordance with previously reported results.[73] This finding is attributed to the activation of E-cadherin in the MSC spheroids by enhanced cell-cell interactions.[178] More importantly, we demonstrate for the first time that the addition of RGO flakes to cell culture further enhances the expression of the growth factors, in both monolayer and spheroid cultures (Figure 4.7b). As a result, spheroid formation and RGO incorporation additively enhanced the expression of growth factors (Figure 4.7b). The expression of growth factors was highest in the hybrid spheroids with 5 μg/ml RGO flakes (Figure 4.7b). This result is likely because cell-cell and cell-ECM interactions, which upregulate the expression of growth factors, in MSC spheroids are optimal and that

RGO is not cytotoxic at an RGO concentration of 5 μg/ml (Figure 4.3 and 4.5). Similar to the gene expression data, MSC-RGO hybrid spheroids with 5 μg/ml RGO flakes (Sph-5) showed significantly enhanced secretion of paracrine factors compared with spheroids without RGO (Figure 4.7c). To the best of our knowledge, this study provides the first demonstration that RGO enhances the secretion of growth factors.

Hypoxia is known to stimulate the growth factor expression of the cells in spheroids.[73] Hypoxia, which is caused by the limited diffusion of oxygen,[198] is dependent on the size of the spheroids. In this study, the quantification of the spheroid sizes showed that the sizes were not influenced by the incorporation of RGO flakes (Figure 4.8). Therefore, the effect of hypoxia on MSC functions induced by RGO incorporation was not investigated in this study.

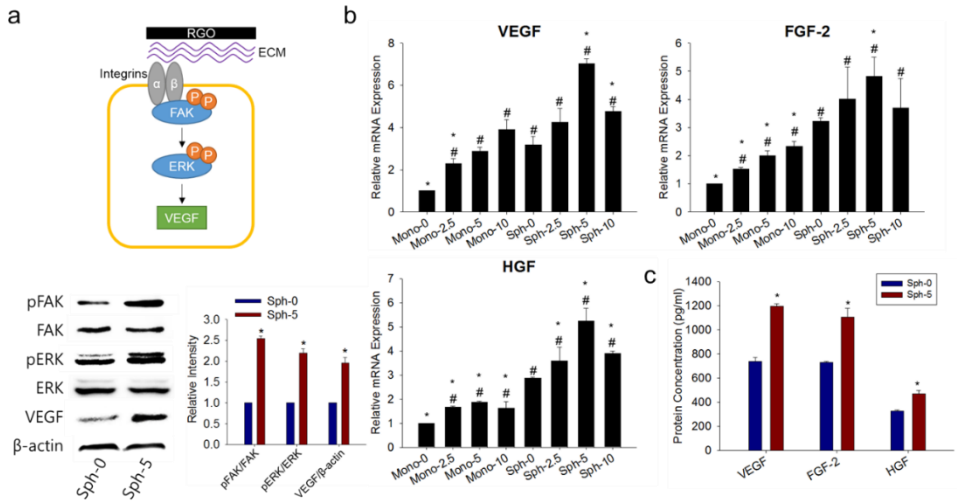

Figure 4.7. Enhanced angiogenic factor expression in MSC-RGO hybrid spheroids. a) Changes in the expression of cell signaling molecules due to RGO incorporation. b) mRNA expression of angiogenic growth factors evaluated by qRT-PCR. c) Amounts of secreted growth factors determined by ELISA. #$p < 0.05$ versus Mono-0 (monolayer culture that contains 0 μg/ml RGO flakes.) *$p < 0.05$ versus Sph-0.

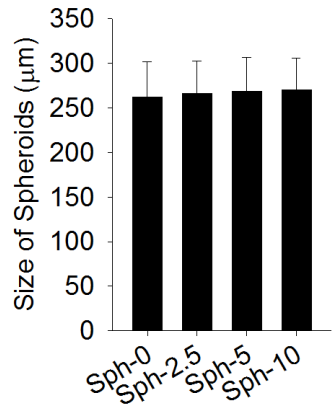

Figure 4.8. Quantification of sizes of spheroids that contain various concentrations of RGO flakes.

4.2.5. Enhanced Cx43 expression in MSC-RGO spheroids

MI not only causes fibrosis of the heart, but also may trigger ventricular arrhythmia due to electrical remodeling of the heart.[199] Excessive deposition of fibrotic tissue and loss of functional cardiac cells impair linear electrical propagation and lead to arrhythmia,[200] at least in part, due to a reduced level of Cx43.[201,202] Therefore, post-injury arrhythmia may be reduced by activating Cx43.[203] In addition, the engraftment of Cx43-expressing cells into the infarct region can reduce the propensity for arrhythmogenesis.[172] However, the expression of Cx43 in naïve MSCs is very low,[173] possibly limiting the antiarrhythmogenic potential of MSC therapy. In addition, Hahn *et al.* showed that MSCs with augmented Cx43 expression exert an enhanced cytoprotective effect on cardiomyocytes, reduce the infarct size, and improve cardiac function.[175]

It has been previously reported that VEGF[184] and electrically conductive materials[113] can enhance the expression of Cx43. In the present study, RGO incorporation into MSC spheroids increased VEGF expression (Figure 4.7). In addition, RGO is an electrically conductive material.[204] Therefore, we hypothesized that MSC-RGO hybrid spheroids upregulate Cx43 expression compared with MSC spheroids without RGO, likely due to increased VEGF expression and the conductivity of RGO flakes (Figure 4.9a).

To test this hypothesis, Cx43 expression was assessed in MSC spheroids with or without RGO. The qRT-PCR analysis indicated that Sph-5 and Sph-10 showed the highest Cx43 mRNA expression levels (Figure 4.9b). The western blot analysis showed that the protein level of Cx43 was also enhanced by RGO incorporation (Figure 4.9c). The immunostaining of Cx43 demonstrated that Cx43 was hardly observed in Sph-0 and Sph-2.5 (Figure 4.9d). In contrast, Cx43 was found

to be well expressed in Sph-5 and Sph-10 (Figure 4.9d). To verify that the conductivity of RGO contributes to the upregulation of Cx43, we compared the Cx43 expression levels between RGO-incorporated spheroids (Sph-RGO) and graphene oxide (GO)-incorporated spheroids (Sph-GO). GO is electrically insulating, and RGO is conductive.[205] For this comparison, we used GO flakes with dimensions that are similar to those of the RGO flakes. Despite the abilities of GO to adsorb FN and activate FAK,[125] which resemble those of RGO (Figure 4.6a and 4.7a), GO significantly reduced the Cx43 expression in MSCs (Figure 4.9e). This finding demonstrates that the conductivity of RGO indeed contributes to the upregulation of Cx43. The functionality of Cx43 was examined by dye transfer analysis. We labeled half of the MSCs with DiI and the other half of the MSCs with calcein AM, which is transferred to adjacent cells through Cx43,[206] and then used these cells to form spheroids. If functional gap junctions exist, calcein AM would transfer to adjacent cells.[207] In Sph-0, no notable dye transfer was observed (Figure 4.9f). In contrast, the transfer of calcein AM to DiI-labeled MSCs was observed in Sph-5 (Figure 4.9f). These results demonstrate that the presence of functional gap junctions in Sph-5.

Although other conductive materials that can adsorb proteins could also promote paracrine factor secretion and Cx43 expression, it is hard to process the materials into thin, two-dimensional shape. For example, gold is generally fabricated into nano-[208] or micro-sized particles[209]. However, gold nanoparticles would not be able to provide cell-ECM interactions because the nanoparticles would be easily uptaken by the cells.[210] On the other hand, the use of microparticles would require a larger amount of conductive materials to provide cell-ECM interactions compared with the use of two-dimensional flakes due to the lower ratio of surface area to volume, which would not be appropriate for *in vivo* implantation.

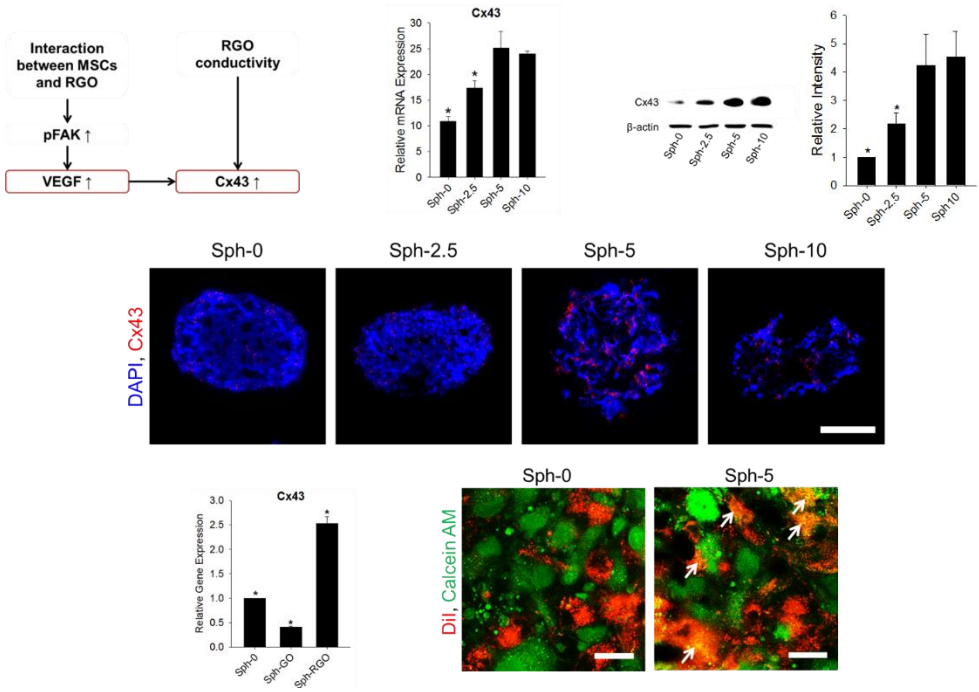

Figure 4.9. Enhanced Cx43 expression in MSC-RGO hybrid spheroids. a) Schematic diagram of mechanisms for enhanced Cx43 expression through RGO incorporation into MSC spheroids.[113,184] b) qRT-PCR analyses of Cx43 expression. c) Cx43 protein expression analyzed by western blot. d) Immunostaining of Cx43 in MSC spheroids incorporated with various concentrations of RGO flakes. Scale bar, 100 μm. e) Effect of incorporation of either non-conductive GO flakes or conductive RGO flakes into MSC spheroids on Cx43 expression in the MSCs, as evaluated by qRT-PCR analyses. f) Dye transfer analysis of Sph-0 and Sph-5. The arrows (yellow) show the transfer of calcein AM (green) dye from calcein AM-labeled MSCs to DiI (red)-labeled MSCs. Calcein AM is known to transfer to neighboring cells through functional gap junctions (Cx43).[206] Scale bars, 20 μm. *$p < 0.05$ versus any other group.

4.2.6. Improved cardiac repair by MSC-RGO hybrid spheroid implantation

In general, the number of MSCs implanted to mouse MI model ranges between 5×10^5 and 5×10^6 cells.[211-213] Meanwhile, in the present study, we implanted 3×10^5 MSCs per mouse. This dose of MSCs was implanted to demonstrate that the incorporation of RGO flakes was able to show a significant therapeutic efficacy even with the reduced amount of the implanted cells.

The amount of RGO flakes implanted to a mouse is approximately 0.75 mg RGO/kg mouse body weight. This RGO amount is much lower than 20 mg/kg which has been reported to exhibit no appreciable *in vivo* toxicity.[214] In addition, our *in vitro* data demonstrated that there was no significant induction of cell apoptosis or reduction in cell functions such as secretion of paracrine factors (Figures 4.3 and 4.7). Therefore, although RGO flakes are not biodegradable,[215] the amount of RGO flakes used for *in vivo* implantation in this study would not exhibit significant toxicity.

Vascularization was evaluated by determining the density of capillaries in the border zone of infarcted myocardium 14 days after cell implantation. Capillaries were identified by immunohistochemical staining with antibodies specific to vWF. Although the MSC spheroids (Sph-0) were able to promote angiogenesis compared with the injection of either PBS or RGO flakes, the MSC-RGO hybrid spheroids (Sph-5) further enhanced the vascularization in the infarcted myocardium (Figure 4.10a). This result may be attributed to the enhanced secretion of angiogenic growth factors in MSCs obtained by the incorporation of RGO flakes (Figure 4.7b and c).

The promotion of angiogenesis attenuates cardiac remodeling after MI.[197] In this study, the incorporation of RGO flakes into MSC spheroids enhanced vascularization and attenuated cardiac remodeling. Masson's trichrome staining of

the longitudinal sections of the heart was performed 14 days after the treatment to quantify the fibrous tissue area (Figure 4.10b). The results showed large fibrotic areas (blue) in the PBS and RGO groups and a small fibrotic area in the Sph-0 group. Importantly, the implantation of Sph-5 showed the smallest fibrotic area, which indicates attenuated cardiac remodeling.

To evaluate the electrical remodeling of the heart, the expression of Cx43 in the border zone of the infarcted myocardium was analyzed. Cx43 is the most abundant type of connexin and is a critical determinant for the electrical properties of the heart.[216,217] It has been reported that the enhanced expression of Cx43 in implanted cells contributes to the prevention of post-infarct arrhythmia.[172] In the PBS and RGO groups, the expression levels of Cx43 were relatively low (Figure 4.10c). Although Sph-0 showed an increase in Cx43 expression, a marked increase in the Cx43 level was apparent in the Sph-5 group. Therefore, the incorporation of RGO flakes into MSC spheroids attenuated the electrical remodeling of the heart after MI.

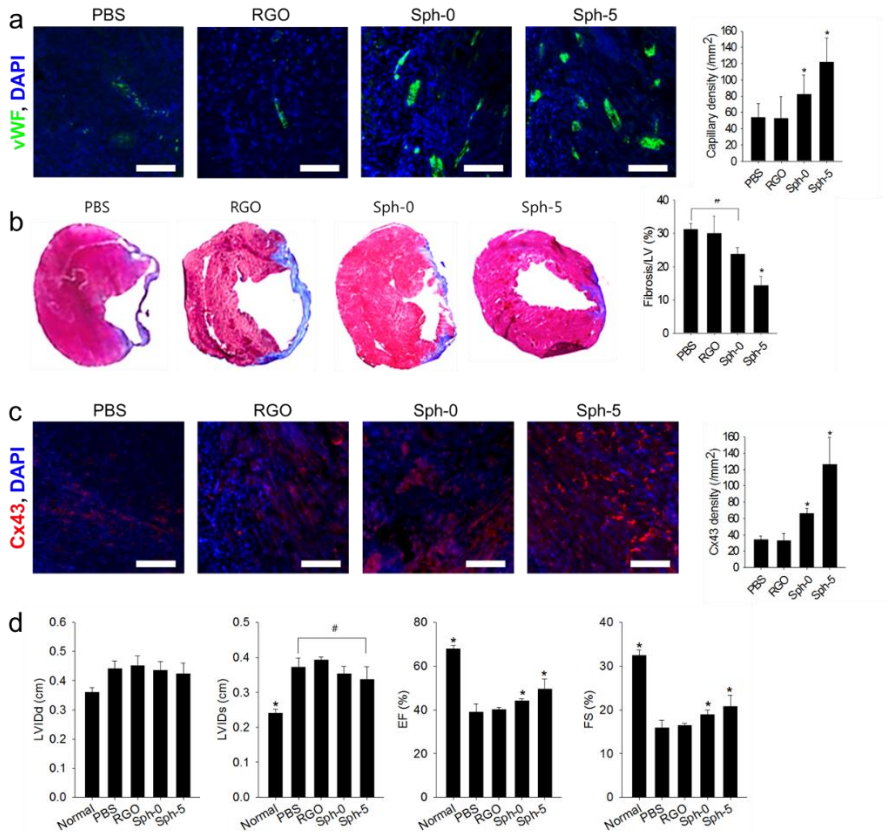

Figure 4.10. Enhanced cardiac repair and cardiac function restoration by implantation of MSC-RGO hybrid spheroids. Infarcted hearts were treated through the injection of PBS, RGO flakes, MSC spheroids (Sph-0), or MSC-RGO hybrid spheroids (Sph-5). a) Capillary density in the peri-infarct border zone assessed by immunostaining for vWF (green). Scale bars, 100 μm. b) Cardiac fibrosis indicated by Masson's trichrome staining (blue) and quantification of the fibrotic area. c) Expression of Cx43 (red) examined by immunohistochemical staining in the infarct border zone. Scale bars, 100 μm. d) Cardiac functions analyzed by echocardiography. $^{*}p < 0.05$ versus any other group. $^{\#}p < 0.05$.

4.2.7. Improvement in cardiac function by MSC-RGO hybrid spheroid implantation

The implantation of Sph-5 improved cardiac function, as demonstrated through transthoracic echocardiography of the infarcted hearts 14 days after the treatment. (Figure 4.10d). In terms of ejection fraction (EF) and fractional shortening (FS), RGO itself did not exert any therapeutic effect. There was no significant difference in the left ventricular internal diameter at end diastole (LVIDd) between the groups. Although the implantation of Sph-0 and Sph-5 showed significantly improved EF and FS, along with the reduction of fibrosis, remarkable improvement in cardiac functions was observed in the Sph-5 group compared with the Sph-0 group. The EF was higher in the Sph-5 group (49.6 ± 4.6%, $p < 0.05$) compared with the Sph-0 group (44.2 ± 0.9%, $p < 0.05$) and the PBS group (38.9 ± 3.7%, $p < 0.05$). The adverse cardiac remodeling was also attenuated in the Sph-5 group, showing a significant reduction of left ventricular internal diameter at end systole (LVIDs) compared with the PBS group (Figure 4.10d). Collectively, echocardiographic parameters showed better cardiac performance in the Sph-5 group than in the Sph-0 group.

Chapter 5.

Graphene oxide flakes as a cellular adhesive: prevention of reactive oxygen species-mediated death of implanted cells for cardiac repair

5.1. Introduction

Cardiovascular diseases continue to be one of the major causes of death around the world.[2,218] Serum deprivation and hypoxia due to restricted blood flow in MI lead to cardiac cell death.[219] Previous studies have demonstrated that the implantation of MSCs can contribute to heart repair mainly by secreting paracrine factors.[75,167] However, the therapeutic benefit of MSC implantation remains very limited due to the poor engraftment and survival of implanted MSCs.[87,88] One of the main causes for the poor survival are ROS generated in the infarcted region after the restoration of blood flow.[220,221] ROS in the infarcted area hinder the adhesion of MSCs to the ECM of the heart tissue by disrupting focal contacts.[222] The loss of MSC adhesion induces the MSC apoptosis, which is known as anoikis,[223] thereby limiting the therapeutic efficacy of MSCs implanted for cardiac repair.[224]

GO is a two-dimensional hydrophilic nano-sheet composed of carbon, oxygen, and hydrogen.[225,226] GO has drawn much attention for their biomedical applications, such as bioimaging,[227,228] drug delivery,[229] gene delivery,[77,230] and tissue engineering.[231,232] The functional groups on the GO surface enable GO to efficiently adsorb proteins from the serum.[124] GO can adsorb proteins though hydrophobic interactions, electrostatic forces, and hydrogen bonding.[125] The proteins from the serum contained in cell culture media include ECM proteins.[233] The adsorption of ECM proteins on GO promotes cell adhesion to GO.[125] Therefore, we hypothesized that the attachment of GO to MSCs (MSC-GO) may preserve the cell-ECM interactions even when cell adhesion to the heart tissue damaged by MI is impaired. While unmodified MSCs would undergo anoikis when implanted into the infarcted region due to hindered cell adhesion by ROS in ischemia and reperfusion injury, MSCs adhering to GO prior to implantation would be able to escape anoikis due to

cell-ECM interactions between MSCs and the ECM proteins adsorbed on GO (Figure 5.1). To test this hypothesis, we first investigated whether MSC adhesion to GO attenuates ROS-mediated deterioration in adhesion, viability, and paracrine factor secretion of MSCs *in vitro*. The signaling mechanisms involved in the adhesion and apoptosis of MSCs were also analyzed. Next, we investigated whether the implantation of MSCs-GO to the reperfused MI region improved the survival, growth factor secretion, and therapeutic efficacy of implanted MSCs by examining angiogenesis, cardiac repair, and heart functions. Here, we introduce a new application of GO as a cellular adhesive to improve the therapeutic efficacy of MSC implantation therapy for the treatment of ROS-abundant ischemia and reperfusion injury.

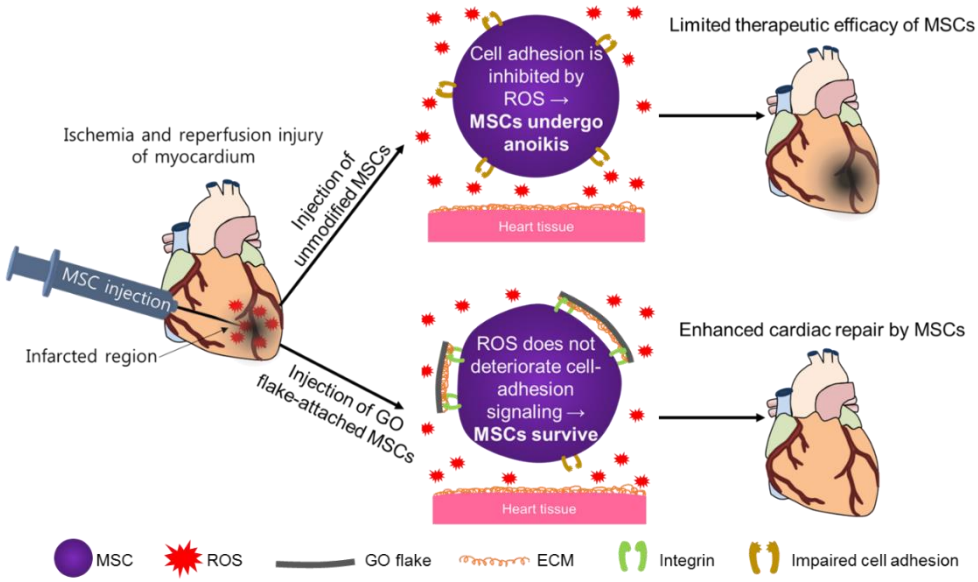

Figure 5.1. Schematic representation of the effects of GO adhesion on the MSCs prior to MSC implantation on the therapeutic efficacy of the MSCs injected into the infarcted myocardium. ROS, which are generated in the ischemic myocardium after the restoration of blood flow, limit the adhesion of implanted MSCs to ECM of the myocardium, which causes the apoptosis of the MSCs due to lack of MSC-ECM interaction (i.e. anoikis). Therefore, allowing MSCs to adhere to GO flakes prior to implantation, which provides the cell-ECM interaction between MSCs and the ECM adsorbed on GO flakes, allows MSCs to escape anoikis when implanted into ROS-abundant injured heart tissue.

5.2. Results and discussion

5.2.1. Characterization of GO flakes

The AFM image of GO flakes showed that the height of flakes was ~1.5 nm, indicating that the GO flakes are monolayer (Figure 5.2a). The size distribution of GO flakes showed that the size of GO flakes ranged from 1 to 6 μm (Figure 5.2a). Figure 5.2b shows a representative TEM image and Figure 5.2c shows the corresponding SAED patterns of a GO flake. The six-fold rotational symmetry of SAED patterns showed graphene-like crystallinity (Figure 5.2c).[234] FT-IR spectrum of GO (Figure 5.2d) showed intense peaks corresponding to hydroxyl groups at 3355 cm^{-1} and 1630 cm^{-1}. A strong band at 1225 cm^{-1} was assigned to the C-OH stretching vibrations, and the bands at 1414 cm^{-1} and 1055 cm^{-1} were attributed to the C-O stretching vibrations. The FT-IR spectra showed same peaks with the previously reported FT-IR spectra of typical GO.[234] Therefore, there was no sign of organic pollutants in GO flakes. The inductively coupled plasma mass spectrometry (ICP-MS) analyses of GO flakes detected negligible amounts[235] of heavy metal pollutants: Ni (0.004 mg/L), Cr (0.010 mg/L), Mn (0.036 mg/L), and Fe (0.118 mg/L). In addition, we confirmed that the Raman spectrum of GO included two broad peaks, which are known as the G and D bands (1590 cm^{-1} and 1350 cm^{-1} respectively) (Figure 5.2e).

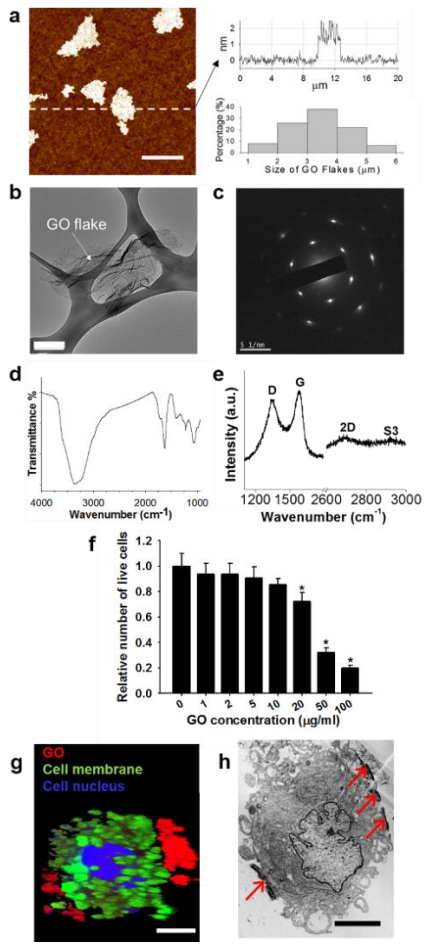

Figure 5.2. Characterization of GO flakes and their adhesion on MSCs. a) Tapping-mode AFM image of GO flakes, the height along the line shown in the AFM image, and the size distribution of GO flakes. Scale bar, 4 μm. b) TEM image of GO flake. Scale bar, 1 μm. c) SAED pattern, d) FT-IR spectra, and e) Raman spectra of GO flakes. f) Viability of MSCs cultured for 3 days with various concentrations of GO flakes added to the culture. *$p < 0.05$ compared to any group. n = 3. g) Adhesion of DiI (red)-labeled GO flakes on MSC. The MSC nucleus was stained with DAPI (blue). The MSC membrane was stained with PKH67 (green). Scale bar, 20 μm. h) TEM image of GO flakes (arrows) attached to MSC surface. Scale bar, 20 μm.

5.2.2. GO adhesion on MSCs

The cytotoxicity of GO flakes was examined by measuring the viability of MSCs after being treated with various concentrations of GO flakes because previous study showed that GO may be cytotoxic in a dose-dependent manner.[236] The analysis of the MSC viability, as assessed using a CCK-8, indicated that the cytotoxicity of GO flakes was not significant at concentrations below 20 μg/ml (Figure 5.2f), which coincides with the results of a previous study.[237] Therefore, we used GO flakes at 10 μg/ml for further experiments.

The attachment of GO flakes to MSCs was examined by fluorescence staining and TEM. Although GO is known to quench fluorescence,[238] GO sheets can be labeled with DiI via adsorption,[110] and increasing the DiI concentration can overcome the fluorescence quenching.[239] Therefore, we labeled GO with high concentrations of DiI to avoid fluorescence quenching to examine GO flake adhesion to MSCs. The DiI labeling of GO flakes, 4'-6-diamidino-2-phenylindole (DAPI) staining of cell nuclei, and PKH67 staining of cell membrane demonstrated that GO flakes attached to MSC membrane (Figure 5.2g). The TEM image of MSC-GO also showed the adherence of several GO flakes on the membrane of a MSC (Figure 5.2h). The relative area of GO adherent to MSCs, as quantified using TEM images, was 25.6 ± 10.1% of the cell surface area. Although there were several literatures that showed cellular uptake of GO nanoparticles (20-300 nm in size),[240,241] there was no sign of GO flake internalization by MSCs in this study (Figures 5.2g and h). This may be due to the micro-scale size of GO flakes (1-6 μm, Figure 5.2a) as particle sizes can influence the cellular uptake of the particles.[240,242]

A previous study demonstrated that GO can effectively adsorb proteins via hydrophobic interactions, electrostatic forces, and hydrogen bonding.[125] Therefore,

it would be possible to control the protein adsorption by modifying GO chemistry. It has previously been reported that the protein adsorption can be controlled by the oxygenous content of GO.[125] For example, GO shows enhanced adsorption of proteins such FGF and FN compared to reduced GO.[125] In the present study, GO prepared by the modified Hummer's method was used as it can effectively facilitate the cell adhesion.[231]

The adsorption of ECM proteins on GO can induce cell adhesion to GO.[141] Therefore, as an example, we analyzed the capability of GO flakes to adsorb FN, a kind of ECM protein. The adsorption of FN to GO flakes immersed in serum-containing medium was examined. The results demonstrated that FN from the culture medium was adsorbed to GO, while no FN was detected on GO flakes immersed in phosphate buffered saline (PBS), which was used as a control (Figure 5.3).

Figure 5.3. FN adsorption to GO flakes after incubation in serum-containing medium for 1 day, as evaluated by western blot analysis.

5.2.3. Enhanced cell adhesion and survival under ROS condition *in vitro*

Paracrine factors secreted from MSCs can promote cardiac regeneration after MI.[243] High engraftment and survival rates of implanted MSCs are necessary for a sustained supply of paracrine factors.[244] However, a burst of ROS is generated at the lesion site after blood restoration in the infarcted region,[245] which significantly impairs the adhesion of implanted MSCs to the infarcted region and results in apoptosis of the MSCs caused by a loss of cell-ECM interaction. This lack of interaction leads to poor engraftment and survival of the implanted MSCs.[224]

To determine whether MSC adhesion to GO flakes can attenuate ROS-mediated cell anoikis, we examined the cell adhesion to culture surfaces and viabilities of MSCs and MSCs-GO in the presence of ROS. To simulate the ROS levels produced by ischemia and reperfusion injury *in vitro*, hydrogen peroxide (H_2O_2), a common model of an exogenous ROS source, was added to the culture medium. First, the initial cell adhesion was visualized by staining filamentous actin (F-actin) with phalloidin. The F-actin staining showed that unmodified MSCs displayed a round morphology in the presence of ROS and the number of adherent cells was significantly decreased, which demonstrated that their ability to adhere was significantly disrupted (Figure 5.4a). The impairment MSC adhesion by H_2O_2 was likely due to impaired integrin-mediated cell adhesion to ECM molecules.[246] Conversely, the morphology of MSCs-GO was more spread out and similar to control MSCs, which were cultured in the absence of H_2O_2. This morphology, along with the number of adherent cells, demonstrated that these cells could more easily attach to the culture surface (Figure 5.4a), which may be due to decreased anoikis of MSCs-GO, which retained the interactions with the ECM via their adhesion to the

ECM-adsorbed GO flakes. The loss of cell-ECM interactions in unmodified MSCs led to anoikis. Therefore, the number of live cells significantly decreased when unmodified MSCs were exposed to ROS, while the adhesion of MSCs to GO could protect the cells from anoikis (Figure 5.4b).

To further examine whether GO flake adhesion to MSCs attenuates MSC anoikis, MSCs and MSCs-GO were cultured on agar-coated plates. The culture plates were coated with agar to inhibit cell adhesion to the plate and mimic the *in vivo* condition of ischemia and reperfusion injury, in which cell adhesion to the heart tissue is disturbed by ROS.[224] After 24 h, only 15 ± 1% of the cells survived on the agar-coated plate compared to MSCs cultured on cell culture plates without agar coating (Figure 5.4c). The dramatic decrease in the cell survival rate was due to the inhibition of cell adhesion (i.e., anoikis). Conversely, MSC adhesion to GO flakes significantly increased the survival rate (Figure 5.4c). This improved cell survival in MSCs-GO was likely due to the cell-ECM interactions that result from MSCs adhering to the FN adsorbed to GO, which attenuated anoikis.

The enhanced cell survival of MSCs-GO increased the secretion of paracrine factors *in vitro* (Figure 5.4d). Treating MSCs with ROS significantly reduced the secretion of FGF-2 and VEGF, which are important paracrine angiogenic factors for ischemic tissue repair.[247,248] The reduced paracrine factor secretion may be due to the poor MSC survival after ROS treatment. Conversely, the amounts of FGF-2 and VEGF secreted by MSC-GO in the presence of ROS were similar to those of MSCs and MSCs-GO cultured without ROS (Figure 5.4d). These results suggest that the number of live MSCs can determine the amount of secreted paracrine factors.

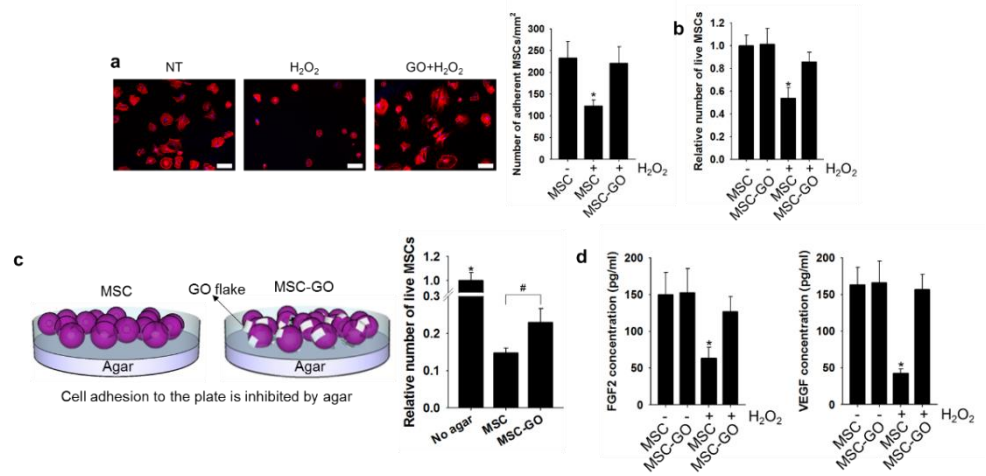

Figure 5.4. Attenuation of ROS-mediated deterioration in adhesion, viability, and paracrine factor secretion of MSCs by MSC adhesion to GO flakes *in vitro*. ROS were generated in the culture by adding H_2O_2. a) The adhesion of MSCs and MSCs-GO to the culture plates 90 min after culture in the medium containing 0 (no treatment, NT) or 200 μM H_2O_2 as evaluated by F-actin staining. Scale bars, 10 μm. b) Relative number of live cells assessed 24 h after the culture of MSCs and MSCs-GO in medium containing 0 (NT) or 200 μM H_2O_2. c) Viability of MSCs and MSCs-GO when cultured on an agar plate, which completely inhibits cell adhesion. The result was compared with MSCs cultured in a culture plate without agar. H_2O_2 was not added to the culture for all groups. Importantly, the result indicates that GO flake adhesion to MSCs attenuates the anoikis of MSCs. d) The amounts of FGF-2 and VEGF secreted by MSCs and MSCs-GO with or without H_2O_2. $^*p < 0.05$ compared to any group. $^{\#}p < 0.05$. n = 3.

5.2.4. The mechanism of enhanced cell survival

The underlying mechanisms by which MSC adhesion to GO flakes prevents anoikis were examined by investigating the expression of cell signaling molecules (Figure 5.5a). Both H_2O_2 treatment and cell detachment downregulate FAK phosphorylation, which in turn enhances the activation of p38 and caspase-3, suggesting that ROS plays a role in cell anoikis.[249,250] To confirm that the disruption of cell adhesion by ROS produced these sequential cell signaling events, we analyzed the expression of these signaling molecules in MSCs cultured in H_2O_2-containing medium. First, we examined the expression of integrin β1, which is one of the major receptors by which cells can attach to ECM molecules.[251] The presence of H_2O_2 significantly downregulated the expression of integrin β1 (Figure 5.5b), indicating deteriorated cell-adhesion to the culture plate. However, the downregulation of integrin β1 was rescued when MSCs were allowed to adhere to GO flakes because integrins could bind to the ECM proteins adsorbed on GO (Figure 5.5b). The downregulation of integrin β1 (i.e., loss of cell adhesion) by ROS led to the downregulation of pFAK and the activation of p38 and caspase-3 (Figure 5.5c). Importantly, the impairment of cell adhesion and upregulation of apoptosis due to the exposure of MSCs to ROS were significantly ameliorated by allowing MSC to attach to GO (Figure 5.5c). This finding confirmed that GO flakes act as a cellular adhesive that provides surfaces for cell adhesion and protects MSCs from anoikis. However, MSC adhesion to GO flakes could not completely reduce the level of activated caspase-3 (Figure 5.5c), the activation of which leads to cell apoptosis. This phenomenon may be observed because ROS not only hinder cell adhesion, but also induce cell apoptosis by regulating the phosphorylation of proteins related to apoptosis.[252]

To investigate whether the adsorption of ECM proteins on GO flakes induces integrin β1 expression for MSC adhesion to GO flakes and prevents apoptotic signaling, MSCs were cultured in a serum-free medium in the presence of ECM protein-adsorbed GO flakes, and transferred to H_2O_2-containing medium. FN and VN are main ECM proteins contained in serum that mediate cell adhesion.[253] Therefore, MSCs were incubated with FN-adsorbed GO [MSC+GO (FN)] and VN-adsorbed GO [MSC+GO (VN)] in serum-free medium prior to being placed under ROS condition. MSC+GO (FN) and MSC+GO (VN) were compared with MSCs incubated with bare GO in serum-free medium (MSC+GO). After incubation in H_2O_2-containing medium, the expression of integrin β1 and the activation of p38 were analyzed. The results demonstrated that ECM protein (FN or VN)-adsorbed GO flakes promoted integrin β1 expression and prevented the activation of p38 in MSCs cultured under ROS condition, while MSC+GO showed a similar tendency to MSCs alone under ROS condition (Figure 5.6). Therefore, ECM proteins adsorbed on GO flakes played a major role in mediating MSC adhesion to GO and preventing ROS-mediated anoikis.

In order to determine whether free ECM proteins in serum-containing medium compete with ECM proteins adsorbed on GO flakes for their interactions with MSCs, we compared the adhesion of GO flakes on MSCs after incubating MSCs with ECM protein-adsorbed GO flakes in either serum-free medium or serum-containing medium for 24 h. The serum-containing medium has free ECM proteins. Unattached GO flakes were removed by washing several times with PBS. ECM protein-adsorbed GO flakes were also incubated in serum-free medium and serum-containing medium without MSCs for 24 h in order to confirm GO attachment to MSCs, rather than the dish. The results demonstrated no attachment of GO flakes in

the absence of MSCs (Figure 5.7), demonstrating GO flakes attached to MSCs, rather than the dish. The presence of free ECM proteins in serum-containing medium did not influence the attachment of GO flakes to MSCs (Figure 5.7). Therefore, free ECM proteins in serum-containing medium did not compete with ECM proteins adsorbed on GO flakes to interact with MSCs.

A previous study reported that GO can reduce oxidative stress by scavenging hydroxyl radicals,[254] which could be a possible mechanism for the attenuation of ROS-mediated MSC death by GO flakes. In the present study, to address this possibility, we examined whether GO can reduce the level of ROS by incubating GO flakes in H_2O_2 (200 μM)-containing solution. After 24 h, the concentration of H_2O_2 in the solution incubated with GO flakes was 199.0 ± 1.1 μM, showing no significant difference compared with that (200 μM) of H_2O_2-containing solution without GO flakes. In addition, the DCFDA staining of intracellular ROS showed no difference between MSCs and MSCs-GO cultured in H_2O_2-containing medium, demonstrating that the adhesion of GO flakes on MSCs did not alter the intracellular ROS in the MSCs (Figure 5.8). These results collectively demonstrate that GO flakes did not significantly scavenge ROS. This may be because the GO concentration (10 μg/ml) used in this study was much lower than the minimal GO concentration (100 μg/ml) that exhibits significant ROS scavenging effect.[254] Furthermore, our data showed only 25.6 ± 10.1% of MSC surfaces were covered with GO flakes (Figure 5.2h), suggesting that GO flakes could not act as a physical barrier to inhibit ROS from damaging MSCs. Therefore, the enhanced MSC survival under ROS condition would be attributed to the interaction between GO flakes and MSCs rather than the ROS scavenging and physical barrier effects of GO flakes.

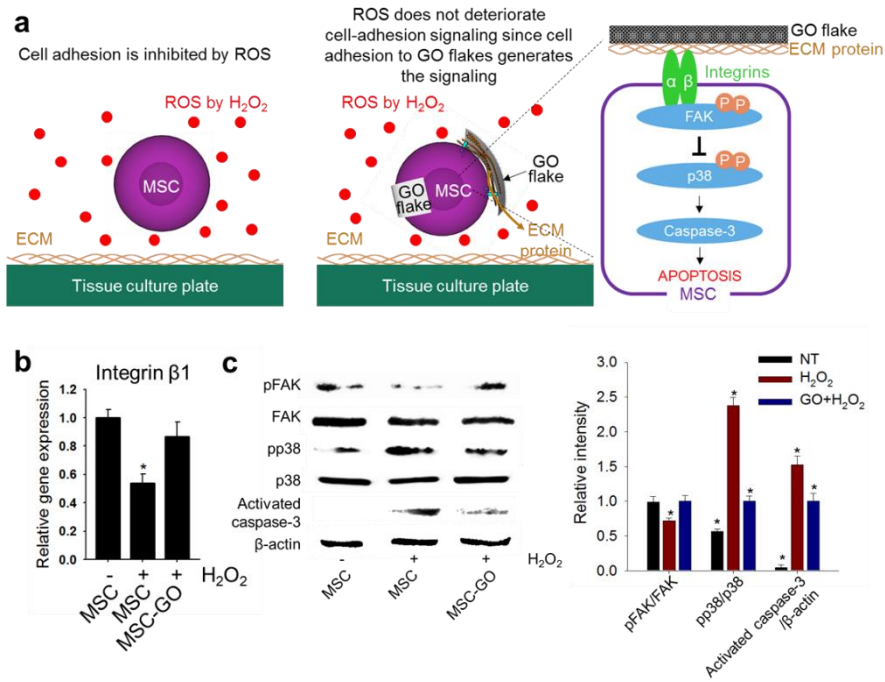

Figure 5.5. The attenuation of ROS-mediated deterioration in cell adhesion signaling and subsequent apoptosis of MSCs by MSC adhesion to GO flakes *in vitro*. a) Schematic representation of anoikis signaling. b) The expression of integrin β1 evaluated by qRT-PCR, indicated that MSC adhesion to GO flakes avoids ROS-mediated deterioration in cell adhesion. c) The expression of activated intracellular signaling molecules related to anoikis as evaluated by western blot analyses. NT indicates no treatment (no H_2O_2). *$p < 0.05$ compared to any group. n =3.

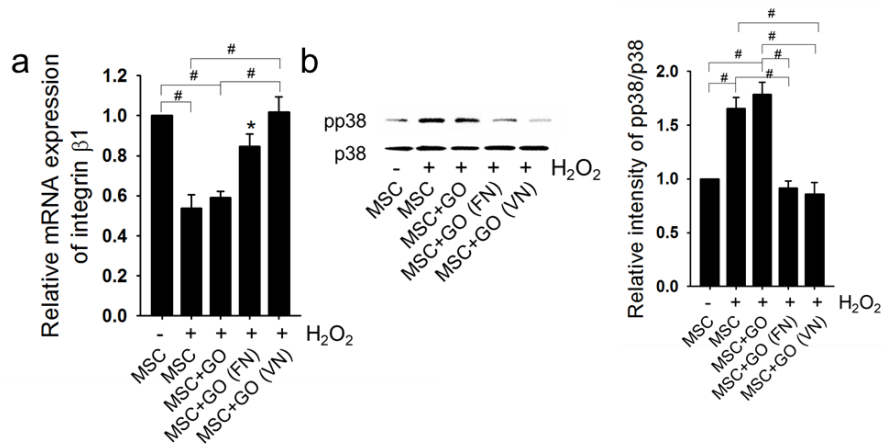

Figure 5.6. The expression of a) integrin β1 evaluated by qRT-PCR and b) activated p38 evaluated by western blot analyses. MSCs cultured in medium with or without H_2O_2 was used as negative and positive controls, respectively. MSCs incubated with GO flakes in medium without serum (MSC+GO) showed a similar tendency to MSCs alone. MSCs incubated with FN-adsorbed GO [MSC+GO (FN)] or VN-adsorbed GO [MSC+GO (VN)] significantly prevented the ROS-mediated reduction of integrin β1 expression and activation of p38. $^{*}p < 0.05$ compared to any group. $^{\#}p < 0.05$. n =3.

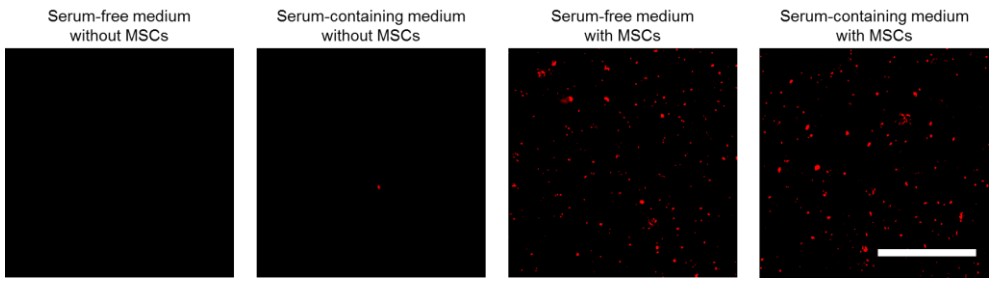

Figure 5.7. Competition between free ECM proteins, which are contained in serum in medium, and ECM proteins adsorbed on GO for their interactions with MSCs. MSCs were incubated with ECM protein-adsorbed GO flakes in either serum-free medium or serum-containing medium for 24 h. After incubation, unattached GO flakes were removed by washing several times with PBS. Serum protein-adsorbed GO flakes were also incubated in serum free medium and serum-containing medium without MSCs for 24 h in order to confirm GO attachment to MSCs, rather than the dish. The presence of serum in the medium did not influence the adhesion of GO flakes on MSCs. Red indicates DiI-labeled GO flakes. Scale bar, 2 mm.

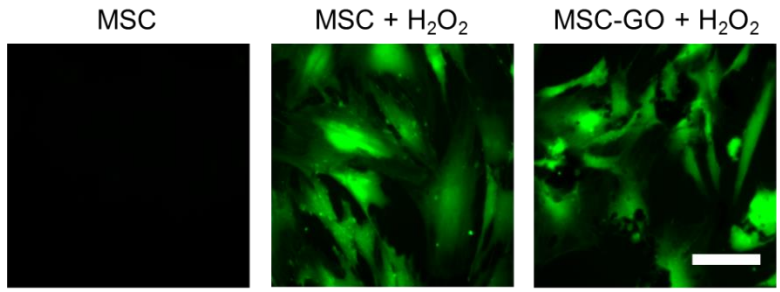

Figure 5.8. DCFDA staining (green) of intracellular ROS in MSCs and MSCs-GO after incubating them in H_2O_2-containing solution for 30 min. Scale bar, 50 μm.

5.2.5. Enhanced survival of MSCs implanted in a myocardial ichemia and reperfusion model

The presence of ROS after reperfusion in the infarcted region is known to inhibit the adhesion of the implanted cells, which results in the apoptosis of the implanted cells due to a loss of cell adhesion (i.e., anoikis).[224] To assess the engraftment of MSCs implanted in the infarcted region, we implanted MSCs labeled with DAPI prior to implantation. The initial engraftment of MSCs was assessed by counting the number of DAPI-labeled cells on day 3. The implantation of MSCs-GO allowed a significantly larger number of MSCs to engraft at the lesion site of ischemia and reperfusion injury (Figure 5.9a). A similar trend in the MSC retention at the injury site was observed on day 14; the number of MSCs at the site increased by more than 7-fold in the MSC-GO group compared to the MSC group (Figure 5.9a). In addition, the MSC dispersion in injury region notably changed on day 14 (Figure 5.9a). MSCs remained localized at the site of injection in the MSC-GO group (Figure 5.9a), which may be due to the strong adhesion of grafted MSCs at the lesion site, as demonstrated *in vitro* in Figure 5.4a. In addition, we examined the TUNEL expression of implanted MSCs to analyze their apoptotic activity. Significantly more MSCs were stained with TUNEL in the MSC group compared to the MSC-GO group (Figure 5.9b), which suggests that unmodified MSCs are more susceptible to ROS-mediated apoptosis, as demonstrated in the *in vitro* results.

Growing evidences suggest that the major mechanism of cardiac repair by stem cell implantation is reparative paracrine factor secretion from the implanted stem cells, rather than the differentiation of the engrafted stem cells into cardiac cells.[1] In addition, although there are some controversies, it has been reported that electromechanical integration is incomplete following therapeutic-cell implantation

as demonstrated by limited expression of adherens and gap junction proteins.[255,256] Therefore, in this study, we focused on the paracrine effect of implanted MSCs and MSCs-GO after they survived in the infarct region (Figure 5.9a), rather than their formation of adherens junctions with the host cells.

Paracrine factors promote angiogenesis in a dose-dependent manner in the ischemic regions, and this effect could be enhanced by increasing the number of implanted cells.[257] In this study, we have increased the number of MSCs engrafted in the ischemic heart by promoting their survival rather than administrating more MSCs (Figure 5.9a and b). The enhanced survival of MSCs significantly enhanced the secretion of proangiogenic growth factors, such as VEGF and FGF-2, *in vitro* (Figure 5.4d). *In vivo*, the secretion of human VEGF by the implanted human MSCs was analyzed as an example for paracrine factor secretion. The secretion of VEGF was increased in the MSC-GO group (Figure 5.9c). By calculating the relative amount of VEGF secreted by each MSC, which did not significantly differ between MSCs and MSCs-GO (Figure 5.9c), we demonstrated that the increased number of engrafted MSCs is responsible for the enhanced secretion of VEGF in the MSC-GO group. This finding also demonstrates that the bio-functionality of the implanted MSCs was preserved irrespective of the use of GO flakes.

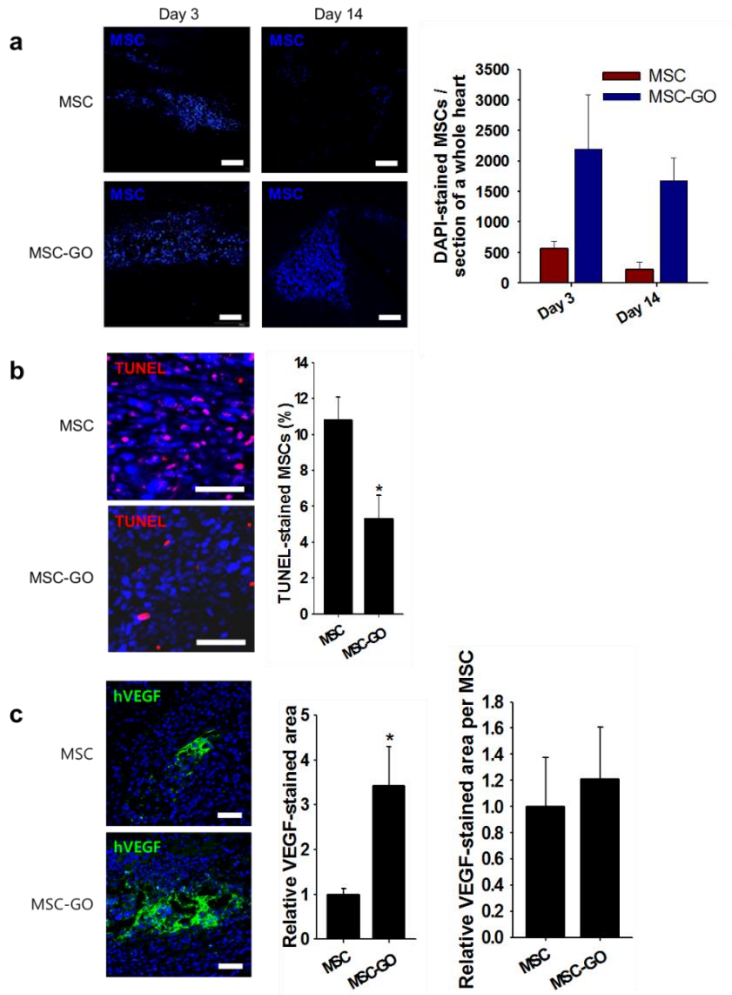

Figure 5.9. Survival and VEGF secretion from MSCs or MSCs-GO implanted into the reperfused MI region evaluated by immunohistochemistry. a) Detection of DAPI (blue)-labeled MSCs 3 and 14 days after MSC implantation. Scale bars, 100 μm. b) TUNEL (red) staining 3 days after MSC implantation. The MSCs were labeled with DAPI (blue). Scale bars, 50 μm. c) Human VEGF (green) staining 3 days after human MSC or human MSC-GO implantation. All cells (not only MSCs) were counterstained with DAPI (blue). Scale bars, 50 μm. *$p < 0.05$ compared to any group. $^{\#}p < 0.05$. n = 3

5.2.5. Improvement in myocardial repair by MSC-GO

Previous studies have demonstrated that the secretion of proangiogenic growth factors contributes to the neovascularization in the ischemic myocardium, and promotes myocardial repair.[248] In the present study, the enhanced growth factor secretion by MSCs-GO enhanced the neovascularization in the infarcted region (Figure 5.10). The heart sections retrieved 14 days after cell implantation were stained for smooth muscle actin alpha (SMA-α) and vWF. To quantify the number of vessels in the infarct region, arterioles were assigned as SMA-α-positive vessels, and capillaries were assigned as vWF-positive minus SMA-α-positive vessels.[258] While MSCs could promote angiogenesis in the infarcted myocardium compared to the PBS injection group, MSCs-GO could further enhance neovascularization (Figure 5.10).

Enhanced angiogenesis contributes to heart repair after MI.[197] The promotion of angiogenesis due to enhanced paracrine secretion by MSCs-GO attenuated left ventricular remodeling (Figure 5.11).[28] Masson's trichrome staining and TTC staining were performed 14 days after the treatment to assess the area of collagen-containing fibrous tissue and infarcted left ventricle, respectively. The Masson's trichrome staining of the longitudinal sections of the heart showed a large fibrotic area (blue) in the PBS and MSC groups, while the fibrotic area was significantly smaller in the MSC-GO group (Figure 5.11a). TTC staining demonstrated that MSCs-GO significantly decreased the infarct size (Figure 5.11b). TUNEL staining showed that the cardiac cells in the infarct region of the PBS and MSC groups continued to undergo apoptosis (Figure 5.11c), which further aggravated the infarction. However, significantly fewer cells were stained with

TUNEL in the MSC-GO group (Figure 5.11c), which demonstrated that the progress of infarction was slowed.

In vivo toxicity of GO flakes was not significant in this study even though GO flakes showed no sign of degradation 14 days after implantation (Figure 5.12 and 5.13). Previous studies have reported that the implantation of GO particles did not exhibit obvious *in vivo* toxicity.[259,260] Yang *et al.* have demonstrated that GO implanted into mice at a concentration of 50 mg/kg is retained in the body for more than 30 days, yet, no significant toxicity was observed even after 90 days.[260] GO exhibits dose-dependent toxicity; GO implantation to mice at a dosage less than 100 mg/kg body weight does not elicit obvious toxicity.[261] In this study, a GO concentration of 10 μg/ml was not cytotoxic to MSCs *in vitro* (Figure 5.2f). For *in vivo* implantation, a GO dosage of 1 mg/kg body weight was used. We carried out a TUNEL assay at the site of cell implantation (peri-infarct region rather than infarct region) to examine the toxic effects of GO on the surrounding cells, including the implanted MSCs and native heart cells. The TUNEL staining demonstrated that GO flakes did not induce significant apoptosis as a notable increase in TUNEL-stained cells was not detected near the GO flakes (Figure 5.12).

In addition to the TUNEL assay, we have carried out hematoxylin and eosin staining of the implantation site to assess inflammatory cell infiltration. Inflammation plays an important role in determining the foreign body response to the implanted materials.[262] The hematoxylin and eosin staining results showed that there were inflammatory cells in both MSC and MSC-GO group, which is in accordance with previous studies that showed large amounts of inflammatory cell infiltration in the infarcted heart at day 14.[263,264] However, the implantation of MSCs-GO did not significantly aggravate the inflammatory cell invasion compared to the

implantation of MSCs alone (Figure 5.13), indicating that there was no significant foreign body response against the implanted GO flakes. A previous study has also demonstrated that a combination of GO and hydrogel injected into the peri-infarct regions of the heart after MI induction did not stimulate inflammatory responses.[77] Therefore, although overcoming the long-time retention of GO flakes post-implantation *in vivo* remains a challenge, this retention may not be of consequence for the *in vivo* use given appropriate doses.

The implantation of MSC-GO also improved cardiac function (Figure 5.14). The implantation of MSC-GO increased the number of engrafted MSCs and the amount of secreted paracrine factors, which enhanced angiogenesis and prevented further remodeling of the infarcted myocardium. The enhanced therapeutic angiogenesis and the inhibition of cardiomyocyte apoptosis contribute to the functional improvement of the infarcted heart.[265] Herein, a transthoracic echocardiography showed that the LVIDd did not significantly differ among groups (Figure 5.14). However, the implantation of MSCs-GO markedly decreased the LVIDs compared to the PBS group, but this parameter did not significantly differ when compared with the normal group (Figure 5.14). In contrast, unmodified MSCs showed significantly larger LVIDs than the normal group (Figure 5.14). The left ventricular EF and FS were significantly enhanced in the MSC-GO group compared to the PBS and MSC groups and did not significantly differ from the normal group (Figure 5.14). In summary, the enhanced survival of implanted MSCs in the MSC-GO group resulted in enhanced paracrine factor secretion and reduced cardiac tissue apoptosis by promoting angiogenesis, attenuating the remodeling of the infarcted heart, and improving cardiac function after ischemia and reperfusion injury.

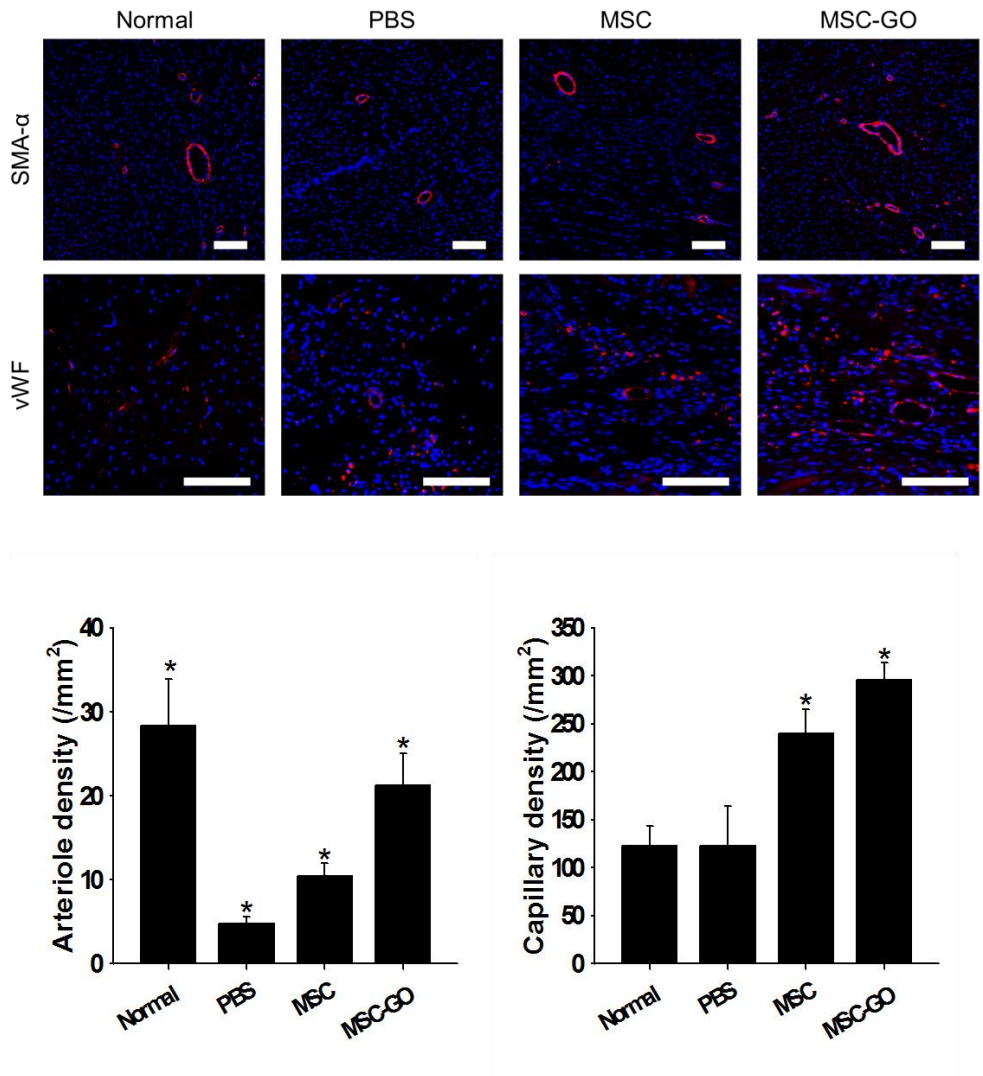

Figure 5.10. Microvessel density in the infarcted region 14 days after MSC or MSC-GO implantation. The arteriole densities were quantified by counting the SMA-α (red)-positive vessels. The capillary densities were quantified by subtracting the SMA-α-positive vessels from vWF (red)-positive vessels. *$p < 0.05$ compared to any group.

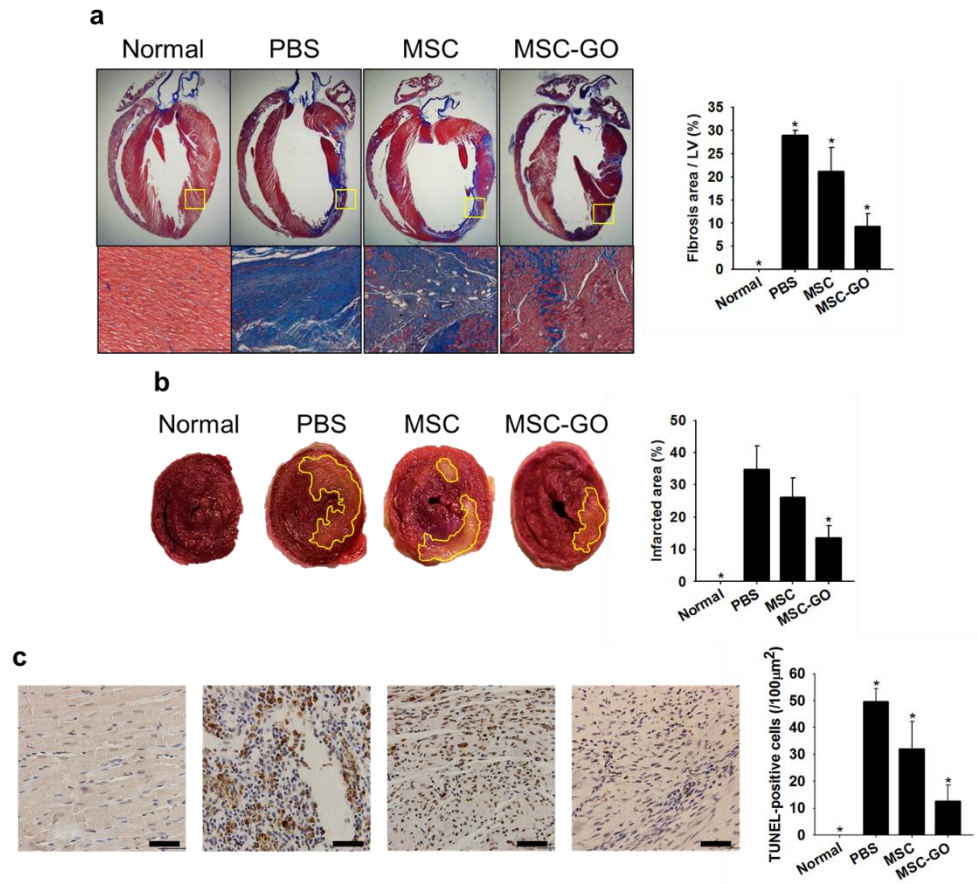

Figure 5.11. Enhanced cardiac repair by MSC-GO implantation (14 days after implantation). a) Fibrosis evaluated based on a histological analysis with Masson's trichrome staining. Blue indicates fibrosis. b) Infarct area evaluated based on the TTC staining of heart sections. The infarct area is marked with a yellow line. c) Tissue apoptosis in the infarct zone as evaluated by TUNEL staining (brown color). Scale bars, 50 μm. *$p < 0.05$ compared to any group.

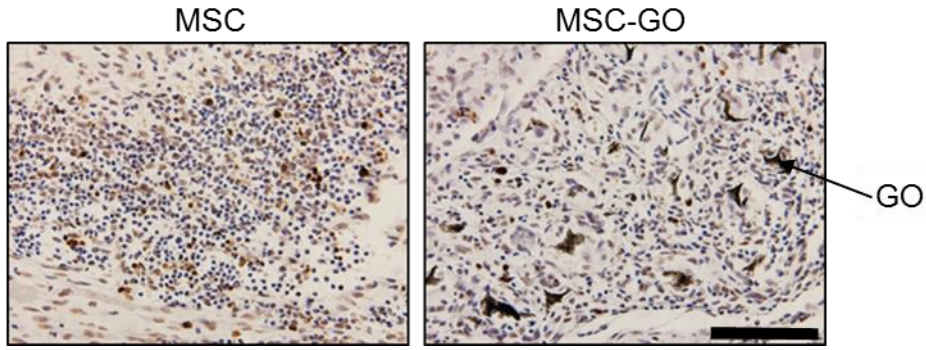

Figure 5.12. *In vivo* biocompatibility of GO flakes as evaluated by TUNEL (brown) staining of the site (peri-infarct region rather than infarct region) of MSC or MSC-GO implantation at day 14. Cells were counterstained with hematoxylin. Scale bar, 100 μm.

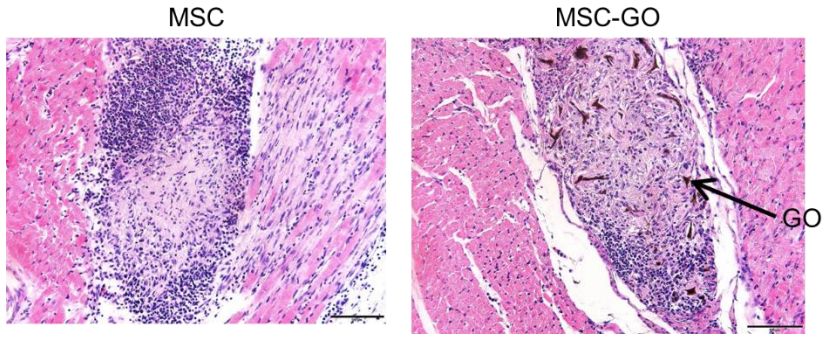

Figure 5.13. Hematoxylin and eosin staining images of the MSC or MSC-GO implantation area to observe the local inflammation at day 14. Black color indicate GO flakes. Scale bar, 100 μm.

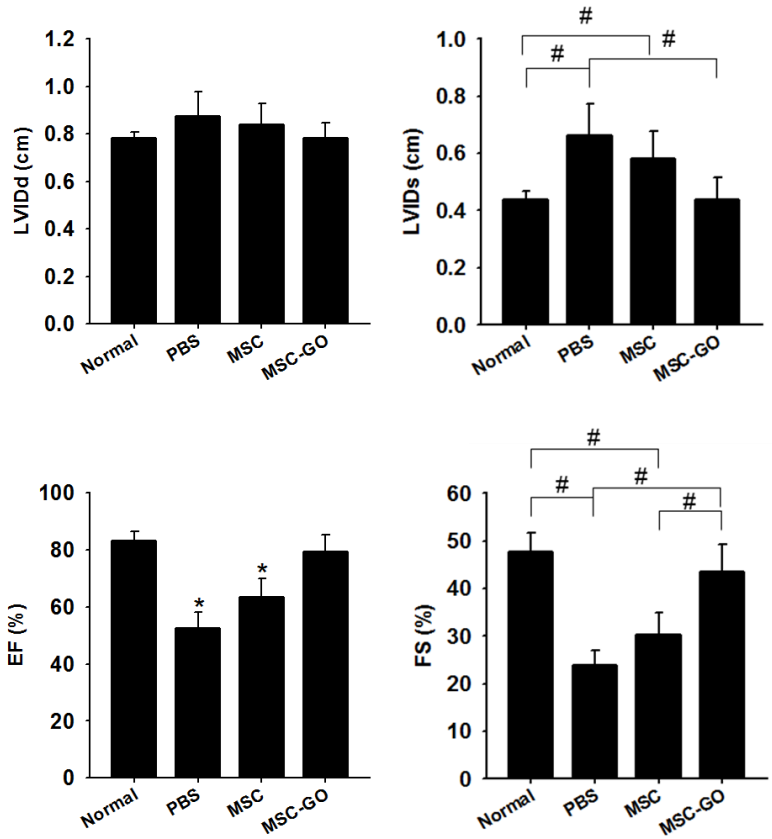

Figure 5.14. Heart functions and left ventricular size 14 days after treatments, as evaluated by echocardiography. $^{*}p < 0.05$ compared to any group. $^{\#}p < 0.05$.

Chapter 6.

Conclusions

This dissertation presents the studies on utilizing graphene and graphene derivatives to improve the efficacy of stem cell therapy for MI treatment.

Chapter 3 provides the first demonstration that graphene could be used as a stem cell culture substrate to promote the cardiomyogenic differentiation process of MSCs without the use of any exogenous chemical inducers. Graphene exhibited no sign of cytotoxicity for stem cell culture, and provided a suitable environment for MSC proliferation. The MSC commitment towards cardiomyogenic lineage was stimulated by simply culturing the MSCs on graphene, even in the absence of chemical inducers for cardiomyogenic differentiation. This finding may be attributed, at least in part, to the upregulation of the gene expression of ECM proteins that are known to promote the cardiomyogenic differentiation of stem cells. In addition, the cell signaling molecules involved in the cardiomyogenic differentiation of stem cells were also upregulated in the MSCs cultured on graphene. Our results suggest that graphene is a novel platform for the cardiomyogenic differentiation of MSCs and could aid the improvement of the therapeutic efficacy to advance the current stem cell therapies used for the treatment of ischemic heart diseases.

Chapter 4 demonstrates that the incorporation of RGO flakes into MSC spheroids promoted the expression of angiogenic growth factors and Cx43 in the MSCs, both of which are important for cardiac repair, likely due to their high affinity toward FN and the high electrical conductivity of RGO. The implantation of MSC-RGO hybrid spheroids into the infarcted myocardium enhanced cardiac repair and cardiac function restoration compared with the injection of either RGO flakes or MSC spheroids. Therefore, RGO can enhance the therapeutic efficacy of MSCs for the treatment of MI.

Chapter 5 shows that GO flakes could effectively prevent a series of adverse cell-signaling cascades that result in the anoikis of MSCs in response to ROS that are generated in the ischemia-damaged and reperfused myocardium. This effect was due to the ability of GO flakes to provide a platform for MSC adhesion. The improved survival of MSCs following the implantation of MSCs-GO into the infarcted and reperfused myocardium resulted in the enhanced secretion of reparative paracrine factors and reduced apoptosis of cardiac tissue, which enhanced angiogenesis and improved cardiac function. Therefore, GO may be utilized to protect therapeutic cells implanted into various ROS-abundant damaged tissues as part of stem cell implantation therapies for ischemic diseases after reperfusion.

References

1. Mirotsou, M.; Jayawardena, T. M.; Schmeckpeper, J.; Gnecchi, M.; Dzau, V. J. Paracrine mechanisms of stem cell reparative and regenerative actions in the heart. *J. Mol. Cell. Cardiol.* **2011,** *50*, 280-289.
2. Lloyd-Jones, D.; Adams, R. J.; Brown, T. M.; Carnethon, M.; Dai, S.; De Simone, G.; Ferguson, T. B.; Ford, E.; Furie, K.; Gillespie, C., *et al.* Heart disease and stroke statistics-2010 update: A report from the american heart association. *Circulation* **2010,** *121*, e46-e215.
3. Park, H. J.; Yang, F.; Cho, S. W. Nonviral delivery of genetic medicine for therapeutic angiogenesis. *Adv. Drug Delivery Rev.* **2012,** *64*, 40-52.
4. Aguirre, A.; Sancho-Martinez, I.; Izpisua Belmonte, J. C. Reprogramming toward heart regeneration: Stem cells and beyond. *Cell Stem Cell* **2013,** *12*, 275-284.
5. McMurray, J. J.; Pfeffer, M. A. Heart failure. *Lancet* **2005,** *365*, 1877-1889.
6. Bramucci, E.; Repetto, A.; Ferrario, M.; Canosi, U.; Boschetti, E.; Brambilla, N.; Gnecchi, M.; Merlini, P. A.; Ardissino, D.; Angoli, L., *et al.* Effectiveness of adjunctive stent implantation following directional coronary atherectomy for treatment of left anterior descending ostial stenosis. *Am. J. Cardiol.* **2002,** *90*, 1074-1078.
7. Gnecchi, M.; Danieli, P.; Cervio, E. Mesenchymal stem cell therapy for heart disease. *Vascul. Pharmacol.* **2012,** *57*, 48-55.
8. Hastings, C. L.; Roche, E. T.; Ruiz-Hernandez, E.; Schenke-Layland, K.; Walsh, C. J.; Duffy, G. P. Drug and cell delivery for cardiac regeneration. *Adv. Drug Delivery Rev.* **2014**.

9. Pascual-Gil, S.; Garbayo, E.; Diaz-Herraez, P.; Prosper, F.; Blanco-Prieto, M. J. Heart regeneration after myocardial infarction using synthetic biomaterials. *J. Control. Release* **2015,** *203*, 23-38.
10. Reis, L. A.; Chiu, L. L.; Feric, N.; Fu, L.; Radisic, M. Biomaterials in myocardial tissue engineering. *J. Tissue Eng. Regen. Med.* **2014**.
11. Huikuri, H. V.; Kervinen, K.; Niemela, M.; Ylitalo, K.; Saily, M.; Koistinen, P.; Savolainen, E. R.; Ukkonen, H.; Pietila, M.; Airaksinen, J. K., *et al.* Effects of intracoronary injection of mononuclear bone marrow cells on left ventricular function, arrhythmia risk profile, and restenosis after thrombolytic therapy of acute myocardial infarction. *Eur. Heart J.* **2008,** *29*, 2723-2732.
12. Meyer, G. P.; Wollert, K. C.; Lotz, J.; Pirr, J.; Rager, U.; Lippolt, P.; Hahn, A.; Fichtner, S.; Schaefer, A.; Arseniev, L., *et al.* Intracoronary bone marrow cell transfer after myocardial infarction: 5-year follow-up from the randomized-controlled boost trial. *Eur. Heart J.* **2009,** *30*, 2978-2984.
13. Assmus, B.; Rolf, A.; Erbs, S.; Elsasser, A.; Haberbosch, W.; Hambrecht, R.; Tillmanns, H.; Yu, J.; Corti, R.; Mathey, D. G., *et al.* Clinical outcome 2 years after intracoronary administration of bone marrow-derived progenitor cells in acute myocardial infarction. *Circ. Heart Fail.* **2010,** *3*, 89-96.
14. Leistner, D. M.; Fischer-Rasokat, U.; Honold, J.; Seeger, F. H.; Schachinger, V.; Lehmann, R.; Martin, H.; Burck, I.; Urbich, C.; Dimmeler, S., *et al.* Transplantation of progenitor cells and regeneration enhancement in acute myocardial infarction (topcare-AMI): Final 5-year results suggest long-term safety and efficacy. *Clin. Res. Cardiol.* **2011,** *100*, 925-934.
15. Hodgson, D. M.; Behfar, A.; Zingman, L. V.; Kane, G. C.; Perez-Terzic, C.; Alekseev, A. E.; Puceat, M.; Terzic, A. Stable benefit of embryonic stem cell

therapy in myocardial infarction. *Am. J. Physiol. Heart Circ. Physiol.* **2004,** *287*, H471-479.

16. Min, J. Y.; Yang, Y.; Converso, K. L.; Liu, L.; Huang, Q.; Morgan, J. P.; Xiao, Y. F. Transplantation of embryonic stem cells improves cardiac function in postinfarcted rats. *J. Appl. Physiol.* **2002,** *92*, 288-296.
17. Xie, C. Q.; Zhang, J.; Xiao, Y.; Zhang, L.; Mou, Y.; Liu, X.; Akinbami, M.; Cui, T.; Chen, Y. E. Transplantation of human undifferentiated embryonic stem cells into a myocardial infarction rat model. *Stem Cells Dev.* **2007,** *16*, 25-29.
18. Ye, L.; Chang, Y. H.; Xiong, Q.; Zhang, P.; Zhang, L.; Somasundaram, P.; Lepley, M.; Swingen, C.; Su, L.; Wendel, J. S., *et al.* Cardiac repair in a porcine model of acute myocardial infarction with human induced pluripotent stem cell-derived cardiovascular cells. *Cell Stem Cell* **2014,** *15*, 750-761.
19. Templin, C.; Zweigerdt, R.; Schwanke, K.; Olmer, R.; Ghadri, J. R.; Emmert, M. Y.; Muller, E.; Kuest, S. M.; Cohrs, S.; Schibli, R., *et al.* Transplantation and tracking of human-induced pluripotent stem cells in a pig model of myocardial infarction: Assessment of cell survival, engraftment, and distribution by hybrid single photon emission computed tomography/computed tomography of sodium iodide symporter transgene expression. *Circulation* **2012,** *126*, 430-439.
20. Xiong, Q.; Ye, L.; Zhang, P.; Lepley, M.; Tian, J.; Li, J.; Zhang, L.; Swingen, C.; Vaughan, J. T.; Kaufman, D. S., *et al.* Functional consequences of human induced pluripotent stem cell therapy: Myocardial atp turnover rate in the in vivo swine heart with postinfarction remodeling. *Circulation* **2013,** *127*, 997-1008.

21. Hong, K. U.; Guo, Y.; Li, Q. H.; Cao, P.; Al-Maqtari, T.; Vajravelu, B. N.; Du, J.; Book, M. J.; Zhu, X.; Nong, Y., *et al.* C-kit+ cardiac stem cells alleviate post-myocardial infarction left ventricular dysfunction despite poor engraftment and negligible retention in the recipient heart. *PLoS One* **2014,** *9*, e96725.

22. Schaefer, A.; Zwadlo, C.; Fuchs, M.; Meyer, G. P.; Lippolt, P.; Wollert, K. C.; Drexler, H. Long-term effects of intracoronary bone marrow cell transfer on diastolic function in patients after acute myocardial infarction: 5-year results from the randomized-controlled boost trial-an echocardiographic study. *Eur. J. Echocardiogr.* **2010,** *11*, 165-171.

23. Kudo, M.; Wang, Y.; Wani, M. A.; Xu, M.; Ayub, A.; Ashraf, M. Implantation of bone marrow stem cells reduces the infarction and fibrosis in ischemic mouse heart. *J. Mol. Cell. Cardiol.* **2003,** *35*, 1113-1119.

24. Orlic, D.; Kajstura, J.; Chimenti, S.; Bodine, D. M.; Leri, A.; Anversa, P. Bone marrow stem cells regenerate infarcted myocardium. *Pediatr. Transplant.* **2003,** *7 Suppl 3*, 86-88.

25. Pittenger, M. F.; Martin, B. J. Mesenchymal stem cells and their potential as cardiac therapeutics. *Circ. Res.* **2004,** *95*, 9-20.

26. Hu, X.; Yu, S. P.; Fraser, J. L.; Lu, Z.; Ogle, M. E.; Wang, J. A.; Wei, L. Transplantation of hypoxia-preconditioned mesenchymal stem cells improves infarcted heart function via enhanced survival of implanted cells and angiogenesis. *J. Thorac. Cardiovasc. Surg.* **2008,** *135*, 799-808.

27. Gnecchi, M.; He, H.; Noiseux, N.; Liang, O. D.; Zhang, L.; Morello, F.; Mu, H.; Melo, L. G.; Pratt, R. E.; Ingwall, J. S., *et al.* Evidence supporting

paracrine hypothesis for akt-modified mesenchymal stem cell-mediated cardiac protection and functional improvement. *FASEB J.* **2006,** *20*, 661-669.

28. Uemura, R.; Xu, M.; Ahmad, N.; Ashraf, M. Bone marrow stem cells prevent left ventricular remodeling of ischemic heart through paracrine signaling. *Circ. Res.* **2006,** *98*, 1414-1421.
29. Rane, A. A.; Christman, K. L. Biomaterials for the treatment of myocardial infarction: A 5-year update. *J. Am. Coll. Cardiol.* **2011,** *58*, 2615-2629.
30. Ungerleider, J. L.; Christman, K. L. Concise review: Injectable biomaterials for the treatment of myocardial infarction and peripheral artery disease: Translational challenges and progress. *Stem Cells Transl. Med.* **2014,** *3*, 1090-1099.
31. Binsalamah, Z. M.; Paul, A.; Khan, A. A.; Prakash, S.; Shum-Tim, D. Intramyocardial sustained delivery of placental growth factor using nanoparticles as a vehicle for delivery in the rat infarct model. *Int. J. Nanomedicine* **2011,** *6*, 2667-2678.
32. Che, H. L.; Muthiah, M.; Ahn, Y.; Son, S.; Kim, W. J.; Seonwoo, H.; Chung, J. H.; Cho, C. S.; Park, I. K. Biodegradable particulate delivery of vascular endothelial growth factor plasmid from polycaprolactone/polyethylenimine electrospun nanofibers for the treatment of myocardial infarction. *J. Nanosci. Nanotechnol.* **2011,** *11*, 7073-7077.
33. Davis, M. E.; Hsieh, P. C. H.; Takahashi, T.; Song, Q.; Zhang, S. G.; Kamm, R. D.; Grodzinsky, A. J.; Anversa, P.; Lee, R. T. Local myocardial insulin-like growth factor 1 (IGF-1) delivery with biotinylated peptide nanofibers improves cell therapy for myocardial infarction. *Proc. Natl. Acad. Sci. U.S.A.* **2006,** *103*, 8155-8160.

34. Hao, X. J.; Silva, E. A.; Mansson-Broberg, A.; Grinnemo, K. H.; Siddiqui, A. J.; Dellgren, G.; Wardell, E.; Brodin, L. A.; Mooney, D. J.; Sylven, C. Angiogenic effects of sequential release of VEGF-A(165) and PDGF-BB with alginate hydrogels after myocardial infarction. *Cardiovasc. Res.* **2007,** *75*, 178-185.

35. Hsieh, P. C. H.; Davis, M. E.; Gannon, J.; MacGillivray, C.; Lee, R. T. Controlled delivery of PDGF-BB for myocardial protection using injectable self-assembling peptide nanofibers. *J. Clin. Invest.* **2006,** *116*, 237-248.

36. Kraehenbuehl, T. P.; Zammaretti, P.; Van der Vlies, A. J.; Schoenmakers, R. G.; Lutolf, M. P.; Jaconi, M. E.; Hubbell, J. A. Three-dimensional extracellular matrix-directed cardioprogenitor differentiation: Systematic modulation of a synthetic cell-responsive peg-hydrogel. *Biomaterials* **2008,** *29*, 2757-2766.

37. Tokunaga, M.; Liu, M. L.; Nagai, T.; Iwanaga, K.; Matsuura, K.; Takahashi, T.; Kanda, M.; Kondo, N.; Wang, P.; Naito, A. T., *et al.* Implantation of cardiac progenitor cells using self-assembling peptide improves cardiac function after myocardial infarction. *J. Mol. Cell. Cardiol.* **2010,** *49*, 972-983.

38. Au, H. T.; Cheng, I.; Chowdhury, M. F.; Radisic, M. Interactive effects of surface topography and pulsatile electrical field stimulation on orientation and elongation of fibroblasts and cardiomyocytes. *Biomaterials* **2007,** *28*, 4277-4293.

39. Zong, X. H.; Bien, H.; Chung, C. Y.; Yin, L. H.; Fang, D. F.; Hsiao, B. S.; Chu, B.; Entcheva, E. Electrospun fine-textured scaffolds for heart tissue constructs. *Biomaterials* **2005,** *26*, 5330-5338.

40. Hsiao, C. W.; Bai, M. Y.; Chang, Y.; Chung, M. F.; Lee, T. Y.; Wu, C. T.; Maiti, B.; Liao, Z. X.; Li, R. K.; Sung, H. W. Electrical coupling of isolated

cardiomyocyte clusters grown on aligned conductive nanofibrous meshes for their synchronized beating. *Biomaterials* **2013,** *34*, 1063-1072.

41. Kim, D. H.; Kshitiz; Smith, R. R.; Kim, P.; Ahn, E. H.; Kim, H. N.; Marban, E.; Suh, K. Y.; Levchenko, A. Nanopatterned cardiac cell patches promote stem cell niche formation and myocardial regeneration. *Integr. Biol.* **2012,** *4*, 1019-1033.
42. Lin, Y. D.; Ko, M. C.; Wu, S. T.; Li, S. F.; Hu, J. F.; Lai, Y. J.; Harn, H. I. C.; Laio, I. C.; Yeh, M. L.; Yeh, H. I., *et al.* A nanopatterned cell-seeded cardiac patch prevents electro-uncoupling and improves the therapeutic efficacy of cardiac repair. *Biomater. Sci.* **2014,** *2*, 567-580.
43. Stout, D. A.; Basu, B.; Webster, T. J. Poly(lactic-co-glycolic acid): Carbon nanofiber composites for myocardial tissue engineering applications. *Acta Biomater.* **2011,** *7*, 3101-3112.
44. Wickham, A. M.; Islam, M. M.; Mondal, D.; Phopase, J.; Sadhu, V.; Tamas, E.; Polisetti, N.; Richter-Dahlfors, A.; Liedberg, B.; Griffith, M. Polycaprolactone-thiophene-conjugated carbon nanotube meshes as scaffolds for cardiac progenitor cells. *J. Biomed. Mater. Res.* **2014,** *102*, 1553-1561.
45. You, J. O.; Rafat, M.; Ye, G. J.; Auguste, D. T. Nanoengineering the heart: Conductive scaffolds enhance connexin 43 expression. *Nano Lett.* **2011,** *11*, 3643-3648.
46. Dvir, T.; Timko, B. P.; Brigham, M. D.; Naik, S. R.; Karajanagi, S. S.; Levy, O.; Jin, H. W.; Parker, K. K.; Langer, R.; Kohane, D. S. Nanowired three-dimensional cardiac patches. *Nat. Nanotechnol.* **2011,** *6*, 720-725.
47. Mooney, E.; Mackle, J. N.; Blond, D. J. P.; O'Cearbhaill, E.; Shaw, G.; Blau, W. J.; Barry, F. P.; Barron, V.; Murphy, J. M. The electrical stimulation of

carbon nanotubes to provide a cardiomimetic cue to mscs. *Biomaterials* **2012,** *33*, 6132-6139.

48. Martins, A. M.; Eng, G.; Caridade, S. G.; Mano, J. F.; Reis, R. L.; Vunjak-Novakovic, G. Electrically conductive chitosan/carbon scaffolds for cardiac tissue engineering. *Biomacromolecules* **2014,** *15*, 635-643.
49. Crowder, S. W.; Liang, Y.; Rath, R.; Park, A. M.; Maltais, S.; Pintauro, P. N.; Hofmeister, W.; Lim, C. C.; Wang, X. T.; Sung, H. J. Poly(epsilon-caprolactone)-carbon nanotube composite scaffolds for enhanced cardiac differentiation of human mesenchymal stem cells. *Nanomed.* **2013,** *8*, 1763-1776.
50. Kharaziha, M.; Shin, S. R.; Nikkhah, M.; Topkaya, S. N.; Masoumi, N.; Annabi, N.; Dokmeci, M. R.; Khademhosseini, A. Tough and flexible cnt-polymeric hybrid scaffolds for engineering cardiac constructs. *Biomaterials* **2014,** *35*, 7346-7354.
51. Han, J.; Kim, B.; Shin, J. Y.; Ryu, S.; Noh, M.; Woo, J.; Park, J. S.; Lee, Y.; Lee, N.; Hyeon, T., *et al.* Iron oxide nanoparticle-mediated development of cellular gap junction crosstalk to improve mesenchymal stem cells' therapeutic efficacy for myocardial infarction. *ACS Nano* **2015,** *9*, 2805–2819.
52. Hare, J. M.; Fishman, J. E.; Gerstenblith, G.; DiFede Velazquez, D. L.; Zambrano, J. P.; Suncion, V. Y.; Tracy, M.; Ghersin, E.; Johnston, P. V.; Brinker, J. A., *et al.* Comparison of allogeneic vs autologous bone marrow-derived mesenchymal stem cells delivered by transendocardial injection in patients with ischemic cardiomyopathy: The poseidon randomized trial. *JAMA* **2012,** *308*, 2369-2379.

53. Houtgraaf, J. H.; den Dekker, W. K.; van Dalen, B. M.; Springeling, T.; de Jong, R.; van Geuns, R. J.; Geleijnse, M. L.; Fernandez-Aviles, F.; Zijlsta, F.; Serruys, P. W., *et al.* First experience in humans using adipose tissue-derived regenerative cells in the treatment of patients with st-segment elevation myocardial infarction. *J. Am. Coll. Cardiol.* **2012,** *59*, 539-540.

54. Wollert, K. C.; Drexler, H. Clinical applications of stem cells for the heart. *Circ. Res.* **2005,** *96*, 151-163.

55. Laflamme, M. A.; Murry, C. E. Heart regeneration. *Nature* **2011,** *473*, 326-335.

56. Zeng, L. P.; Hu, Q. S.; Wang, X. H.; Mansoor, A.; Lee, J.; Feygin, J.; Zhang, G.; Suntharalingam, P.; Boozer, S.; Mhashilkar, A., *et al.* Bioenergetic and functional consequences of bone marrow-derived multipotent progenitor cell transplantation in hearts with postinfarction left ventricular remodeling. *Circulation* **2007,** *115*, 1866-1875.

57. Anthony, D. F.; Shiels, P. G. Exploiting paracrine mechanisms of tissue regeneration to repair damaged organs. *Transplant. Res.* **2013,** *2*, 10.

58. Baraniak, P. R.; McDevitt, T. C. Stem cell paracrine actions and tissue regeneration. *Regen. Med.* **2010,** *5*, 121-143.

59. Ratajczak, M. Z.; Kucia, M.; Jadczyk, T.; Greco, N. J.; Wojakowski, W.; Tendera, M.; Ratajczak, J. Pivotal role of paracrine effects in stem cell therapies in regenerative medicine: Can we translate stem cell-secreted paracrine factors and microvesicles into better therapeutic strategies? *Leukemia* **2012,** *26*, 1166-1173.

60. Amado, L. C.; Saliaris, A. P.; Schuleri, K. H.; St John, M.; Xie, J. S.; Cattaneo, S.; Durand, D. J.; Fitton, T.; Kuang, J. Q.; Stewart, G., *et al.* Cardiac repair

with intramyocardial injection of allogeneic mesenchymal stem cells after myocardial infarction. *Proc. Natl. Acad. Sci. U.S.A.* **2005,** *102*, 11474-11479.

61. Nishiyama, N.; Miyoshi, S.; Hida, N.; Uyama, T.; Okamoto, K.; Ikegami, Y.; Miyado, K.; Segawa, K.; Terai, M.; Sakamoto, M., *et al.* The significant cardiomyogenic potential of human umbilical cord blood-derived mesenchymal stem cells in vitro. *Stem Cells* **2007,** *25*, 2017-2024.
62. Antonitsis, P.; Ioannidou-Papagiannaki, E.; Kaidoglou, A.; Papakonstantinou, C. In vitro cardiomyogenic differentiation of adult human bone marrow mesenchymal stem cells. The role of 5-azacytidine. *Interact. Cardiovasc. Thorac. Surg.* **2007,** *6*, 593-597.
63. Xu, W. R.; Zhang, X. R.; Qian, H.; Zhu, W.; Sun, X. C.; Hu, J.; Zhou, H.; Chen, Y. C. Mesenchymal stem cells from adult human bone marrow differentiate into a cardiomyocyte phenotype in vitro. *Exp. Biol. Med.* **2004,** *229*, 623-631.
64. Huang, Y.; Jia, X. L.; Bai, K.; Gong, X. H.; Fan, Y. B. Effect of fluid shear stress on cardiomyogenic differentiation of rat bone marrow mesenchymal stem cells. *Arch. Med. Res.* **2010,** *41*, 497-505.
65. Song, H.; Hwang, H. J.; Chang, W.; Song, B. W.; Cha, M. J.; Kim, I. K.; Lim, S.; Choi, E. J.; Ham, O.; Lee, C. Y., *et al.* Cardiomyocytes from phorbol myristate acetate-activated mesenchymal stem cells restore electromechanical function in infarcted rat hearts. *Proc. Natl. Acad. Sci. U.S.A.* **2011,** *108*, 296-301.
66. Bartunek, J.; Croissant, J. D.; Wijns, W.; Gofflot, S.; de Lavareille, A.; Vanderheyden, M.; Kaluzhny, Y.; Mazouz, N.; Willemsen, P.; Penicka, M., *et al.* Pretreatment of adult bone marrow mesenchymal stem cells with

cardiomyogenic growth factors and repair of the chronically infarcted myocardium. *Am. J. Physiol. Heart Circ. Physiol.* **2007,** *292*, H1095-H1104.

67. Pijnappels, D. A.; Schalij, M. J.; Ramkisoensing, A. A.; van Tuyn, J.; de Vries, A. A.; van der Laarse, A.; Ypey, D. L.; Atsma, D. E. Forced alignment of mesenchymal stem cells undergoing cardiomyogenic differentiation affects functional integration with cardiomyocyte cultures. *Circ. Res.* **2008,** *103*, 167-176.

68. Yoon, Y. S.; Wecker, A.; Heyd, L.; Park, J. S.; Tkebuchava, T.; Kusano, K.; Hanley, A.; Scadova, H.; Qin, G. J.; Cha, D. H., *et al.* Clonally expanded novel multipotent stem cells from human bone marrow regenerate myocardium after myocardial infarction. *J. Clin. Invest.* **2005,** *115*, 326-338.

69. Zhang, D. Z.; Gai, L. Y.; Liu, H. W.; Jin, Q. H.; Huang, J. H.; Zhu, X. Y. Transplantation of autologous adipose-derived stem cells ameliorates cardiac function in rabbits with myocardial infarction. *Chin. Med. J.* **2007,** *120*, 300-307.

70. Duran, J. M.; Makarewich, C. A.; Sharp, T. E.; Starosta, T.; Zhu, F.; Hoffman, N. E.; Chiba, Y.; Madesh, M.; Berretta, R. M.; Kubo, H. Bone-derived stem cells repair the heart after myocardial infarction through transdifferentiation and paracrine signaling mechanisms. *Circ. Res.* **2013,** *113*, 539-552.

71. Gnecchi, M.; Zhang, Z.; Ni, A.; Dzau, V. J. Paracrine mechanisms in adult stem cell signaling and therapy. *Circ. Res.* **2008,** *103*, 1204-1219.

72. Zamilpa, R.; Navarro, M. M.; Flores, I.; Griffey, S. Stem cell mechanisms during left ventricular remodeling post-myocardial infarction: Repair and regeneration. *World J. Cardiol.* **2014,** *6*, 610-620.

73. Bhang, S. H.; Cho, S. W.; La, W. G.; Lee, T. J.; Yang, H. S.; Sun, A. Y.; Baek, S. H.; Rhie, J. W.; Kim, B. S. Angiogenesis in ischemic tissue produced by spheroid grafting of human adipose-derived stromal cells. *Biomaterials* **2011,** *32*, 2734-2747.

74. Hwang, H. J.; Chang, W.; Song, B. W.; Song, H.; Cha, M. J.; Kim, I. K.; Lim, S.; Choi, E. J.; Ham, O.; Lee, S. Y., *et al.* Antiarrhythmic potential of mesenchymal stem cell is modulated by hypoxic environment. *J. Am. Coll. Cardiol.* **2012,** *60*, 1698-1706.

75. Kinnaird, T.; Stabile, E.; Burnett, M. S.; Lee, C. W.; Barr, S.; Fuchs, S.; Epstein, S. E. Marrow-derived stromal cells express genes encoding a broad spectrum of arteriogenic cytokines and promote in vitro and in vivo arteriogenesis through paracrine mechanisms. *Circ. Res.* **2004,** *94*, 678-685.

76. Zhao, S. L.; Zhang, Y. J.; Li, M. H.; Zhang, X. L.; Chen, S. L. Mesenchymal stem cells with overexpression of midkine enhance cell survival and attenuate cardiac dysfunction in a rat model of myocardial infarction. *Stem Cell Res. Ther.* **2014,** *5*, 37.

77. Paul, A.; Hasan, A.; Al Kindi, H.; Gaharwar, A. K.; Rao, V. T. S.; Nikkhah, M.; Shin, S. R.; Krafft, D.; Dokmeci, M. R.; Shum-Tim, D., *et al.* Injectable graphene oxide/hydrogel-based angiogenic gene delivery system for vasculogenesis and cardiac repair. *ACS Nano* **2014,** *8*, 8050-8062.

78. Zhang, G.; Nakamura, Y.; Wang, X. H.; Hu, Q. S.; Suggs, L. J.; Zhang, J. Y. Controlled release of stromal cell-derived factor-1alpha in situ increases c-kit(+) cell homing to the infarcted heart. *Tissue Eng.* **2007,** *13*, 2063-2071.

79. Zhang, Y.; Li, W.; Ou, L.; Wang, W.; Delyagina, E.; Lux, C.; Sorg, H.; Riehemann, K.; Steinhoff, G.; Ma, N. Targeted delivery of human vegf gene

via complexes of magnetic nanoparticle-adenoviral vectors enhanced cardiac regeneration. *PLoS One* **2012,** *7*, e39490.

80. Ye, L.; Haider, H. K.; Tan, R.; Toh, W.; Law, P. K.; Tan, W.; Su, L.; Zhang, W.; Ge, R.; Zhang, Y., *et al.* Transplantation of nanoparticle transfected skeletal myoblasts overexpressing vascular endothelial growth factor-165 for cardiac repair. *Circulation* **2007,** *116*, I113-I120.
81. Padin-Iruegas, M. E.; Misao, Y.; Davis, M. E.; Segers, V. F. M.; Esposito, G.; Tokunou, T.; Urbanek, K.; Hosoda, T.; Rota, M.; Anversa, P., *et al.* Cardiac progenitor cells and biotinylated insulin-like growth factor-1 nanofibers improve endogenous and exogenous myocardial regeneration after infarction. *Circulation* **2009,** *120*, 876-887.
82. Paul, A.; Nayan, M.; Khan, A. A.; Shum-Tim, D.; Prakash, S. Angiopoietin-1-expressing adipose stem cells genetically modified with baculovirus nanocomplex: Investigation in rat heart with acute infarction. *Int. J. Nanomedicine* **2012,** *7*, 663-682.
83. Huang, Y. C.; Liu, T. J. Mobilization of mesenchymal stem cells by stromal cell-derived factor-1 released from chitosan/tripolyphosphate/fucoidan nanoparticles. *Acta Biomater.* **2012,** *8*, 1048-1056.
84. Abbott, J. D.; Huang, Y.; Liu, D.; Hickey, R.; Krause, D. S.; Giordano, F. J. Stromal cell-derived factor-1 alpha plays a critical role in stem cell recruitment to the heart after myocardial infarction but is not sufficient to induce homing in the absence of injury. *Circulation* **2004,** *110*, 3300-3305.
85. Schober, A.; Knarren, S.; Lietz, M.; Lin, E. A.; Weber, C. Crucial role of stromal cell-derived factor-1 alpha in neointima formation after vascular injury in apolipoprotein-e-deficient mice. *J. Vasc. Res.* **2004,** *41*, 104-104.

86. Segers, V. F.; Tokunou, T.; Higgins, L. J.; MacGillivray, C.; Gannon, J.; Lee, R. T. Local delivery of protease-resistant stromal cell derived factor-1 for stem cell recruitment after myocardial infarction. *Circulation* **2007,** *116*, 1683-1692.

87. Terrovitis, J.; Lautamaki, R.; Bonios, M.; Fox, J.; Engles, J. M.; Yu, J.; Leppo, M. K.; Pomper, M. G.; Wahl, R. L.; Seidel, J., *et al.* Noninvasive quantification and optimization of acute cell retention by in vivo positron emission tomography after intramyocardial cardiac-derived stem cell delivery. *J. Am. Coll. Cardiol.* **2009,** *54*, 1619-1626.

88. Lee, W. Y.; Wei, H. J.; Lin, W. W.; Yeh, Y. C.; Hwang, S. M.; Wang, J. J.; Tsai, M. S.; Chang, Y.; Sung, H. W. Enhancement of cell retention and functional benefits in myocardial infarction using human amniotic-fluid stem-cell bodies enriched with endogenous ecm. *Biomaterials* **2011,** *32*, 5558-5567.

89. Karam, J. P.; Muscari, C.; Montero-Menei, C. N. Combining adult stem cells and polymeric devices for tissue engineering in infarcted myocardium. *Biomaterials* **2012,** *33*, 5683-5695.

90. Ruvinov, E.; Harel-Adar, T.; Cohen, S. Bioengineering the infarcted heart by applying bio-inspired materials. *J Cardiovasc. Transl. Res.* **2011,** *4*, 559-574.

91. Chiu, L. L.; Iyer, R. K.; Reis, L. A.; Nunes, S. S.; Radisic, M. Cardiac tissue engineering: Current state and perspectives. *Front. Biosci.* **2012,** *17*, 1533-1550.

92. Simpson, D.; Liu, H.; Fan, T. H.; Nerem, R.; Dudley, S. C., Jr. A tissue engineering approach to progenitor cell delivery results in significant cell engraftment and improved myocardial remodeling. *Stem Cells* **2007,** *25*, 2350-2357.

93. Jin, J.; Jeong, S. I.; Shin, Y. M.; Lim, K. S.; Lee, Y. M.; Koh, H. C.; Kim, K. S. Transplantation of mesenchymal stem cells within a poly (lactide-co-ε-caprolactone) scaffold improves cardiac function in a rat myocardial infarction model. *Eur. J. Heart Fail.* **2009,** *11*, 147-153.

94. Fujimoto, K. L.; Tobita, K.; Merryman, W. D.; Guan, J.; Momoi, N.; Stolz, D. B.; Sacks, M. S.; Keller, B. B.; Wagner, W. R. An elastic, biodegradable cardiac patch induces contractile smooth muscle and improves cardiac remodeling and function in subacute myocardial infarction. *J. Am. Coll. Cardiol.* **2007,** *49*, 2292-2300.

95. Piao, H.; Kwon, J. S.; Piao, S.; Sohn, J. H.; Lee, Y. S.; Bae, J. W.; Hwang, K. K.; Kim, D. W.; Jeon, O.; Kim, B. S., *et al.* Effects of cardiac patches engineered with bone marrow-derived mononuclear cells and pgcl scaffolds in a rat myocardial infarction model. *Biomaterials* **2007,** *28*, 641-649.

96. Lin, Y. D.; Yeh, M. L.; Yang, Y. J.; Tsai, D. C.; Chu, T. Y.; Shih, Y. Y.; Chang, M. Y.; Liu, Y. W.; Tang, A. C.; Chen, T. Y., *et al.* Intramyocardial peptide nanofiber injection improves postinfarction ventricular remodeling and efficacy of bone marrow cell therapy in pigs. *Circulation* **2010,** *122*, S132-141.

97. Dubois, G.; Segers, V. F.; Bellamy, V.; Sabbah, L.; Peyrard, S.; Bruneval, P.; Hagege, A. A.; Lee, R. T.; Menasche, P. Self-assembling peptide nanofibers and skeletal myoblast transplantation in infarcted myocardium. *J. Biomed. Mater. Res. B Appl. Biomater.* **2008,** *87*, 222-228.

98. Cui, X. J.; Xie, H.; Wang, H. J.; Guo, H. D.; Zhang, J. K.; Wang, C.; Tan, Y. Z. Transplantation of mesenchymal stem cells with self-assembling

polypeptide scaffolds is conducive to treating myocardial infarction in rats. *Tohoku J. Exp. Med.* **2010,** *222*, 281-289.

99. Guo, H. D.; Cui, G. H.; Wang, H. J.; Tan, Y. Z. Transplantation of marrow-derived cardiac stem cells carried in designer self-assembling peptide nanofibers improves cardiac function after myocardial infarction. *Biochem. Biophys. Res. Commun.* **2010,** *399*, 42-48.
100. Chen, H. S.; Kim, C.; Mercola, M. Electrophysiological challenges of cell-based myocardial repair. *Circulation* **2009,** *120*, 2496-2508.
101. Kang, B. J.; Kim, H.; Lee, S. K.; Kim, J.; Shen, Y.; Jung, S.; Kang, K. S.; Im, S. G.; Lee, S. Y.; Choi, M., *et al.* Umbilical-cord-blood-derived mesenchymal stem cells seeded onto fibronectin-immobilized polycaprolactone nanofiber improve cardiac function. *Acta Biomater.* **2014,** *10*, 3007-3017.
102. Ravichandran, R.; Venugopal, J. R.; Mueller, M.; Sundarrajan, S.; Mukherjee, S.; Pliska, D.; Wintermantel, E.; Ramakrishna, S. Buckled structures and 5-azacytidine enhance cardiogenic differentiation of adipose-derived stem cells. *Nanomed.* **2013,** *8*, 1985-1997.
103. Shin, K. H.; Jang, Y.; Kim, B. S.; Jang, J.; Kim, S. H. Highly conductive reduced graphene oxide produced via pressure-assisted reduction at mild temperature for flexible and transparent electrodes. *Chem. Commun.* **2013,** *49*, 4887-4889.
104. Bandaru, P. R. Electrical properties and applications of carbon nanotube structures. *J. Nanosci. Nanotechnol.* **2007,** *7*, 1239-1267.
105. Shevach, M.; Fleischer, S.; Shapira, A.; Dvir, T. Gold nanoparticle-decellularized matrix hybrids for cardiac tissue engineering. *Nano Lett.* **2014,** *14*, 5792-5796.

106. Severs, N. J.; Bruce, A. F.; Dupont, E.; Rothery, S. Remodelling of gap junctions and connexin expression in diseased myocardium. *Cardiovasc. Res.* **2008,** *80*, 9-19.

107. Webber, M. J.; Han, X. Q.; Murthy, S. N. P.; Rajangam, K.; Stupp, S. I.; Lomasney, J. W. Capturing the stem cell paracrine effect using heparin-presenting nanofibres to treat cardiovascular diseases. *J. Tissue Eng. Regen. Med.* **2010,** *4*, 600-610.

108. Song, D.; Liu, X.; Liu, R.; Yang, L.; Zuo, J.; Liu, W. Connexin 43 hemichannel regulates H9C2 cell proliferation by modulating intracellular atp and [Ca2+]. *Acta Biochim. Biophys. Sin.* **2010,** *42*, 472-482.

109. Christman, J. K. 5-azacytidine and 5-aza-2 '-deoxycytidine as inhibitors of DNA methylation: Mechanistic studies and their implications for cancer therapy. *Oncogene* **2002,** *21*, 5483-5495.

110. Yoon, H. H.; Bhang, S. H.; Kim, T.; Yu, T.; Hyeon, T.; Kim, B. S. Dual roles of graphene oxide in chondrogenic differentiation of adult stem cells: Cell-adhesion substrate and growth factor-delivery carrier. *Adv. Funct. Mater.* **2014,** *24*, 6455-6464.

111. Yamada, K.; Green, K. G.; Samarel, A. M.; Saffitz, J. E. Distinct pathways regulate expression of cardiac electrical and mechanical junction proteins in response to stretch. *Circ. Res.* **2005,** *97*, 346-353.

112. Mitra, S. K.; Schlaepfer, D. D. Integrin-regulated fak-src signaling in normal and cancer cells. *Curr. Opin. Cell Biol.* **2006,** *18*, 516-523.

113. You, J.-O.; Rafat, M.; Ye, G. J. C.; Auguste, D. T. Nanoengineering the heart: Conductive scaffolds enhance connexin 43 expression. *Nano Lett.* **2011,** *11*, 3643-3648.

114. Singelyn, J. M.; DeQuach, J. A.; Seif-Naraghi, S. B.; Littlefield, R. B.; Schup-Magoffin, P. J.; Christman, K. L. Naturally derived myocardial matrix as an injectable scaffold for cardiac tissue engineering. *Biomaterials* **2009,** *30*, 5409-5416.

115. Martens, T. P.; Godier, A. F. G.; Parks, J. J.; Wan, L. Q.; Koeckert, M. S.; Eng, G. M.; Hudson, B. I.; Sherman, W.; Vunjak-Novakovic, G. Percutaneous cell delivery into the heart using hydrogels polymerizing in situ. *Cell Transplant.* **2009,** *18*, 297-304.

116. Geim, A. K.; Novoselov, K. S. The rise of graphene. *Nat. Mater.* **2007,** *6*, 183-191.

117. Choi, W.; Lahiri, I.; Seelaboyina, R.; Kang, Y. S. Synthesis of graphene and its applications: A review. *Crit. Rev. Solid State Mater. Sci.* **2010,** *35*, 52-71.

118. Jakus, A. E.; Secor, E. B.; Rutz, A. L.; Jordan, S. W.; Hersam, M. C.; Shah, R. N. Three-dimensional printing of high-content graphene scaffolds for electronic and biomedical applications. *ACS Nano* **2015,** *9*, 4636-4648.

119. Geim, A. K. Graphene: Status and prospects. *Science* **2009,** *324*, 1530-1534.

120. Zhang, Y.; Nayak, T. R.; Hong, H.; Cai, W. Graphene: A versatile nanoplatform for biomedical applications. *Nanoscale* **2012,** *4*, 3833-3842.

121. Kalbacova, M.; Broz, A.; Kong, J.; Kalbac, M. Graphene substrates promote adherence of human osteoblasts and mesenchymal stromal cells. *Carbon* **2010,** *48*, 4323-4329.

122. Ryoo, S. R.; Kim, Y. K.; Kim, M. H.; Min, D. H. Behaviors of nih-3t3 fibroblasts on graphene/carbon nanotubes: Proliferation, focal adhesion, and gene transfection studies. *ACS Nano* **2010,** *4*, 6587-6598.

123. Nayak, T. R.; Andersen, H.; Makam, V. S.; Khaw, C.; Bae, S.; Xu, X. F.; Ee, P. L. R.; Ahn, J. H.; Hong, B. H.; Pastorin, G., *et al.* Graphene for controlled and accelerated osteogenic differentiation of human mesenchymal stem cells. *ACS Nano* **2011,** *5*, 4670-4678.

124. Lee, W. C.; Lim, C. H.; Shi, H.; Tang, L. A.; Wang, Y.; Lim, C. T.; Loh, K. P. Origin of enhanced stem cell growth and differentiation on graphene and graphene oxide. *ACS Nano* **2011,** *5*, 7334-7341.

125. Shi, X. T.; Chang, H. X.; Chen, S.; Lai, C.; Khademhosseini, A.; Wu, H. K. Regulating cellular behavior on few-layer reduced graphene oxide films with well-controlled reduction states. *Adv. Funct. Mater.* **2012,** *22*, 751-759.

126. Tang, L. A. L.; Lee, W. C.; Shi, H.; Wong, E. Y. L.; Sadovoy, A.; Gorelik, S.; Hobley, J.; Lim, C. T.; Loh, K. P. Highly wrinkled cross-linked graphene oxide membranes for biological and charge-storage applications. *Small* **2012,** *8*, 423-431.

127. Li, N.; Zhang, X. M.; Song, Q.; Su, R. G.; Zhang, Q.; Kong, T.; Liu, L. W.; Jin, G.; Tang, M. L.; Cheng, G. S. The promotion of neurite sprouting and outgrowth of mouse hippocampal cells in culture by graphene substrates. *Biomaterials* **2011,** *32*, 9374-9382.

128. Park, S. Y.; Park, J.; Sim, S. H.; Sung, M. G.; Kim, K. S.; Hong, B. H.; Hong, S. Enhanced differentiation of human neural stem cells into neurons on graphene. *Adv. Mater.* **2011,** *23*, H263-H267.

129. Wang, Y.; Lee, W. C.; Manga, K. K.; Ang, P. K.; Lu, J.; Liu, Y. P.; Lim, C. T.; Loh, K. P. Fluorinated graphene for promoting neuro-induction of stem cells. *Adv. Mater.* **2012,** *24*, 4285-+.

130. Ku, S. H.; Park, C. B. Myoblast differentiation on graphene oxide. *Biomaterials* **2013,** *34*, 2017-2023.

131. Chen, G. Y.; Pang, D. W. P.; Hwang, S. M.; Tuan, H. Y.; Hu, Y. C. A graphene-based platform for induced pluripotent stem cells culture and differentiation. *Biomaterials* **2012,** *33*, 418-427.

132. Zhang, L.; Wang, Z. P.; Xu, C.; Li, Y.; Gao, J. P.; Wang, W.; Liu, Y. High strength graphene oxide/polyvinyl alcohol composite hydrogels. *J. Mater. Chem.* **2011,** *21*, 10399-10406.

133. Lu, B. G.; Li, T.; Zhao, H. T.; Li, X. D.; Gao, C. T.; Zhang, S. X.; Xie, E. Q. Graphene-based composite materials beneficial to wound healing. *Nanoscale* **2012,** *4*, 2978-2982.

134. La, W. G.; Park, S.; Yoon, H. H.; Jeong, G. J.; Lee, T. J.; Bhang, S. H.; Han, J. Y.; Char, K.; Kim, B. S. Delivery of a therapeutic protein for bone regeneration from a substrate coated with graphene oxide. *Small* **2013,** *9*, 4051–4060.

135. Hummers, W. S.; Offeman, R. E. Preparation of graphitic oxide. *J. Am. Chem. Soc.* **1958,** *80*, 1339-1339.

136. Del Duca, D.; Werbowetski, T.; Del Maestro, R. F. Spheroid preparation from hanging drops: Characterization of a model of brain tumor invasion. *J. Neurooncol.* **2004,** *67*, 295-303.

137. Chang, W.; Song, B. W.; Lim, S.; Song, H.; Shim, C. Y.; Cha, M. J.; Ahn, D. H.; Jung, Y. G.; Lee, D. H.; Chung, J. H., *et al.* Mesenchymal stem cells pretreated with delivered Hph-1-Hsp70 protein are protected from hypoxia-mediated cell death and rescue heart functions from myocardial injury. *Stem Cells* **2009,** *27*, 2283-2292.

138. Psaltis, P. J.; Zannettino, A. C.; Worthley, S. G.; Gronthos, S. Concise review: Mesenchymal stromal cells: Potential for cardiovascular repair. *Stem Cells* **2008,** *26*, 2201-2210.

139. Kim, H. N.; Jiao, A.; Hwang, N. S.; Kim, M. S.; Kang, D. H.; Kim, D. H.; Suh, K. Y. Nanotopography-guided tissue engineering and regenerative medicine. *Adv. Drug Delivery Rev.* **2012,** *65*, 36-558.

140. Kim, J.; Kim, Y. R.; Kim, Y.; Lim, K. T.; Seonwoo, H.; Park, S.; Cho, S. P.; Hong, B. H.; Choung, P. H.; Chung, T. D., *et al.* Graphene-incorporated chitosan substrata for adhesion and differentiation of human mesenchymal stem cells. *J. Mater. Chem.* **2013,** *1*, 933-938.

141. Kim, J.; Choi, K. S.; Kim, Y.; Lim, K. T.; Seonwoo, H.; Park, Y.; Kim, D. H.; Choung, P. H.; Cho, C. S.; Kim, S. Y., *et al.* Bioactive effects of graphene oxide cell culture substratum on structure and function of human adipose-derived stem cells. *J. Biomed. Mater. Res. A* **2013,** *101*, 3520-3530.

142. Orza, A.; Soritau, O.; Olenic, L.; Diudea, M.; Florea, A.; Ciuca, D. R.; Mihu, C.; Casciano, D.; Biris, A. S. Electrically conductive gold-coated collagen nanofibers for placental-derived mesenchymal stem cells enhanced differentiation and proliferation. *ACS Nano* **2011,** *5*, 4490-4503.

143. Engler, A. J.; Sen, S.; Sweeney, H. L.; Discher, D. E. Matrix elasticity directs stem cell lineage specification. *Cell* **2006,** *126*, 677-689.

144. Martino, M. M.; Mochizuki, M.; Rothenfluh, D. A.; Rempel, S. A.; Hubbell, J. A.; Barker, T. H. Controlling integrin specificity and stem cell differentiation in 2d and 3d environments through regulation of fibronectin domain stability. *Biomaterials* **2009,** *30*, 1089-1097.

145. Ogura, N.; Kawada, M.; Chang, W. J.; Zhang, Q.; Lee, S. Y.; Kondoh, T.; Abiko, Y. Differentiation of the human mesenchymal stem cells derived from bone marrow and enhancement of cell attachment by fibronectin. *J. Oral Sci.* **2004,** *46*, 207-213.

146. Moore, L.; Fan, D.; Basu, R.; Kandalam, V.; Kassiri, Z. Tissue inhibitor of metalloproteinases (TIMPs) in heart failure. *Heart Fail. Rev.* **2012,** *17*, 693-706.

147. van Laake, L. W.; van Donselaar, E. G.; Monshouwer-Kloots, J.; Schreurs, C.; Passier, R.; Humbel, B. M.; Doevendans, P. A.; Sonnenberg, A.; Verkleij, A. J.; Mummery, C. L. Extracellular matrix formation after transplantation of human embryonic stem cell-derived cardiomyocytes. *Cell. Mol. Life Sci.* **2010,** *67*, 277-290.

148. Kurazumi, H.; Kubo, M.; Ohshima, M.; Yamamoto, Y.; Takemoto, Y.; Suzuki, R.; Ikenaga, S.; Mikamo, A.; Udo, K.; Hamano, K., *et al.* The effects of mechanical stress on the growth, differentiation, and paracrine factor production of cardiac stem cells. *PLoS One* **2011,** *6*, e28890.

149. Eghbali, M.; Weber, K. T. Collagen and the myocardium: Fibrillar structure, biosynthesis and degradation in relation to hypertrophy and its regression. *Mol. Cell. Biochem.* **1990,** *96*, 1-14.

150. Sato, H.; Takahashi, M.; Ise, H.; Yamada, A.; Hirose, S.; Tagawa, Y.; Morimoto, H.; Izawa, A.; Ikeda, U. Collagen synthesis is required for ascorbic acid-enhanced differentiation of mouse embryonic stem cells into cardiomyocytes. *Biochem. Biophys. Res. Commun.* **2006,** *342*, 107-112.

151. Horton, R. E.; Auguste, D. T. Synergistic effects of hypoxia and extracellular matrix cues in cardiomyogenesis. *Biomaterials* **2012,** *33*, 6313-6319.

152. Malan, D.; Reppel, M.; Dobrowolski, R.; Roell, W.; Smyth, N.; Hescheler, J.; Paulsson, M.; Bloch, W.; Fleischmann, B. K. Lack of laminin γ1 in embryonic stem cell-derived cardiomyocytes causes inhomogeneous electrical spreading despite intact differentiation and function. *Stem Cells* **2009,** *27*, 88-99.

153. Subauste, M. C.; Pertz, O.; Adamson, E. D.; Turner, C. E.; Junger, S.; Hahn, K. M. Vinculin modulation of paxillin-fak interactions regulates erk to control survival and motility. *The Journal of cell biology* **2004,** *165*, 371-381.

154. Hynes, R. O. Integrins - versatility, modulation, and signaling in cell-adhesion. *Cell* **1992,** *69*, 11-25.

155. Schaller, M. D.; Hildebrand, J. D.; Shannon, J. D.; Fox, J. W.; Vines, R. R.; Parsons, J. T. Autophosphorylation of the focal adhesion kinase, pp125FAK, directs sh2-dependent binding of pp60Src. *Mol. Cell. Biol.* **1994,** *14*, 1680-1688.

156. Chen, H. C.; Appeddu, P. A.; Isoda, H.; Guan, J. L. Phosphorylation of tyrosine 397 in focal adhesion kinase is required for binding phosphatidylinositol 3-kinase. *J. Biol. Chem.* **1996,** *271*, 26329-26334.

157. Thannickal, V. J.; Lee, D. Y.; White, E. S.; Cui, Z.; Larios, J. M.; Chacon, R.; Horowitz, J. C.; Day, R. M.; Thomas, P. E. Myofibroblast differentiation by transforming growth factor-beta 1 is dependent on cell adhesion and integrin signaling via focal adhesion kinase. *J. Biol. Chem.* **2003,** *278*, 12384-12389.

158. Cantley, L. C. The phosphoinositide 3-kinase pathway. *Science* **2002,** *296*, 1655-1657.

159. Eriksson, M.; Leppa, S. Mitogen-activated protein kinases and activator protein 1 are required for proliferation and cardiomyocyte differentiation of p19 embryonal carcinoma cells. *J. Biol. Chem.* **2002,** *277*, 15992-16001.

160. Naito, A. T.; Akazawa, H.; Takano, H.; Minamino, T.; Nagai, T.; Aburatani, H.; Komuro, I. Phosphatidylinositol 3-kinase–akt pathway plays a critical role in early cardiomyogenesis by regulating canonical wnt signaling. *Circ. Res.* **2005,** *97*, 144-151.

161. Heo, J. S.; Lee, J. C. Beta-catenin mediates cyclic strain-stimulated cardiomyogenesis in mouse embryonic stem cells through ros-dependent and integrin-mediated PI3K/Akt pathways. *J. Cell. Biochem.* **2011,** *112*, 1880-1889.

162. Naito, A. T.; Tominaga, A.; Oyamada, M.; Oyamada, Y.; Shiraishi, I.; Monzen, K.; Komuro, I.; Takamatsu, T. Early stage-specific inhibitions of cardiomyocyte differentiation and expression of Csx/Nkx-2.5 and gata-4 by phosphatidylinositol 3-kinase inhibitor LY294002. *Exp. Cell Res.* **2003,** *291*, 56-69.

163. Polesskaya, A.; Seale, P.; Rudnicki, M. A. Wnt signaling induces the myogenic specification of resident CD45+ adult stem cells during muscle regeneration. *Cell* **2003,** *113*, 841-852.

164. Bond, J.; Sedmera, D.; Jourdan, J.; Zhang, Y. H.; Eisenberg, C. A.; Eisenberg, L. M.; Gourdie, R. G. Wnt11 and wnt7a are up-regulated in association with differentiation of cardiac conduction cells in vitro and in vivo. *Dev. Dyn.* **2003,** *227*, 536-543.

165. Kim, M.-H.; Kino-oka, M.; Maruyama, N.; Saito, A.; Sawa, Y.; Taya, M. Cardiomyogenic induction of human mesenchymal stem cells by altered rho family gtpase expression on dendrimer-immobilized surface with d-glucose display. *Biomaterials* **2010,** *31*, 7666-7677.

166. Auer, M.; Hausott, B.; Klimaschewski, L. Rho gtpases as regulators of morphological neuroplasticity. *Ann. Anat.* **2011,** *193*, 259-266.

167. Orlic, D.; Kajstura, J.; Chimenti, S.; Jakoniuk, I.; Anderson, S. M.; Li, B.; Pickel, J.; McKay, R.; Nadal-Ginard, B.; Bodine, D. M., *et al.* Bone marrow cells regenerate infarcted myocardium. *Nature* **2001,** *410*, 701-705.

168. Zhou, B.; Honor, L. B.; He, H. M.; Ma, Q.; Oh, J. H.; Butterfield, C.; Lin, R. Z.; Melero-Martin, J. M.; Dolmatova, E.; Duffy, H. S., *et al.* Adult mouse epicardium modulates myocardial injury by secreting paracrine factors. *J. Clin. Invest.* **2011,** *121*, 1894-1904.

169. Nagaya, N.; Kangawa, K.; Itoh, T.; Iwase, T.; Murakami, S.; Miyahara, Y.; Fujii, T.; Uematsu, M.; Ohgushi, H.; Yamagishi, M., *et al.* Transplantation of mesenchymal stem cells improves cardiac function in a rat model of dilated cardiomyopathy. *Circulation* **2005,** *112*, 1128-1135.

170. Gandia, C.; Arminan, A.; Garcia-Verdugo, J. M.; Lledo, E.; Ruiz, A.; Minana, M. D.; Sanchez-Torrijos, J.; Paya, R.; Mirabet, V.; Carbonell-Uberos, F., *et al.* Human dental pulp stem cells improve left ventricular function, induce angiogenesis, and reduce infarct size in rats with acute myocardial infarction. *Stem Cells* **2008,** *26*, 638-645.

171. de Jong, S.; van Veen, T. A.; van Rijen, H. V.; de Bakker, J. M. Fibrosis and cardiac arrhythmias. *J. Cardiovasc. Pharmacol.* **2011,** *57*, 630-638.

172. Roell, W.; Lewalter, T.; Sasse, P.; Tallini, Y. N.; Choi, B. R.; Breitbach, M.; Doran, R.; Becher, U. M.; Hwang, S. M.; Bostani, T., *et al.* Engraftment of connexin 43-expressing cells prevents post-infarct arrhythmia. *Nature* **2007,** *450*, 819-824.

173. Wang, D. G.; Zhang, F. X.; Shen, W. Z.; Chen, M. L.; Yang, B.; Zhang, Y. Z.; Cao, K. J. Mesenchymal stem cell injection ameliorates the inducibility of ventricular arrhythmias after myocardial infarction in rats. *Int. J. Cardiol.* **2011,** *152*, 314-320.

174. Chang, M. G.; Tung, L.; Sekar, R. B.; Chang, C. Y.; Cysyk, J.; Dong, P.; Marban, E.; Abraham, M. R. Proarrhythmic potential of mesenchymal stem cell transplantation revealed in an in vitro coculture model. *Circulation* **2006,** *113*, 1832-1841.

175. Hahn, J. Y.; Cho, H. J.; Kang, H. J.; Kim, T. S.; Kim, M. H.; Chung, J. H.; Bae, J. W.; Oh, B. H.; Park, Y. B.; Kim, H. S. Pre-treatment of mesenchymal stem cells with a combination of growth factors enhances gap junction formation, cytoprotective effect on cardiomyocytes, and therapeutic efficacy for myocardial infarction. *J. Am. Coll. Cardiol.* **2008,** *51*, 933-943.

176. Potapova, I. A.; Gaudette, G. R.; Brink, P. R.; Robinson, R. B.; Rosen, M. R.; Cohen, I. S.; Doronin, S. V. Mesenchymal stem cells support migration, extracellular matrix invasion, proliferation, and survival of endothelial cells in vitro. *Stem Cells* **2007,** *25*, 1761-1768.

177. Hsu, S. H.; Huang, G. S.; Lin, S. Y. F.; Feng, F.; Ho, T. T.; Liao, Y. C. Enhanced chondrogenic differentiation potential of human gingival fibroblasts by spheroid formation on chitosan membranes. *Tissue Eng.* **2012,** *18*, 67-79.

178. Lee, E. J.; Park, S. J.; Kang, S. K.; Kim, G. H.; Kang, H. J.; Lee, S. W.; Leo, H. B.; Kim, H. S. Spherical bullet formation via E-cadherin promotes therapeutic potency of mesenchymal stem cells derived from human umbilical cord blood for myocardial infarction. *Mol. Ther.* **2012,** *20*, 1424-1433.

179. Doble, B. W.; Kardami, E. Basic fibroblast growth factor stimulates connexin-43 expression and intercellular communication of cardiac fibroblasts. *Mol. Cell. Biochem.* **1995,** *143*, 81-87.

180. Wang, M.; Cai, J.; Huang, F.; Zhu, M.; Zhang, Q.; Yang, T.; Zhang, X.; Qian, H.; Xu, W. Pre-treatment of human umbilical cord-derived mesenchymal stem cells with interleukin-6 abolishes their growth-promoting effect on gastric cancer cells. *Int. J. Mol. Med.* **2015,** *35*, 367-375.

181. Kim, K. S.; Zhao, Y.; Jang, H.; Lee, S. Y.; Kim, J. M.; Ahn, J. H.; Kim, P.; Choi, J. Y.; Hong, B. H. Large-scale pattern growth of graphene films for stretchable transparent electrodes. *Nature* **2009,** *457*, 706-710.

182. Chung, C.; Kim, Y. K.; Shin, D.; Ryoo, S. R.; Hong, B. H.; Min, D. H. Biomedical applications of graphene and graphene oxide. *Acc. Chem. Res.* **2013,** *46*, 2211-2224.

183. Sheta, E. A.; Harding, M. A.; Conaway, M. R.; Theodorescu, D. Focal adhesion kinase, Rap1, and transcriptional induction of vascular endothelial growth factor. *J. Natl. Cancer Inst.* **2000,** *92*, 1065-1073.

184. Pimentel, R. C.; Yamada, K. A.; Kleber, A. G.; Saffitz, J. E. Autocrine regulation of myocyte Cx43 expression by vegf. *Circ. Res.* **2002,** *90*, 671-677.

185. Moon, I. K.; Lee, J.; Ruoff, R. S.; Lee, H. Reduced graphene oxide by chemical graphitization. *Nat. Commun.* **2010,** *1*.

186. Mu, Q.; Su, G.; Li, L.; Gilbertson, B. O.; Yu, L. H.; Zhang, Q.; Sun, Y.-P.; Yan, B. Size-dependent cell uptake of protein-coated graphene oxide nanosheets. *ACS Appl. Mater. Interfaces* **2012,** *4*, 2259-2266.

187. Schrepfer, S.; Deuse, T.; Reichenspurner, H.; Fischbein, M. P.; Robbins, R. C.; Pelletier, M. P. Stem cell transplantation: The lung barrier. *Transplant. Proc.* **2007,** *39*, 573-576.

188. Datta, S. S.; Strachan, D. R.; Khamis, S. M.; Johnson, A. T. C. Crystallographic etching of few-layer graphene. *Nano Lett.* **2008,** *8*, 1912-1915.

189. Shkumatov, A.; Baek, K.; Kong, H. Matrix rigidity-modulated cardiovascular organoid formation from embryoid bodies. *PLoS One* **2014,** *9*, e94764.

190. Liao, K. H.; Lin, Y. S.; Macosko, C. W.; Haynes, C. L. Cytotoxicity of graphene oxide and graphene in human erythrocytes and skin fibroblasts. *ACS Appl. Mater. Interfaces* **2011,** *3*, 2607-2615.

191. Seo, J.; Lee, J. S.; Lee, K.; Kim, D.; Yang, K.; Shin, S.; Mahata, C.; Jung, H. B.; Lee, W.; Cho, S. W., *et al.* Switchable water-adhesive, superhydrophobic palladium-layered silicon nanowires potentiate the angiogenic efficacy of human stem cell spheroids. *Adv. Mater.* **2014,** *26*, 7043-7050.

192. Hanks, S. K.; Calalb, M. B.; Harper, M. C.; Patel, S. K. Focal adhesion protein-tyrosine kinase phosphorylated in response to cell attachment to fibronectin. *Proc. Natl. Acad. Sci. U.S.A.* **1992,** *89*, 8487-8491.

193. Garcia, A. J.; Boettiger, D. Integrin-fibronectin interactions at the cell-material interface: Initial integrin binding and signaling. *Biomaterials* **1999,** *20*, 2427-2433.

194. Fogerty, F. J.; Akiyama, S. K.; Yamada, K. M.; Mosher, D. F. Inhibition of binding of fibronectin to matrix assembly sites by anti-integrin (alpha 5 beta 1) antibodies. *J. Cell Biol.* **1990,** *111*, 699-708.

195. Toutant, M.; Costa, A.; Studler, J. M.; Kadare, G.; Carnaud, M.; Girault, J. A. Alternative splicing controls the mechanisms of fak autophosphorylation. *Mol. Cell. Biol.* **2002,** *22*, 7731-7743.

196. Bhang, S. H.; Cho, S. W.; Lim, J. M.; Kang, J. M.; Lee, T. J.; Yang, H. S.; Song, Y. S.; Park, M. H.; Kim, H. S.; Yoo, K. J., *et al.* Locally delivered growth factor enhances the angiogenic efficacy of adipose-derived stromal cells transplanted to ischemic limbs. *Stem Cells* **2009,** *27*, 1976-1986.

197. Ma, N.; Stamm, C.; Kaminski, A.; Li, W.; Kleine, H. D.; Muller-Hilke, B.; Zhang, L.; Ladilov, Y.; Egger, D.; Steinhoff, G. Human cord blood cells induce angiogenesis following myocardial infarction in nod/scid-mice. *Cardiovasc. Res.* **2005,** *66*, 45-54.

198. Wang, C. C.; Chen, C. H.; Hwang, S. M.; Lin, W. W.; Huang, C. H.; Lee, W. Y.; Chang, Y.; Sung, H. W. Spherically symmetric mesenchymal stromal cell bodies inherent with endogenous extracellular matrices for cellular cardiomyoplasty. *Stem Cells* **2009,** *27*, 724-732.

199. Pinto, J. M. B.; Boyden, P. A. Electrical remodeling in ischemia and infarction. *Cardiovasc. Res.* **1999,** *42*, 284-297.

200. Khan, R.; Sheppard, R. Fibrosis in heart disease: Understanding the role of transforming growth factor-beta in cardiomyopathy, valvular disease and arrhythmia. *Immunology* **2006,** *118*, 10-24.

201. Poelzing, S.; Rosenbaum, D. S. Altered connexin43 expression produces arrhythmia substrate in heart failure. *Am. J. Physiol. Heart Circ. Physiol.* **2004,** *287*, H1762-H1770.

202. Gutstein, D. E.; Morley, G. E.; Tamaddon, H.; Vaidya, D.; Schneider, M. D.; Chen, J.; Chien, K. R.; Stuhlmann, H.; Fishman, G. I. Conduction slowing and

sudden arrhythmic death in mice with cardiac-restricted inactivation of connexin43. *Circ. Res.* **2001,** *88*, 333-339.

203. O'Quinn, M. P.; Palatinus, J. A.; Harris, B. S.; Hewett, K. W.; Gourdie, R. G. A peptide mimetic of the connexin43 carboxyl terminus reduces gap junction remodeling and induced arrhythmia following ventricular injury. *Circ. Res.* **2011,** *108*, 704-715.
204. Gomez-Navarro, C.; Weitz, R. T.; Bittner, A. M.; Scolari, M.; Mews, A.; Burghard, M.; Kern, K. Electronic transport properties of individual chemically reduced graphene oxide sheets. *Nano Lett.* **2007,** *7*, 3499-3503.
205. Vuluga, D.; Thomassin, J. M.; Molenberg, I.; Huynen, I.; Gilbert, B.; Jerome, C.; Alexandre, M.; Detrembleur, C. Straightforward synthesis of conductive graphene/polymer nanocomposites from graphite oxide. *Chem. Commun.* **2011,** *47*, 2544-2546.
206. Kim, Y. S.; Ahn, Y.; Kwon, J. S.; Cho, Y. K.; Jeong, M. H.; Cho, J. G.; Park, J. C.; Kang, J. C. Priming of mesenchymal stem cells with oxytocin enhances the cardiac repair in ischemia/reperfusion injury. *Cells Tissues Organs* **2012,** *195*, 428-442.
207. Czyz, J.; Irmer, U.; Schulz, G.; Mindermann, A.; Hulser, D. F. Gap-junctional coupling measured by flow cytometry. *Exp. Cell Res.* **2000,** *255*, 40-46.
208. Grzelczak, M.; Perez-Juste, J.; Mulvaney, P.; Liz-Marzan, L. M. Shape control in gold nanoparticle synthesis. *Chem. Soc. Rev.* **2008,** *37*, 1783-1791.
209. Li, Z.; Ravaine, V.; Ravaine, S.; Garrigue, P.; Kuhn, A. Raspberry-like gold microspheres: Preparation and electrochemical characterization. *Adv. Funct. Mater.* **2007,** *17*, 618-622.

210. Chithrani, B. D.; Ghazani, A. A.; Chan, W. C. Determining the size and shape dependence of gold nanoparticle uptake into mammalian cells. *Nano Lett.* **2006,** *6*, 662-668.

211. Behfar, A.; Yamada, S.; Crespo-Diaz, R.; Nesbitt, J. J.; Rowe, L. A.; Perez-Terzic, C.; Gaussin, V.; Homsy, C.; Bartunek, J.; Terzic, A. Guided cardiopoiesis enhances therapeutic benefit of bone marrow human mesenchymal stem cells in chronic myocardial infarction. *J. Am. Coll. Cardiol.* **2010,** *56*, 721-734.

212. Jin, J.; Zhao, Y.; Tan, X.; Guo, C.; Yang, Z.; Miao, D. An improved transplantation strategy for mouse mesenchymal stem cells in an acute myocardial infarction model. *PLoS One* **2011,** *6*, e21005.

213. Noiseux, N.; Gnecchi, M.; Lopez-Ilasaca, M.; Zhang, L.; Solomon, S. D.; Deb, A.; Dzau, V. J.; Pratt, R. E. Mesenchymal stem cells overexpressing akt dramatically repair infarcted myocardium and improve cardiac function despite infrequent cellular fusion or differentiation. *Mol. Ther.* **2006,** *14*, 840-850.

214. Yang, K.; Wan, J.; Zhang, S.; Zhang, Y.; Lee, S. T.; Liu, Z. In vivo pharmacokinetics, long-term biodistribution, and toxicology of pegylated graphene in mice. *ACS Nano* **2011,** *5*, 516-522.

215. Li, Y.; Feng, L.; Shi, X.; Wang, X.; Yang, Y.; Yang, K.; Liu, T.; Yang, G.; Liu, Z. Surface coating-dependent cytotoxicity and degradation of graphene derivatives: Towards the design of non-toxic, degradable nano-graphene. *Small* **2014,** *10*, 1544-1554.

216. Thomas, S. P.; Kucera, J. P.; Bircher-Lehmann, L.; Rudy, Y.; Saffitz, J. E.; Kleber, A. G. Impulse propagation in synthetic strands of neonatal cardiac

myocytes with genetically reduced levels of connexin43. *Circ. Res.* **2003,** *92*, 1209-1216.

217. Jalife, J.; Morley, G. E.; Vaidya, D. Connexins and impulse propagation in the mouse heart. *J. Cardiovasc. Electrophysiol.* **1999,** *10*, 1649-1663.

218. Tofield, A. European cardiovascular disease statistics 2012 summary. *Eur. Heart J.* **2013,** *34*, 1086-1086.

219. Thygesen, K.; Alpert, J. S.; Jaffe, A. S.; Simoons, M. L.; Chaitman, B. R.; White, H. D.; Force, J. E. A. A. W. T. Third universal definition of myocardial infarction. *Rev. Esp. Cardiol.* **2013,** *66*, 2551-2567.

220. Eltzschig, H. K.; Eckle, T. Ischemia and reperfusion-from mechanism to translation. *Nat. Med.* **2011,** *17*, 1391-1401.

221. Angelos, M. G.; Kutala, V. K.; Torres, C. A.; He, G. L.; Stoner, J. D.; Mohammad, M.; Kuppusamy, P. Hypoxic reperfusion of the ischemic heart and oxygen radical generation. *Am. J. Physiol. Heart Circ. Physiol.* **2006,** *290*, H341-H347.

222. Gailit, J.; Colflesh, D.; Rabiner, I.; Simone, J.; Goligorsky, M. S. Redistribution and dysfunction of integrins in cultured renal epithelial cells exposed to oxidative stress. *Am. J. Physiol. Renal Physiol.* **1993,** *264*, F149-157.

223. Chiarugi, P.; Giannoni, E. Anoikis: A necessary death program for anchorage-dependent cells. *Biochem. Pharmacol.* **2008,** *76*, 1352-1364.

224. Song, H.; Cha, M. J.; Song, B. W.; Kim, I. K.; Chang, W.; Lim, S.; Choi, E. J.; Ham, O.; Lee, S. Y.; Chung, N., *et al*. Reactive oxygen species inhibit adhesion of mesenchymal stem cells implanted into ischemic myocardium via interference of focal adhesion complex. *Stem Cells* **2010,** *28*, 555-563.

225. Dreyer, D. R.; Park, S.; Bielawski, C. W.; Ruoff, R. S. The chemistry of graphene oxide. *Chem. Soc. Rev.* **2010,** *39*, 228-240.

226. Cha, C. Y.; Shin, S. R.; Gao, X. G.; Annabi, N.; Dokmeci, M. R.; Tang, X. W.; Khademhosseini, A. Controlling mechanical properties of cell-laden hydrogels by covalent incorporation of graphene oxide. *Small* **2014,** *10*, 514-523.

227. Kanakia, S.; Toussaint, J. D.; Chowdhury, S. M.; Lalwani, G.; Tembulkar, T.; Button, T.; Shroyer, K. R.; Moore, W.; Sitharaman, B. Physicochemical characterization of a novel graphene-based magnetic resonance imaging contrast agent. *Int. J. Nanomedicine* **2013,** *8*, 2821-2833.

228. Lalwani, G.; Sundararaj, J. L.; Schaefer, K.; Button, T.; Sitharaman, B. Synthesis, characterization, in vitro phantom imaging, and cytotoxicity of a novel graphene-based multimodal magnetic resonance imaging-x-ray computed tomography contrast agent. *J. Mater. Chem.* **2014,** *2*, 3519-3530.

229. Liu, J. Q.; Cui, L.; Losic, D. Graphene and graphene oxide as new nanocarriers for drug delivery applications. *Acta Biomater.* **2013,** *9*, 9243-9257.

230. Feng, L.; Zhang, S.; Liu, Z. Graphene based gene transfection. *Nanoscale* **2011,** *3*, 1252-1257.

231. Shin, S. R.; Aghaei-Ghareh-Bolagh, B.; Gao, X.; Nikkhah, M.; Jung, S. M.; Dolatshahi-Pirouz, A.; Kim, S. B.; Kim, S. M.; Dokmeci, M. R.; Tang, X., *et al*. Layer-by-layer assembly of 3d tissue constructs with functionalized graphene. *Adv. Funct. Mater.* **2014,** *24*, 6136-6144.

232. Shen, H.; Zhang, L.; Liu, M.; Zhang, Z. Biomedical applications of graphene. *Theranostics* **2012,** *2*, 283-294.

233. Grinnell, F.; Feld, M. K. Fibronectin adsorption on hydrophilic and hydrophobic surfaces detected by antibody-binding and analyzed during cell-adhesion in serum-containing medium. *J. Biol. Chem.* **1982,** *257*, 4888-4893.

234. Marcano, D. C.; Kosynkin, D. V.; Berlin, J. M.; Sinitskii, A.; Sun, Z. Z.; Slesarev, A.; Alemany, L. B.; Lu, W.; Tour, J. M. Improved synthesis of graphene oxide. *ACS Nano* **2010,** *4*, 4806-4814.

235. Peng, L.; Xu, Z.; Liu, Z.; Wei, Y. Y.; Sun, H. Y.; Li, Z.; Zhao, X. L.; Gao, C. An iron-based green approach to 1-h production of single-layer graphene oxide. *Nat. Commun.* **2015,** *6*.

236. Chang, Y.; Yang, S. T.; Liu, J. H.; Dong, E.; Wang, Y.; Cao, A.; Liu, Y.; Wang, H. In vitro toxicity evaluation of graphene oxide on a549 cells. *Toxicol. Lett.* **2011,** *200*, 201-210.

237. Wojtoniszak, M.; Chen, X.; Kalenczuk, R. J.; Wajda, A.; Lapczuk, J.; Kurzewski, M.; Drozdzik, M.; Chu, P. K.; Borowiak-Palen, E. Synthesis, dispersion, and cytocompatibility of graphene oxide and reduced graphene oxide. *Colloids Surf. B Biointerfaces* **2012,** *89*, 79-85.

238. Treossi, E.; Melucci, M.; Liscio, A.; Gazzano, M.; Samori, P.; Palermo, V. High-contrast visualization of graphene oxide on dye-sensitized glass, quartz, and silicon by fluorescence quenching. *J. Am. Chem. Soc.* **2009,** *131*, 15576-15577.

239. Sinoforoglu, M.; Gur, B.; Arik, M.; Onganer, Y.; Meral, K. Graphene oxide sheets as a template for dye assembly: Graphene oxide sheets induce h-aggregates of pyronin (y) dye. *Rsc Advances* **2013,** *3*, 11832-11838.

240. Talukdar, Y.; Rashkow, J. T.; Lalwani, G.; Kanakia, S.; Sitharaman, B. The effects of graphene nanostructures on mesenchymal stem cells. *Biomaterials* **2014,** *35*, 4863-4877.

241. Chowdhury, S. M.; Lalwani, G.; Zhang, K. V.; Yang, J. Y.; Neville, K.; Sitharaman, B. Cell specific cytotoxicity and uptake of graphene nanoribbons. *Biomaterials* **2013,** *34*, 283-293.

242. Ma, N.; Ma, C.; Li, C.; Wang, T.; Tang, Y.; Wang, H.; Moul, X.; Chen, Z.; Hel, N. Influence of nanoparticle shape, size, and surface functionalization on cellular uptake. *J. Nanosci. Nanotechnol.* **2013,** *13*, 6485-6498.

243. Gnecchi, M.; He, H.; Liang, O. D.; Melo, L. G.; Morello, F.; Mu, H.; Noiseux, N.; Zhang, L.; Pratt, R. E.; Ingwall, J. S., *et al.* Paracrine action accounts for marked protection of ischemic heart by akt-modified mesenchymal stem cells. *Nat. Med.* **2005,** *11*, 367-368.

244. Martinez, E. C.; Kofidis, T. Adult stem cells for cardiac tissue engineering. *J. Mol. Cell. Cardiol.* **2011,** *50*, 312-319.

245. Liu, P.; Hock, C. E.; Nagele, R.; Wong, P. Y. Formation of nitric oxide, superoxide, and peroxynitrite in myocardial ischemia-reperfusion injury in rats. *Am. J. Physiol. Heart Circ. Physiol.* **1997,** *272*, H2327-2336.

246. Zhang, Z. Y.; Turner, D. C.; Drzewiecki, G. J.; Hinshaw, D. B.; Hyslop, P. A. Impairment of integrin-mediated cell-matrix adhesion in oxidant-stressed pc12 cells. *Brain Res.* **1994,** *662*, 189-197.

247. Bhang, S. H.; Lee, T. J.; La, W. G.; Kim, D. I.; Kim, B. S. Delivery of fibroblast growth factor 2 enhances the viability of cord blood-derived mesenchymal stem cells transplanted to ischemic limbs. *J. Biosci. Bioeng.* **2011,** *111*, 584-589.

248. Tang, Y. L.; Zhao, Q.; Zhang, Y. C.; Cheng, L.; Liu, M.; Shi, J.; Yang, Y. Z.; Pan, C.; Ge, J.; Phillips, M. I. Autologous mesenchymal stem cell transplantation induce vegf and neovascularization in ischemic myocardium. *Regul. Pept.* **2004,** *117*, 3-10.

249. Rosen, K.; Shi, W.; Calabretta, B.; Filmus, J. Cell detachment triggers p38 mitogen-activated protein kinase-dependent overexpression of fas ligand - a novel mechanism of anoikis of intestinal epithelial cells. *J. Biol. Chem.* **2002,** *277*, 46123-46130.

250. Wei, H.; Li, Z. W.; Hu, S. S.; Chen, X.; Cong, X. F. Apoptosis of mesenchymal stem cells induced by hydrogen peroxide concerns both endoplasmic reticulum stress and mitochondrial death pathway through regulation of calspases, p38 and jnk. *J. Cell. Biochem.* **2010,** *111*, 967-978.

251. Hynes, R. O. Integrins: Versatility, modulation, and signaling in cell adhesion. *Cell* **1992,** *69*, 11-25.

252. Simon, H. U.; Haj-Yehia, A.; Levi-Schaffer, F. Role of reactive oxygen species (ROS) in apoptosis induction. *Apoptosis* **2000,** *5*, 415-418.

253. Underwood, P. A.; Bennett, F. A. A comparison of the biological-activities of the cell-adhesive proteins vitronectin and fibronectin. *J. Cell Sci.* **1989,** *93*, 641-649.

254. Qiu, Y.; Wang, Z. Y.; Owens, A. C. E.; Kulaots, I.; Chen, Y. T.; Kane, A. B.; Hurt, R. H. Antioxidant chemistry of graphene-based materials and its role in oxidation protection technology. *Nanoscale* **2014,** *6*, 11744-11755.

255. Laflamme, M. A.; Murry, C. E. Regenerating the heart. *Nat. Biotechnol.* **2005,** *23*, 845-856.

256. Reinecke, H.; Poppa, V.; Murry, C. E. Skeletal muscle stem cells do not transdifferentiate into cardiomyocytes after cardiac grafting. *J. Mol. Cell. Cardiol.* **2002,** *34*, 241-249.

257. Kinnaird, T.; Stabile, E.; Burnett, M. S.; Shou, M.; Lee, C. W.; Barr, S.; Fuchs, S.; Epstein, S. E. Local delivery of marrow-derived stromal cells augments collateral perfusion through paracrine mechanisms. *Circulation* **2004,** *109*, 1543-1549.

258. Van't Hof, W.; Mal, N.; Huang, Y.; Zhang, M.; Popovic, Z.; Forudi, F.; Deans, R.; Penn, M. S. Direct delivery of syngeneic and allogeneic large-scale expanded multipotent adult progenitor cells improves cardiac function after myocardial infarct. *Cytotherapy* **2007,** *9*, 477-487.

259. Kanakia, S.; Toussaint, J. D.; Mullick Chowdhury, S.; Tembulkar, T.; Lee, S.; Jiang, Y. P.; Lin, R. Z.; Shroyer, K. R.; Moore, W.; Sitharaman, B. Dose ranging, expanded acute toxicity and safety pharmacology studies for intravenously administered functionalized graphene nanoparticle formulations. *Biomaterials* **2014,** *35*, 7022-7031.

260. Yang, K.; Gong, H.; Shi, X. Z.; Wan, J. M.; Zhang, Y. J.; Liu, Z. In vivo biodistribution and toxicology of functionalized nano-graphene oxide in mice after oral and intraperitoneal administration. *Biomaterials* **2013,** *34*, 2787-2795.

261. Wang, K.; Ruan, J.; Song, H.; Zhang, J. L.; Wo, Y.; Guo, S. W.; Cui, D. X. Biocompatibility of graphene oxide. *Nanoscale Res. Lett.* **2011,** *6*, 1-8.

262. Gerullis, H.; Georgas, E.; Boros, M.; Klosterhalfen, B.; Eimer, C.; Arndt, C.; Otto, S.; Barski, D.; Ysebaert, D.; Ramon, A., *et al.* Inflammatory reaction as

determinant of foreign body reaction is an early and susceptible event after mesh implantation. *Biomed Res. Int.* **2014**.

263. Morales, C.; Gonzalez, G. E.; Rodriguez, M.; Bertolasi, C. A.; Gelpi, R. J. Histopathologic time course of myocardial infarct in rabbit hearts. *Cardiovasc. Pathol.* **2002,** *11*, 339-345.
264. Takemura, G.; Ohno, M.; Hayakawa, Y.; Misao, J.; Kanoh, M.; Ohno, A.; Uno, Y.; Minatoguchi, S.; Fujiwara, T.; Fujiwara, H. Role of apoptosis in the disappearance of infiltrated and proliferated interstitial cells after myocardial infarction. *Circ. Res.* **1998,** *82*, 1130-1138.
265. Takahashi, M.; Li, T.-S.; Suzuki, R.; Kobayashi, T.; Ito, H.; Ikeda, Y.; Matsuzaki, M.; Hamano, K. Cytokines produced by bone marrow cells can contribute to functional improvement of the infarcted heart by protecting cardiomyocytes from ischemic injury. *Am. J. Physiol. Heart Circ. Physiol.* **2006,** *291*, H886-H893.

요약 (국문초록)

심근경색은 인류의 가장 큰 사망 원인 중의 하나이다. 그럼에도 불구하고 현재의 임상 치료법은 매우 제한적이며, 환자들은 매년 늘어간다. 따라서 심근 경색 치료를 위한 대체치료법의 개발이 절실하다. 최근 줄기세포 및 조직공학의 발전으로 인해, 줄기세포에 기반을 둔 재생의학은 통한 심근 경색의 치료에 희망적인 전략을 제시한다. 그래핀은 특이적인 전기적, 화학적, 시각적 그리고 물리적 특성으로 인해 최근 몇 년간 차세대 소재로써 각광을 받고 있다. 생명공학 분야에서도 그래핀을 다양한 질환과 손상된 조직을 치료하기 위한 재료로써 주목하기 시작하였다.

본 학위논문에서는 그래핀과 그래핀 유도체들을 사용한 심근경색의 치료방법을 탐구하였다. 이에 따른 본 논문의 구체적인 목표는 다음과 같다. (1) 심근경색을 치료에 좀 유리하도록 줄기세포의 심근 분화를 유도하기 위한 2 차원 그래핀 플랫폼 개발과, 그래핀이 줄기세포의 분화에 미치는 영향의 메커니즘 규명. (2) 환원된 그래핀 옥사이드 (reduced graphene oxide, RGO)를 이용한 줄기세포의 성장인자 분비 및 간극 결함 단백질 발현 촉진을 통해 줄기세포의 심근 재생 효과 향상. (3) 그래핀 옥사이드 (graphene oxide, GO)를 사용해 심근 경색 부위에서 줄기세포의 생존 및 생착 유도.

본 논문의 주요 결과는 다음과 같다. 첫째, 그래핀은 줄기세포의 심근 분화 과정을 촉진시킨다. 줄기세포는 대량으로 얻을 수 있으며, 비교적 쉽게 분리할 수 있고, 증식 속도가 빠르며, 다양한 세포로 분화할

수 있다. 따라서 허혈성 심장질환 치료를 위한 재료로써 많은 주목을 받고 있다. 하지만 기존의 줄기세포의 심근 분화는 가격이 비싼 성장인자나 줄기세포에 독성이 있을 수 있는 화학물질을 사용해야만 가능했다. 하지만 그래핀 위에서 줄기세포를 배양하게 되면, 세포 배양 배지 외에 기타 추가적인 물질 없이도 줄기세포가 심근 분화 과정을 시작하게 된다. 이의 원인으로는 그래핀 위에서 줄기세포를 배양하게 되면 심근 분화에 유리한 세포외기질 단백질이 많이 발현되게 되기 때문이라고 생각된다. 또한 그래핀 위에서 배양된 줄기세포에서는 심근 분화에 필요한 세포 신호전달 물질들이 많이 발현되게 된다. 결과적으로, 그래핀 위에서 줄기세포가 심근 분화를 할 때 발현되는 인자들의 유전자가 증가하는 것을 확인할 수 있었다.

둘째, 줄기세포 치료요법은 심근경색 치료의 대안으로 떠오르고 있다. 줄기세포는 주로 성장인자를 분비함으로써 손상된 심근을 재생시킨다. 또한 간극 결합 단백질인 connexin 43 (Cx43)이 과발현되면 심장의 재생과 기능 향상이 촉진된다. 하지만 일반적으로 이식되는 줄기세포의 양으로는 충분한 성장인자와 Cx43 이 발현되지 않는데, 기존 논문들은 줄기세포를 spheroid 형태로 뭉치게 되면 세포 간 상호작용이 증가하여 이러한 효능이 향상된다는 것을 밝혔다. 하지만 줄기세포 spheroid는 성장인자의 분비를 더욱 촉진할 수 있는 세포와 세포외기질의 상호작용이 매우 제한적이다. RGO 는 세포외기질 단백질을 잘 흡착할 수 있다. 이 연구에서는 세포외기질 단백질이 흡착된 RGO 를 줄기세포 spheroid에 결합시킴으로써 세포와 세포외기질의 상호작용 증가시키고, 이에 의

해 성장인자의 분비를 촉진시킬 수 있었다. 증가된 성장인자의 분비와 RGO 의 전도성은 Cx43 의 발현도 증가시킬 수 있었다. RGO 가 결합된 줄기세포 spheroid 는 RGO 나 줄기세포 spheroid 에 비해 심근경색 치료에 뛰어난 효과를 보였다.

마지막으로, 심근경색 부위에 이식된 줄기세포의 낮은 생존율은 치료의 효능을 감소시킨다. 이러한 낮은 생존율의 주된 원인은 허혈 심근 부위를 재관류 하면서 분비된 활성산소이다. 줄기세포는 활성산소에 의해 손상된 조직의 세포외기질에 부착되지 못해 anoikis (세포가 부착되지 못해 일어나는 세포사)가 일어나게 된다. 따라서 이 연구에서는, GO 를 사용해 줄기세포를 활성산소에 의한 세포사로부터 보호하여 줄기세포의 치료효능을 개선하였다. GO 는 세포외기질 단백질을 흡착할 수 있다. 세포외기질 단백질이 흡착된 GO 에 부착된 줄기세포는 *in vitro* 에서 활성산소에 노출되거나 허혈 및 재관류 된 심근에 이식되었을 때, 아무 처리되지 않은 줄기세포보다 좋은 생존율을 보였다. 또한, GO 에 부착된 줄기세포는 심근에 더 많이 생착됨으로써 더 많은 양의 성장인자를 분비해서 심장 조직의 재생과 기능의 회복을 촉진시켰다. 따라서 GO 는 활성산소가 많은 심장의 허혈 및 재관류 부위에 이식된 줄기세포의 생존과 생착에 도움을 줌으로써 줄기세포의 치료 효율을 증가시킬 수 있다.

주요어: 중간엽줄기세포, 그래핀, 심근경색, 세포기능, 세포이식

학번: 2010-23330